ISTANBUL TECHNICAL UNIVERSITY ★ GRADUATE SCHOOL

MITIGATING ALKALI SILICA REACTION USING WASTE GLASS POWDER

M.Sc. THESIS

Abed ALIOGLU

Department of Civil Engineering

Structure Engineering Program

FEBRUARY 2024

ISTANBUL TECHNICAL UNIVERSITY ★ GRADUATE SCHOOL

MITIGATING ALKALI SILICA REACTION USING WASTE GLASS POWDER

M.Sc. THESIS

Abed ALIOGLU
(501201032)

Department of Civil Engineering

Structure Engineering Program

Thesis Advisor: Asst. Prof. Dr. Özgür EKİNCİOĞLU

FEBRUARY 2024

ISTANBUL TEKNİK ÜNİVERSİTESİ ★ LİSANSÜSTÜ EĞİTİM ENSTİTÜSÜ

ALKALİ SİLİKA REAKSİYONUNUN AZALTILMASI İÇİN ATIK CAM TOZU KULLANIMI

YÜKSEK LİSANS TEZİ

Abed ALIOGLU
(501201032)

İnşaat Mühendisliği Anabilim Dalı

Yapı Mühendisliği Programı

Tez Danışmanı: Dr. Öğr. Üyesi Özgür EKİNCİOĞLU

ŞUBAT 2024

Abed ALIOGLU, a M.Sc. student of İTU Graduate School student ID 501201032, successfully defended the thesis/dissertation entitled "**MITIGATING ALKALI SILICA REACTION USING WASTE GLASS POWDER**", which he prepared after fulfilling the requirements specified in the associated legislations, before the jury whose signatures are below.

Thesis Advisor:	**Asst. Prof. Dr. Özgür EKİNCİOĞLU** İstanbul Technical University	.....
Jury Members:	**Prof. Dr. Mustafa Hulusi ÖZKUL** Beykent University	.....
	Asst. Prof. Dr. Ünal Anıl DOĞAN İstanbul Technical University	.....

Date of Submission : 05 January 2024
Date of Defense : 23 February 2024

FOREWORD

I want to express my profound appreciation to Asst. Prof. Dr. Özgür EKİNCİOĞLU, my thesis advisor, for his invaluable assistance, guidance, and motivation throughout my laboratory studies and in the preparation of my thesis. This acknowledgment is a small token of appreciation for your substantial contributions to my academic and personal development.

I am also immensely thankful to the dedicated academicians who have helped me apply some tests throughout my studies. Prof. Dr. Ahmet SİRKECİOĞLU helped me through TGA tests, Dr. Türkan DOĞAN used SEM, and Dr. Hasan GÖKÇE applied XRD tests for me.

I would also like to thank the technicians of the Building Materials laboratory, Mr. Murat MEYDAN and Mr. Oktay YALÇINKAYA, for their support and expertise during my research.

This study was supported by the Scientific Research Projects Department of Istanbul Technical University with Project Number 44099.

Finally, I thank my parents for their unwavering support throughout my academic journey and life.

December 2023

Abed ALIOGLU
Civil Engineer

TABLE OF CONTENTS

ABBREVIATIONS

AAR : Alkali Aggregate Reaction
ACR : Alkali Carbonate Reaction
ASR : Alkali-Silica Reaction
C-S-H : Calcium Silicate Hydrate
CH: : Calcium Hydroxide
FA : Fly Ash
GGBFS : Ground Granulated Blast Furnace
MCPT : Miniature concrete prism test
NS : Nano-Silica
SBR : Styrene butadiene rubber
SEM : Scanning Electronic Microscope
SF : Silica Fume
TGA : Thermogravimetric Analysis
WGP : Waste Glass Powder
XRD : X-Ray Diffraction
XRF : X-Ray Fluorescence

SYMBOLS

°C	: Degree Celsius
Na	: Sodium
NaOH	: Sodium Hydroxide
K	: Potassium
H_2SiO_2	: Silicic Acid
Ca^{+2}	: Calcium ions
mm	: Millimeter
m	: Meter
MPa	: Mega Pascale
µm	: Micrometer

LIST OF TABLES

Page

LIST OF FIGURES

Page

MITIGATING ALKALI-SILICA REACTION USING WASTE GLASS POWDER

SUMMARY

Alkali silica reaction (ASR), the most widespread alkali-aggregate reaction (AAR), is a significant durability problem affecting concrete. A deleterious gel is formed due to the reaction between alkali oxides and reactive aggregates containing silica. This gel causes expansion, which in turn causes small cracks that affect the durability and mechanical properties of the concrete later. Although ASR causes cracks in concrete, the fundamental issue with ASR is the prevalence of additional durability concerns, such as corrosion in steel, that could ultimately lead to extreme results.

Much research has been done to keep ASR expansion within the safe limits mentioned in related standards. Chemical and mineral additives, such as lithium and different supplementary cementitious materials (SCMs), can mitigate the expansion of ASR. Recently, some studies introduced waste glass in powder form as a mineral additive to mitigate ASR, and they found promising results with some problems in mechanical properties. However, more research is needed to understand how waste glass mitigates ASR and how we can solve its negative effect on mechanical properties.

Environmental problems are considered one of the most significant problems in scientific society. Waste glass is an important environmental problem due to its large volume and slow decomposition rate. Glass is non-biodegradable and can take thousands of years to decompose in landfills. Improperly disposed of waste glass can contribute to environmental problems such as pollution, climate change, and habitat destruction. Therefore, using waste glass to produce cement-based materials can contribute to sustainability by reducing environmental issues.

This experimental study proposes using waste glass powder (WGP) and nano silica (NS) as mineral additives to mitigate ASR. Different percentages of (WGP): 10%, 15%, 20%, and 25%, with 1%, 1.5%, and 2% of nano silica as cementitious replacement were examined. Nano-silica accelerates the early-age hydration reactions in mortar, while waste glass powder mitigates.

Waste glass powder and cement used for the production were tested using an X-ray fluorescence test (XRF) to learn the elemental composition of both materials. The average particle size of WGP was 60μm before production to increase the effectiveness in mitigating ASR. Different tests were conducted to investigate the effect of WGP-NS combinations on mortar properties. A flowability test determined the workability of mortars with glass powder and Nano silica. Air content for mortars containing different amounts of WGP and NS was calculated during the production phase. An accelerated mortar bar test was conducted for different combinations to measure the expansion in each mortar. Flexural and compressive strength tests were conducted on prismatic specimens at 7 and 28 days. First, three flexural strength tests were conducted on samples to divide each specimen into two pieces (6). Three of the six pieces were tested in a compression machine, and the other three were used for a

capillary water absorption test to see the influence of WGP and NS on the permeability of mortar. The results showed a positive effect of WGP-NS on mitigating ASR and limiting the reduction in the mechanical properties of mortars, especially at an early age.

Scanning Electronic Microscope (SEM) and Thermo Gravimetric Analysis (TGA) tests were performed to examine the pozzolanic reaction of glass powder and see the cracks and different hydration products in the specimens. Also, X-ray diffraction analysis was performed to investigate the effect of WGP and NS on CH consumption C-S-H formation and quartz formation. SEM showed the ability of WGP to reduce the cracks that resulted from alkali-silica gel formation. Also, results showed a denser microstructure in mortars produced with WGP and NS. XRD and TGA tests presented the pozzolanic activity of WGP. The fine particles of glass powder, which contain high levels of Si+4 and Ca2+, conduct a pozzolanic reaction, and they dissolve completely in the hydration process to form C-S-H. This pozzolanic reaction causes insufficient presence of SiO_2 to form the ASR gel. In addition to the improvements in the properties of mortars, replacing the cement with these mineral additives (WGP and NS) can be considered a recycling process and contribute to sustainability principles.

ALKALİ SİLİKA REAKSİYONUNUN AZALTILMASI İÇİN ATIK CAM TOZU KULLANIMI

ÖZET

Alkali agrega reaksiyonunun (AAR) en yaygın şekli olan alkali silika reaksiyonu (ASR), betonu etkileyen önemli bir dayanıklılık sorunu olarak bilinmektedir. Na^+ ve K^+ gibi alkali oksitler ile reaktif silis içeren bazı agregalar arasındaki reaksiyon nedeniyle zararlı bir jel oluşur. Bu jel suyun da etkisi ile şişerek genleşmeye ve iç gerilmelerin artmasına neden olur ve bu da daha sonra betonun dayanıklılığını ve mekanik özelliklerini etkileyen ve harita şekilli olarak adlandırılan ince çatlaklara neden olur. Bununla birlikte, ASR ile ilgili asıl endişe kaynağı bu çatlaklar değil, geçirimliliğin artması ile çelik çubukların korozyonu gibi diğer dayanıklılık problemlerinin ortaya çıkma potansiyelidir.

ASR kaynaklı genleşmeleri ilgili standartların belirttiği sınırlar dahilinde tutmak için birçok araştırma yapılmıştır. Mümkünse reaktif olmayan bir agrega ile düşük alkali içeriğine sahip bir çimento kullanmak ve ortamdan nemi uzak tutmak en başta gelen çözüm yöntemlerinden olmakla birlikte bu durum her zaman kolay veya mümkün olmayabilir. ASR genleşmelerini azaltmak için lityum gibi kimyasal katkılar ve uçucu kül, silis dumanı, metakaolin, yüksek fırın cürufu gibi çok çeşitli mineral katkı maddeleri de kullanılabilir. Mineral katkıların kullanılmasının arkasındaki temel neden, hidratasyonun erken aşamalarında amorf silisin salınmasını kolaylaştıran puzolanik reaksiyon göstermeleridir. Bu reaksiyon, kalsiyum silikat hidrate (C-S-H) oluşturmak için kalsiyum hidroksit (CH) tüketir. Sonuç olarak, agrega kaynaklı reaktif silis, alkaliler ile reaksiyona girerek alkali silis hidratı (zararlı jel) oluşturmak için yeterli kalsiyumdan yoksundur.

Son zamanlarda yapılan bazı çalışmalarda, beton ve harç gibi çimento esaslı malzemelerde ASR'yi azaltmak için toz haline getirilmiş atık camlar da mineral katkı maddesi olarak kullanılmış ve her ne kadar mekanik özelliklerde bazı problemler gözlenmiş olsa da ASR genleşmelerinde umut verici sonuçlar elde edilmiştir. Bazı çalışmalara göre atık cam tozu kullanılarak üretilen harç ve betonların erken yaş dayanımlarında düşmeler gözlenmiştir. Bununla birlikte, atık camın ASR kaynaklı genleşmeleri nasıl azalttığını ve mekanik özellikler üzerindeki olumsuz etkisini nasıl giderebileceğimizi anlamak için daha fazla araştırma yapılmasına ihtiyaç vardır.

Günümüzde çevre sorunları bilim camiasının en önemli sorunlarından biri olarak kabul edilmektedir. Atık camlar, Dünya'mızdaki en yaygın katı atıklardan biridir ve yavaş ayrışma hızı nedeniyle önemli bir çevre sorunudur. Camın biyolojik olarak parçalanması mümkün değildir ve çöplüklerde parçalanması binlerce yıl alabilir. Uygun şekilde atılmayan atık camlar kirlilik, iklim değişikliği ve habitat tahribatı gibi çevresel sorunlara katkıda bulunabilir. Bu nedenle atık camların çimento esaslı malzemelerin üretiminde kullanılması çevresel sorunları azaltarak sürdürülebilirliğe katkı sağlayabilir. Günümüzde atık camlar agrega olarak veya çimento ile ikame olarak kullanılabilmektedir. Çimento ile ikame edildiğinde tane boyutuna bağlı olarak ASR'nin olumsuz etkisini azalttığı gözlenmiştir. Bunun sebepleri üzerine çok çeşitli teoriler öne sürülmesine rağmen bu konuda araştırmalar devam etmektedir.

Bu çalışmada ASR'yi azaltmak amacıyla atık cam tozu (ACT) ve nano silikanın (NS) mineral katkı maddesi olarak kullanılması önerilmiştir. Çimento yerine ikame olarak %10, %15, %20 ve %25 ACT ile %1, %1.5 ve %2 nano silikanın farklı yüzdelerde kullanılması ile toplam 20 farklı harç karışımı üretilmiştir. Atık cam tozu diğer mineral katkı malzemelerine benzer şekilde hidratasyon reaksiyonlarını yavaşlatarak çimento esaslı malzemelerin erken yaş mukavemetini azaltmaktadır. Nano silika ise daha büyük yüzey alanı nedeniyle daha reaktif bir malzemedir ve erken yaş dayanımlarını artırması beklenmektedir. Bu iki malzeme birlikte farklı oranlarda kullanılarak ikisinin optimum bir kombinasyonu bulunmaya çalışılmıştır.

ACT-NS kombinasyonlarının harç özelliklerine etkisini araştırmak amacıyla farklı testler yapılmıştır. Taze harçların işlenebilirliği yayılma testi ile belirlenmiş ve hava miktarları hesaplanmıştır. ASR kaynaklı genleşmeleri ölçmek için farklı oranlarda ACT-NS içeren kombinasyonlara hızlandırılmış harç çubuğu deneyi uygulanmış ve boy değişimleri ölçülmüştür. Mekanik özellikleri belirlemek için 4x4x16 cm boyutunda üretilen prizmatik numunelere ise 7 ve 28. günlerde eğilme ve basınç dayanımı testleri uygulandı. Öncelikle prizmatik numunelere eğilme dayanımı testi uygulanarak numuneler iki parçaya bölünmüş ve bu iki parçanın biri üzerinde basınç dayanımı testi yapılırken diğer parça daha sonra kılcal su emme deneyi yapılmak üzere ayrılmıştır. Sonuçlar, ACT ve NS'nın ASR'yi azaltmada olumlu etkisi olduğunu ve ayrıca harçların mekanik özelliklerindeki azalmanın sınırlı kaldığını gösterdi. Elde edilen sonuçlara göre, %20 ACT ve %1,5 NS ile üretilen harç karışımının hem ASR genleşmelerini azaltmada hem de yeterli dayanımlara ulaşmada en uygun karışım olduğu sonucuna varılmıştır.

Cam tozu ve çimentonun kristal yapısı arasındaki farkın anlaşılması amacıyla çimento ve cam tozu üzerine X-Işını Kırınımı (XRD) testleri uygulandı. Ayrıca, bazı harç numuneleri de toz haline getirilerek onlar üzerinde de XRD deneyleri yapıldı ve ACT ve NS'nın CH tüketimi ile CSH jeli ve quartz oluşumuna etkileri incelendi. Atık cam tozunun puzolanik etkisini incelemek ve numunelerdeki çatlakları ve farklı hidratasyon ürünlerini görmek amacıyla da Taramalı Elektron Mikroskobu (SEM) ve Termogravemetrik Analiz (TGA) deneyleri yapıldı. SEM sonuçlarına göre, kullanılan ACT'nun ASR kaynaklı çatlakları azaltmada etkili olduğu gözlendi. Aynı zamanda, sonuçlar ACT ve NS ile üretilen harçların daha sıkı bir içyapıya sahip olduğunu da göstermiştir. XRD ve TGA deneyleri ACT'nun puzolanik aktivite gösterdiğini ortaya koymuştur. İnce taneli atık cam tozu yüksek oranda Si^{+4} ve Ca^{+2} içermektedir ve puzolanik reaksiyon sonucunda tamamen çözünerek C-S-H oluşturur. Bu puzolanik reaksiyon sonucunda ortamdaki SiO_2, ASR jeli oluşumu için yetersiz kalmaktadır. Harç özelliklerindeki iyileşmelere ilave olarak, çimentonun ACT ve NS gibi mineral katkılar ile ikame edilmesi geri dönüşüm olarak da düşünülebilir ve sürdürülebilirlik ilkelerine katkıda bulunur.

Sonuç olarak bu çalışmanın, biyobozunur atıklardan biri olmayan camın harç ve beton gibi çimento esaslı malzemelerin üretiminde kullanılmasıyla hem çevresel kaynaklı problemleri azaltarak sürdürülebilirliğe katkıda bulunmayı hem de ASR gibi önemli bir dayanıklılık sorununa çözüm olmasını umuyoruz. Bununla birlikte atık cam tozlarının çimento esaslı malzemelerdeki etki mekanizmasını anlamak için daha fazla sayıda çalışma yapılmasına ihtiyaç duyulmaktadır ve bu tezin de bu tarz çalışmalara katkıda bulunmasını umuyoruz.

1. INTRODUCTION

Alkali-silica reaction (ASR), the most common form of alkali-aggregate response, is a significant concern for the durability of concrete structures, particularly in regions with high levels of reactive aggregates. ASR is a chemical reaction between the alkalis from cement and reactive forms of silica from aggregates, which can lead to the formation of a harmful gel. This gel absorbs water and swells, causing interior stress and cracks in concrete. These cracks cause considerable damage to concrete structures. ASR is a significant concern for the durability of concrete structures, particularly in regions that use aggregates with a high content of reactive silica. Reactive silica can exist in several forms, including opal, chert, flint, and volcanic glass. The higher the amount of reactive silica in the aggregate, the more susceptible the concrete is to ASR. Humidity and temperature also affect the expansion of the deleterious gel formed. The third factor that controls the presence of ASR is cement with high alkali content.

Many studies have been completed to investigate the methods of reducing deleterious expansion. The most effective additives used to mitigate ASR gel are fly ash, metakaolin, and ground granulated blast furnace slag (GGBFS), which are known as supplementary cementitious materials (SCM) (Lindgårda et al., 2012). The primary concept behind using supplementary cementitious materials (SCM) is their pozzolanic reaction, which facilitates the release of amorphous silica during the early stages of hydration. This reaction consumes calcium hydroxide to form C-S-H (calcium silicate hydrate). As a result, the reactive silica from the aggregate lacks sufficient calcium to react and form the alkali silicate hydrate (the deleterious gel).

Various materials are used in different studies to test the ability of their pozzolanic reaction to mitigate ASR. One of these materials is waste glass (Topcu and Canbaz, 2004; Johnston, 1974). Waste glass can have several negative effects on the environment and human health. Some potential negative effects include air pollution from the fine particles of waste glass powder, which can become airborne and

contribute to air pollution. Inhaling these particles can cause respiratory problems, especially for people with asthma or other respiratory conditions. Waste glass powder can also contaminate water sources if improperly disposed of. When mixed with water, waste glass powder can release harmful chemicals and heavy metals, harming aquatic life and human health. Recycling waste glass powder helps decrease these harmful damages and creates a cleaner environment.

1.1 Aim and Content of the Study

This research focuses on reducing alkali-silica reaction (ASR) in mortars by partially substituting cement with waste glass in powder form. The waste glass undergoes a pozzolanic reaction, aiding in ASR mitigation. Previous studies have shown that glass powder delays hydration (Cai et al., 2019). Nano silica is introduced to the mixtures to counter this and accelerate the hydration process (Nigam and Verma, 2023). Incorporating nano silica leads to faster hydration during the early stages (Nigam and Verma, 2023). The investigation also includes assessing the impact of waste glass powder (WGP) and nano silica (NS) on mechanical properties, workability, and air content of the mortars. A capillary water absorption test is conducted on each specimen to observe the distribution of voids through water absorption via capillary action. Moreover, X-ray diffraction (XRD) analyses are performed on the mortars after immersing them in NaOH solution to identify any chemical composition changes resulting from adding WGP and nano-silica. Scanning electron microscopy (SEM) images are taken for various WGP and NS contents to observe the microstructure changes after immersion in NaOH solution.

In summary, this study will be a step towards a purer future and contribute to sustainability by introducing effective ways of using non-biodegradable wastes in concrete and mitigating a durability concern such as ASR. However, more studies are needed to understand the mechanism of waste glass powder in concrete and mortar, and I hope this study will be part of that investigation.

2. ALKALI AGGREGATE REACTION (AAR)

Alkali aggregate reaction is between alkalis from different sources (mainly Portland cement) and specific aggregates containing silica, carbonate, and silicate. This chemical reaction occurs between hydroxyl ions (OH) of alkalis such as sodium and potassium from hydraulic cement and carbonate from some aggregates in the case of alkali carbonate reaction (ACR) and reactive silica in the case of alkali-silica reaction (ASR). These reactions can occur in concrete and mortar (Thomas et al., 2013).

2.1 Different Sources of Alkalis

There are different sources of alkalis contributing to the alkali-aggregate reactions. These are;

- Portland cement.
- Supplementary cementitious materials (SCM) (e.g., fly ash, slag, silica fume, natural pozzolans).
- Aggregates.
- Chemical admixtures.
- External sources (e.g., seawater and deicing salts).
- Wash water (if used).

Among these, the primary source of alkali is Portland cement. The total alkali content is generally limited by 0.6% in Portland Cement to avoid any risks of contributing deleterious gel.

2.2 Types of Alkali Aggregate Reaction

Two types of AAR are known. These are;

1. Alkali carbonate reaction (ACR)
2. Alkali silica Reaction (ASR)

These reactions occur when OH^- ions from alkalis present in Portland cement interact with varying chemical compositions found in different reactive aggregates (ACR – ASR). This reaction produces a deleterious gel that can absorb water from surroundings in the appearance of temperature, leading to expansion and swelling. This swelling produces internal stresses, which appear as map cracking. A summary of different types of AAR will be mentioned in the following paragraphs.

2.2.1 ACR

It is a reaction between hydroxyl ions of alkalis such as Sodium and Potassium from hydraulic cement or other sources, and carbonate comes from certain carbonate rocks, particularly calcitic, dolostone, and dolomitic limestone, present in some aggregates. As shown by equation (2.1), the primary chemical reaction in rocks is the decomposition of the dolomite ($CaMg(CO_3)_2$), or dedolomitization, to calcite ($CaCO_3$) and brucite ($Mg(OH)_2$) where M represents an alkali element. The reaction is usually accompanied by dedolomitization and expansion of the affected aggregate particles, leading to abnormal expansion and cracking of concrete in service (Thomas et al., 2013).

$$CaMg(CO_3)_2 + 2MOH \rightarrow Mg(OH)_2 + CaCO_3 + M_2CO_3 \quad \text{(Ozol, 1994)} \quad (2.1)$$

Alkali carbonate reaction (ACR) was first discovered by Swenson as the underlying cause of concrete deterioration in Canada, coinciding with the initial documentation of alkali-silica reaction (ASR) in the same country (Swenson, 1957a; Sweson, 1957b). Following its identification, ACR was subsequently implicated in cases of concrete structure degradation in the USA, as reported by (Hadley, 1961). Over time, alleged occurrences of ACR have been reported in various regions, including Virginia, West Virginia, Kentucky, Missouri, Tennessee, Iowa, Illinois, Indiana, and New York, as well as in England, Bahrain, Iraq, and China (Thomas et al., 2013).

However, unlike ASR, the issues associated with ACR remain confined to a few isolated locations worldwide. As a result, comparatively limited research has been conducted on this particular topic.

2.2.2 ASR

Alkali-silica reaction (ASR) is a significant concern for the durability of concrete structures, particularly in regions with high levels of reactive aggregates, and it is the most common form of AAR. ASR is a chemical reaction between the alkalis in concrete and reactive forms of silica, which can form a gel-like substance that can cause considerable damage to concrete structures.

ASR was initially identified in the USA in the 1930s while looking into the early deterioration of concrete buildings in California (Figure 2.1). There was no discovered reason that might be responsible for the deterioration, which seemed to be caused by internal expansion stress. Stanton started evaluating the cement used in concrete in a

laboratory in 1940. No excessive expansion was observed when different curing conditions, such as immersion, drying, and high temperatures, were used (Naik, 2008). Nevertheless, after a year, comparable samples with high-alkali cement and high humidity experienced excessive expansion (Stanton, 1942). Stanton noted that no excessive expansion happened when low-alkali cements were utilized. He concluded that the minerals expand significantly when high-alkali cement is used with particular minerals found in the aggregates (Stanton, 1942). It was proposed that the maximum amount of cement alkalis in concrete containing these aggregates should be at most 0.6%.

Figure 2.1: Thomas Stanton of the California State Division of Highways and a Bridge Parapet Wall that shows signs of Damage due to an Alkali-Silica Reaction (Thomas et al., 2013).

2.3 ASR's Mechanisms

Understanding the mechanisms behind Alkali-Silica Reaction (ASR) is essential for mitigating the harmful effects on concrete structures. Since ASR was discovered in the 1940s, many theories have started to appear to explain the mechanism by which this deleterious gel was formed. The following parts will explain some explanations, such

as forming alkali-silica gel, the swelling process, and the role of calcium ions in forming ASR.

2.3.1 Formation of alkali-silica gel

Powers and Steinour (1955) thoroughly examined the ASR mechanism. Silica phases vary greatly, from highly disordered amorphous forms like opal and volcanic glass to densely structured crystals like quartz. Alkali hydroxides can damage the silica structure, causing sodium or potassium to replace the hydroxyl ions on the surface. The process continues as the silica structure dissolves and the silica-oxygen linkages break down (Powers and Steinour, 1955). Chatterji (1989) aligns with the above theory and introduces the impact of cation size on the absorption rate into silica. Larger cations like Ca^{++} will not penetrate as quickly as smaller cations like Na^{+}.

Diamond (1989) provided similar explanations but focused on the crucial distinction between the formation of alkali-silica gel and the swelling process.

2.3.2 Swelling mechanism

Powers and Steinour (1955) explained swelling due to the energy gradient. Because of a rise in energy states between the pore solution and the alkali-silica gel, swelling happens when water travels from the cement paste toward the reaction site (Powers and Steinour, 1955). Osmotic pressure pulls the pore solution into the alkali-silica gel, where it reacts with the silica structure, dislodging alkalis and binding to the oxygen exposed to form an enlarged structure. Swelling causes volume expansion and has enough energy to exert net pressure on the underlying concrete matrix (Powers and Steinour, 1955). Diamond (1989) emphasizes the role of osmotic pressure and a semi-permeable membrane. The pore solution is absorbed into the gel due to the different energy levels of the alkali-silica gel and the pore solution. The swelling brought on by the absorption puts pressure on the surrounding matrix. Alkali-silica gel cannot dissolve in pore solution; hence, it works as a semi-permeable membrane to separate the pore solution from the solution contained within the gel. This enables the formation of an osmotic pressure gradient and a concentration gradient (Diamond, 1989). Wang (1991) introduced the concept of a colloidal alkali-silica structure. This structure exhibits a high affinity for water and is frequently formed by alkali-silica groups. These groups generate along the surface of materials, leading to swelling at the reaction site.

Helmuth et al. (1993) mentioned the expansion of alkali-silica gel to silanol group exposure. Due to hydroxyl ions in the pore solution, the reaction starts with the degradation of silanol groups along the surface. Protons (H^+) are then substituted by alkalis (K^+, Na^+) in the silanol groups (Helmuth et al., 1993). Following this action, hydroxyl ions attack the siloxane bonds to generate more silanol sites for alkalis to form bonds with. Continued exposure to silanol groups causes the expansion of reactive aggregate's alkali-silica gel as the process draws more pore solution into it. Rajabipour (2015) links swelling to transforming nano-colloidal silica into a gel.

2.3.3 Role of calcium

The significance of calcium in mitigating excessive swelling is a common thread. Powers and Steinour (1955) focus on limited calcium transport to the reaction site as it has a much lower solubility than alkalis. Powers and Steinour (1955) propose a layer of lime (calcium) alkali-silica to limit calcium transfer. This layer blocks the transfer of further calcium to the reaction site, preventing an excess of calcium. They claimed that calcium hydroxide contributes to the formation of alkali-silica gel (Powers and Steinour, 1955).

Chatterji (1989) concluded that the rate at which silica diffuses out of the mineral during the reaction is determined by the amount of Ca^{++} in the pore solution. He confirmed the importance of Ca^{++}'s existence in forming alkali silica gel. Contradictory, Diamond (1989) emphasizes the need for calcium to prevent harmful swelling. He claimed that alkali-silica gel can be created without causing dangerous swelling when there is insufficient Ca^{++}.

Wang and Gillott (1991) discussed calcium-ion exchange: the hydrogen proton (H^+), which is present on the silica surface as silanol (Si-O-H) groups, is first exchanged for an alkali ion before being released into solution (Si-O-R^+). In exchange for calcium, sodium or potassium may be released from the surface, attacking the siloxane bonds inside the silica mineral. More silanol bonds are consequently made available to the pore solution, enabling the process to proceed. Then, the available calcium ions are used to replace the alkali ions, which had formed bonds with the exposed silanol groups, freeing the alkalis to continue the reaction.

Helmuth et al. (1993) explained calcium's role in forming calcium-silicate hydrates. He claimed that the development of ASR depends on calcium, but calcium hydroxide's solubility is smaller than alkalis. Calcium hydroxide has saturated the pore solution, although calcium concentrations in alkali-containing fluids are lower. This is because calcium-silicate hydrates (C-S-H) develop inside the reactive silica, releasing alkalis to feed the reaction (Helmuth et al., 1993). Alkali-silica gels are transported away from the reaction site and contain additional calcium products due to exposure to calcium-rich pore fluid (Helmuth et al., 1993).

Blezynski and Thomas (1998) mapped a high calcium concentration along the reactive particle's outer border. They discovered a band of high calcium along the reactive particles outside edge while mapping the alkali-silica gel concentration within reactive aggregate particles using backscatter electron imaging. However, more silica and less calcium were found along the reaction rim's leading edge. The research also identified a layer of potassium-rich silica between this layer and the calcium-rich layer below and a layer of sodium-rich silica at the aggregate interface. The study supports the need for Ca^{++} and alkali in producing alkali-silica gels. Rajabipour et al. (2015) demonstrated that silica phases can dissolve into solution up until the cement pore solution is saturated with Si, which contributed to our understanding of the reaction mechanism. The nucleation and condensation of nano-colloidal silica solution occur in the cement pore solution when Ca^{2+} (and lesser concentrations of Fe^{2+} and Al^{3+}) are present. This goes on until the creation of larger metal silicate formations, such as silicate gel or macro-scale precipitates (Rajabipour et al., 2015).

2.4 The Pessimum Ratio

The appearance of ASR depends not only on alkali content and type of aggregate but also on their ratios in concrete. The specific combination of alkali content and reactive aggregate type that causes the highest ASR expansion expresses the pessimum ratio term. This ratio represents an essential barrier at which ASR induces the highest damage level. Researchers have observed that moving away from the pessimum ratio in either direction (higher or lower alkali content) can reduce expansion. It was first discovered by Stanton, who claimed that expansion didn’t necessarily increase with the increase in reactive aggregate content. Also, at a fixed proportion of reactive aggregates, the expansion became maximum at a specific particle size, and the

expansion decreased when the particle size increased or decreased from the pessimum size (Stanton et al., 1942).

Much research has investigated the pessimum ratio for reactive aggregate content and grain size for different types of reactive aggregates (Binal, 2015). They found that the maximum expansion level (0.66) happened at 20% replacement of sand for opal (Figure 2.2). It decreased with an increase in opal content of more than 20% (Binal, 2015). They stated the reason as the amount of amorphous silica content in the reactive aggregate (Binal, 2015). Figure 2.3 shows the pessimum ratio for grain size. It can be noticed that the range between 0.15 and 0.3 mm in grain size offers the maximum expansion level (0.88) for opal as a reactive aggregate (Binal, 2015). A reduction in expansion level can be noticed for higher and lower grain sizes.

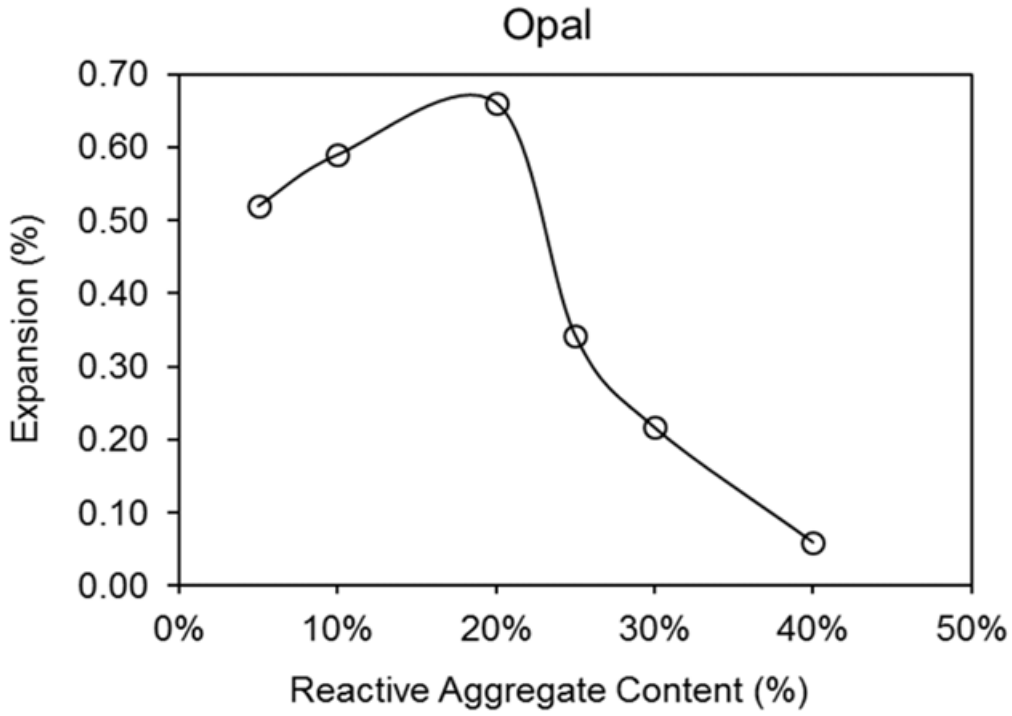

Figure 2.2: The graph of the pessimum ratio of opal aggregate (Binal, 2015).

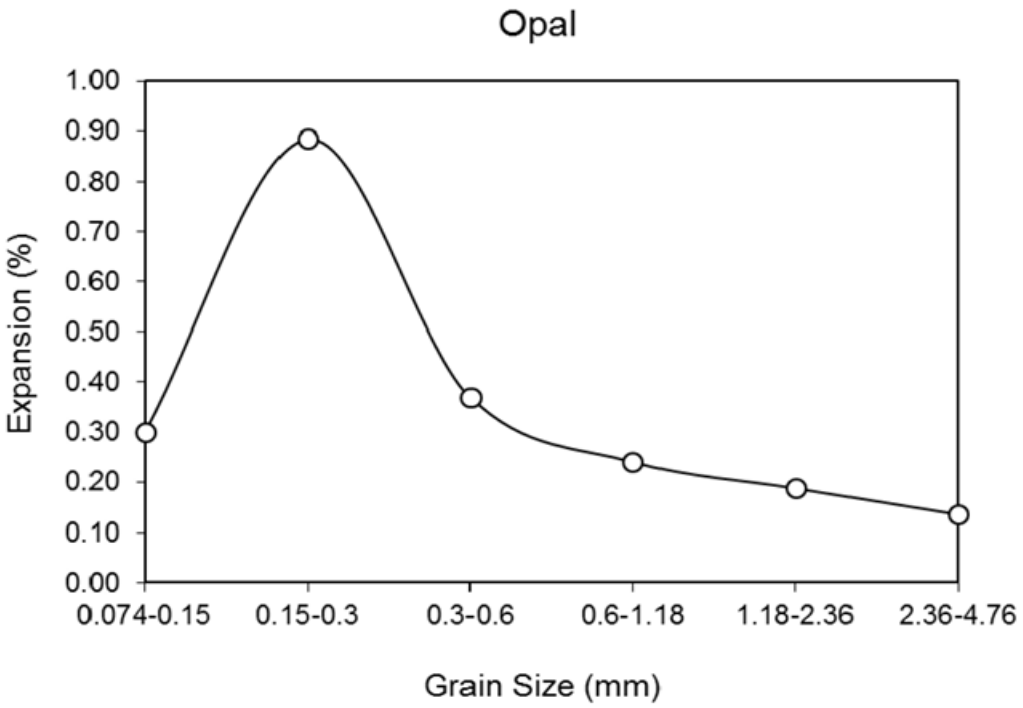

Figure 2.3: The grain size effect of expansion for opal aggregate (Binal, 2015).

2.5 Factors Affecting ASR

Numerous factors have been found to affect ASR, and these factors can be broadly divided into two categories: aggregate-related factors and cement-related factors.

2.5.1 Aggregate-related factors

Among the aggregate-related factors, the reactive silica content of the aggregate is a critical factor in the development of ASR (ACI, 2016). Aggregates with a high reactive silica content are more likely to cause ASR. Other aggregate-related factors that can affect ASR include the size and shape of the aggregate particles and the moisture content of the aggregate. Fine aggregates with a high surface area to volume ratio are more susceptible to ASR than coarse aggregates. Angular and irregularly shaped aggregates are more reactive than rounded aggregates (Diamond S., 1999). High moisture content in the aggregate can also accelerate the reaction, and aggregates stored in damp conditions are more prone to ASR.

2.5.2 Cement-related factors

Cement-related factors that can influence ASR include the cement's alkali content, the concrete's curing conditions, the type of cement used, and the concrete mix design.

Alkalis, such as sodium and potassium, can react with the reactive silica in the aggregate, forming a gel-like substance. Therefore, a high alkali content in the cement can increase the rate of ASR (Mindess and Young, 1981). The curing conditions of the concrete can also affect the rate and extent of ASR. Concrete structures can experience more severe ASR if not adequately cured (Thomas, 2003). The type of cement used can also affect the development of ASR. Cements with high tricalcium aluminate (C_3A) content tend to produce more alkaline solutions, which can accelerate ASR (Neville, 2011). On the other hand, cements with low C_3A and high slag content are less susceptible to ASR (Puertas, 2000). Finally, the mix design of the concrete can also influence ASR. A low water-to-cement ratio and using pozzolanic materials such as fly ash and slag can reduce the risk of ASR (Dhir et al., 1996).

2.6 Symptoms of Alkali-Silica Reaction

As mentioned before, the three conditions needed to start ASR are:
(1) Reactive silica, which exists in the aggregate.
(2) The concentration of alkalis hydroxides ([Na^+, K^+, OH^-]) in the concrete.
(3) Appropriate amount of moisture.
These three conditions help in forming ASR which appears as different types of visual symptoms, such as:

- Cracking
- Expansion causing deformation, relative movement, and displacement.
- Localized crushing of concrete.
- Extrusion of joint (sealant) material.
- Surface pop-outs.
- Surface discoloration and gel exudations (Thomas et al., 2013).

Several variables, including the concrete member's shape or geometry, the surrounding environment, the presence and placement of reinforcement, and the load or stress fields (restraint) placed on the material, might affect the ASR-related cracking pattern. Map cracking, also known as pattern cracking, is a common sign of ASR and appears as randomly oriented cracks on the surface of concrete parts that are primarily uncontrolled and free to move in all directions (Figure 2.4). However, a pattern of cracks displaying a random orientation can also be caused by drying shrinkage, freezing/thawing cycles, and sulfate attacks (Thomas et al., 2013).

Figure 2.4: Severe map-cracking and associated gel staining around cracks in a median (Thomas et al., 2013).

2.7 Mitigating ASR

Mitigating ASR depends on two main methods:

1. Preventing ASR from occurring
2. Using additives to concrete, which divides into two different types:

a) Chemical additives.

b) Mineral additives (supplementary cementitious materials).

The following parts will mention the most popular mitigating and preventing methods.

2.7.1 Preventing formation of ASR

The factors leading to ASR must be eliminated from concrete and mortar production to prevent ASR gel formation. So, the prevention methods can be summarized as:

1. Using non-reactive aggregate.
2. Using cement with low alkali content.
3. There is a low amount of moisture in the surroundings.

As must be noted, these methods cannot be applied to different sites. Often, transporting non-reactive aggregates to construction sites is considered non-economical and cannot be practical. Also, the alkali content in cement cannot always be controlled. Obviously, moisture cannot be controlled on construction sites. For

these reasons, the researchers looked at some other methods that would be more economical and easier to apply. They found out that, in some cases, we cannot prevent ASR gel formation; however, we can limit its effect.

2.7.2 Using additives

Adding two different types of additives into concrete and mortar mitigates ASR. The first type of additive is chemical additives, and the second is mineral additives, also called supplementary cementitious materials (SCMs). Much research has been completed to investigate the advantages and disadvantages of each method. The following chapters will review the effects of chemical and mineral additives on ASR.

2.7.2.1 Chemical additives

According to most studies, out of more than 100 tested chemical compounds, various lithium salts are the only compounds effective in mitigating ASR. Lithium is an alkali metal like sodium and potassium. Consequently, it is paradoxical that lithium compounds are effective ASR suppressants. Although numerous hypotheses have been made, the specific mechanism by which lithium regulates ASR is unknown (Feng et al., 2005). Lithium salts will react with reactive silica like sodium and potassium salts, but the reaction product is an insoluble lithium silicate with little propensity to absorb water and swell. This is the simplest and most widely accepted explanation. Lithium silicate envelops the reactive aggregate particles, shielding them from the alkali hydroxides' attack on the reactive silica underneath (Thomas et al., 2013). The amount of lithium needed to control the expansion was related to two factors: a) the amount of alkalis in the pore solution and b) the aggregate type.

In 1951, McCoy and Caldwell found that the amount of lithium needed to control the expansion is a function of alkalis' content (Na^++ K^+) (McCoy et al., 1951). They concluded that lithium to sodium and potassium ratio must be greater than 0.74. After that, all of the following researchers found the same conclusion. The percentage of (Li/Na+K) depends on various factors such as the form of lithium, the nature of reactive aggregate, and, perhaps, the method of test used (Feng et al., 2005).

The second factor was the type of aggregate used. The effect of aggregate type on the quantity of lithium needed to control expansion owing to ASR has been emphasized by Trembly et al. (2007). Figure 2.5 illustrates the expansion of concrete prisms during two years with 12 different reactive aggregates, one non-reactive aggregate (NF), and

various lithium doses (the standard amount is [Li]/[Na+K] = 0.74. 75% to 100% of the usual dose was sufficient to control expansion (0.040% at two years) for 6 of the 12 aggregates. It was necessary to use 125% to 150% of the usual dose for 3 of the aggregates, but even at 150% of the regular amount, expansion could not be stopped for the other three aggregates (Trembly et al., 2007). Islam and Ghafoori (2016) also got the same results for six types of aggregates. He used AMBT instead of a concrete prism test and compared the six types of aggregates after 14 days of immersion in the pore solution. Figure 2.6 shows the results of expansion for the six different aggregates with six [Li]/[Na+K] ratios. According to the results, the optimum lithium dosages in suppressing the expansion of control mortar bars below the safe limit of 0.10% at 14 days were: 0.74 for the AG-A, AG-B, and AG-D aggregates, 0.89 for the AG-C and AG-E aggregates, and 1.04 for the AG-F aggregate, respectively (Islam and Ghafoori, 2016).

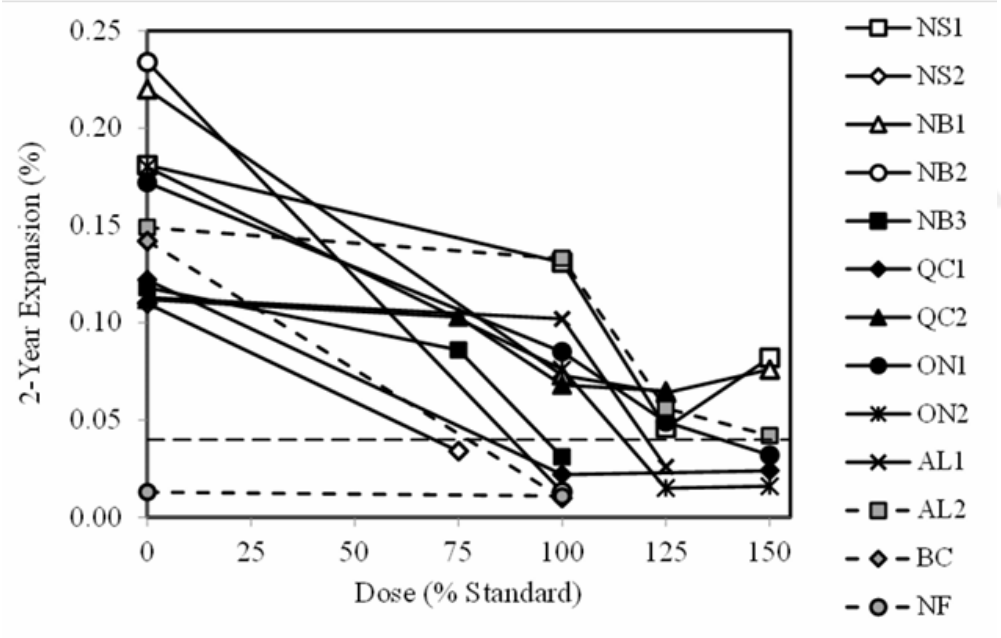

Figure 2.5: Effect of lithium dose on concrete expansion with different reactive aggregates (Trembly et al., 2007).

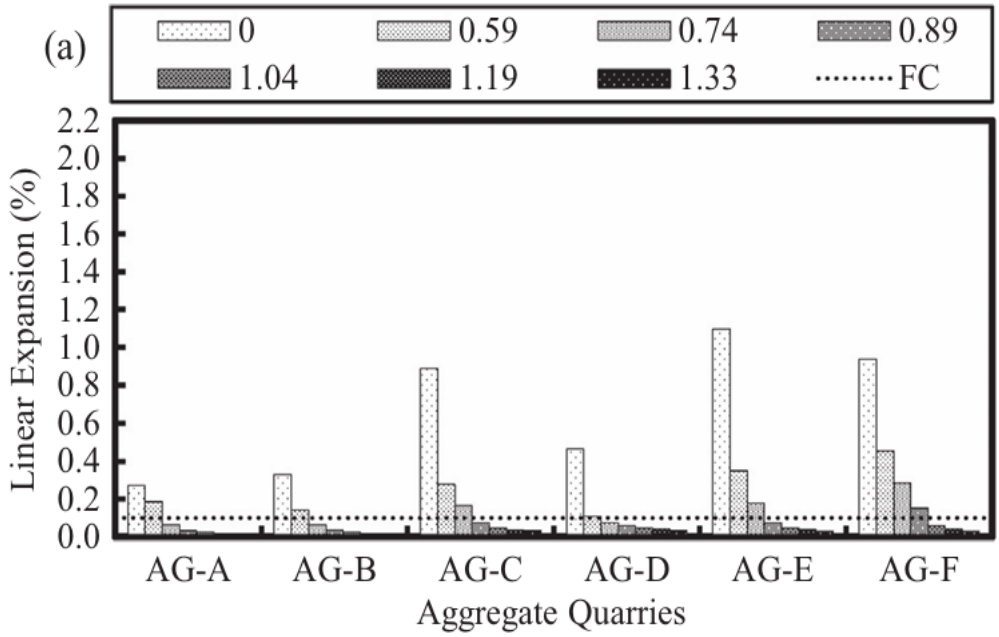

Figure 2.6: The expansions of the mortar bars made with various lithium dosages at 14 days (Islam and Ghafoori, 2016).

2.7.2.2 Supplementary cementitious materials (SCM)

Many methods have been proposed to reduce concrete ASR damage. The most effective and successful strategy for reducing the undesirable effects of ASR is to use supplementary cementitious materials (SCMs) at the proper dose level (Shehata and Thomas, 2002). In previous efforts to successfully control ASR expansion, fly ash, silica fume, ground granulated blast-furnace slag (GGBS), and metakaolin are a few SCMs that have been used in place of Portland cement to some extent (Johnston, 1974). Metakaolin and silica fumes are rarely used due to their high cost. The pore structure of the cement matrix can be improved by the pozzolanic supplementary cementitious materials (SCMs) such as FA and SF. As a result, the diffusivity of alkali ions in concrete is reduced. These SCMs perform a pozzolanic reaction to form C-S-H with a low Ca/Si ratio and a negatively charged C-S-H. Cations, particularly alkali ions, are taken up by the negatively charged C-S-H. It is by this mechanism that pozzolanic SCMs reduce ASR (Thomas, 2011; Monteiro et al., 1997; Aquino et al., 2001). Large, agglomerated SF, on the other hand, has been implicated in ASR as reactive aggregates rather than pozzolanic materials (Maas et al., 2007). In Figure 2.7, we can observe the expansion in concrete after two years, depending on the type and quantity of supplementary cementitious materials (SCM) employed. These tests were conducted in a single laboratory using reactive aggregate from a specific source, namely siliceous limestone from the Spratt quarry in Ontario, Canada. The testing

largely adhered to ASTM C 1293 standards. Among the SCMs, silica fume and metakaolin proved to be the most effective in minimizing expansion over the two years, followed by low-calcium fly ash. On the other hand, slag, high calcium fly ash, and high-alkali fly ash were less effective and required higher replacement levels to keep the expansion below 0.040% after two years. In general, the impact of various SCMs on the expansion of concrete prisms corresponded to their influence on the alkalinity of the pore solution (Thomas, 2011).

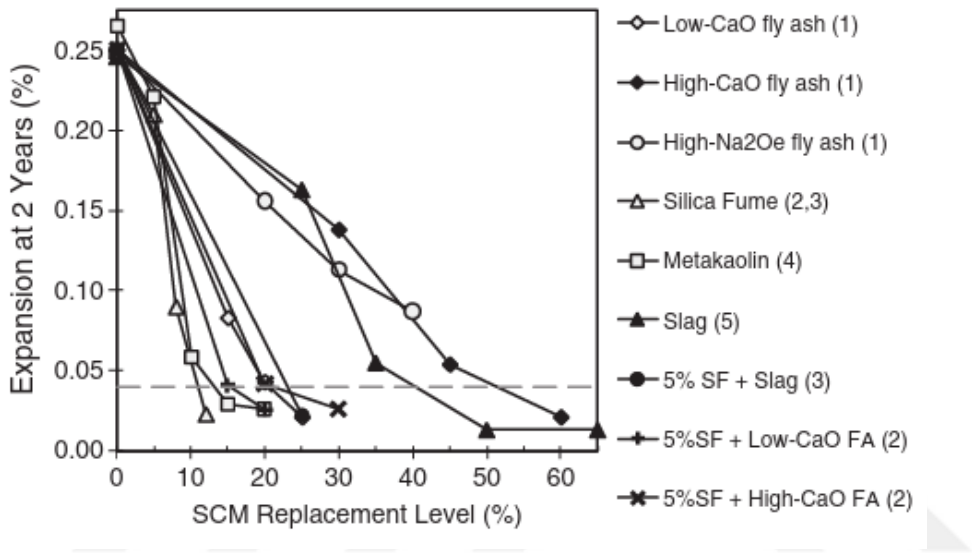

Figure 2.7: Effect of SCMs on the two-year expansion of concrete (Thomas, 2011).

2.7.2.2.1 Fly Ash

One of the most popular SCMs is fly ash because it is an economical option among the other SCMs. The primary mitigation mechanism of using fly ash is because of the pozzolanic reaction, which results in producing C-S-H. According to ASTM C618 (2022), fly ash with low alkali and low calcium is classified as class F, and the one with high alkali and high calcium content is classified as class C. It was found from different studies that the effect of class F fly ash in mitigating ASR is better than class C fly ash (Shehata and Thomas, 2000; Shehata and Thomas, 2006). As a result, the studies focused on the chemical composition of fly ash. Table 2.1 shows the difference between types of fly ash in mitigating ASR with different replacement levels. Observations indicate that using lower proportions of class F fly ash effectively reduces the expansion caused by alkali-silica reaction (ASR) in both the accelerated mortar bar test (AMBT) and concrete prism test (CPT). Per testing standards, the

allowable expansion limits are 0.04% after two years for CPT and 0.01% after 16 days for AMBT (Saha et al., 2018).

Table 2.1: A literature review of using type C and type F fly ashes for mitigating ASR (Saha et al., 2018).

Fly ash type	Test type	Cement replacement level (%)										References
		10	15	20	25	30	35	40	45	50	60	
						Expansion%						
Class F	AMBT	-	-	-	-	0.08	-	-	-	-	-	(Saha and Sarker, 2016)
Class C	CPT	-	-	-	-	0.14	-	-	0.06	-	0.03	(Shehata and Thomas, 2002)
Class F		-	0.08	0.04	-	-	-	-	-	-	-	
Class F	AMBT	0.55	-	0.18	-	0.06	-	-	-	-	-	(Choi and Choi, 2015)
Class C	CPT	-	-	0.123	-	0.10	-	0.068	-	0.042	-	(Shehata and Thomas, 2002)
Class F		-	0.083	0.043	0.03	-	-	-	-	-	-	
Class F	AMBT	-	-	-	-	0.03	-	-	-	-	-	(García et al., 2007)
Class C	AMBT	-	-	-	0.485	-	-	-	-	-	-	(Moser et al., 2010)
Class C	AMBT	-	-	0.41	-	0.38	-	-	-	-	-	(Esteves et al., 2012)
Class F		-	-	0.38	-	0.33	-	-	-	-	-	
Class C	AMBT	-	-	0.23	-	-	0.11	-	-	-	-	(Shon et al., 2004)
Class F		-	-	0.27	-	-	0.10	-	-	-	-	
Class F	AMBT	0.15	-	-	-	0.12	-	-	-	0.07	-	(Awal and Hussin, 1997)

2.7.2.2.2 Silica Fume

Silica fume, a by-product of silicon and ferrosilicon alloy production, has been extensively studied and proven effective in mitigating alkali-silica reaction (ASR) in concrete. Numerous research studies have demonstrated the efficacy of silica fume in mitigating ASR. A study by Shehata and Thomas (2002) investigated the influence of silica fume on ASR in concrete. The results showed that adding silica fume significantly reduced the expansion caused by ASR, leading to improved durability and increased service life of the concrete (Shehata and Thomas, 2002). Silica fume is considered one of the most effective SCMs as it needs a small amount of replacement to control the short- and long-term expansion. It works like any other SCM but in a more effective way. It reduces the number of OH- ions in the pore solution rapidly by comparing it with other SCMs (in the first 28 days), but OH^- ions start to increase slowly with time beyond three months. This behavior is observed only in pastes containing silica fume (not observed for other types of SCMs) (Shehata and Thomas, 2002). Studies show that a small amount of silica fume is enough for controlling ASR (between 3.5 and 7%). It also enhances the durability of concrete by increasing the density and reducing the permeability of concrete and mortar (Thomas and Blezynski, 2001).

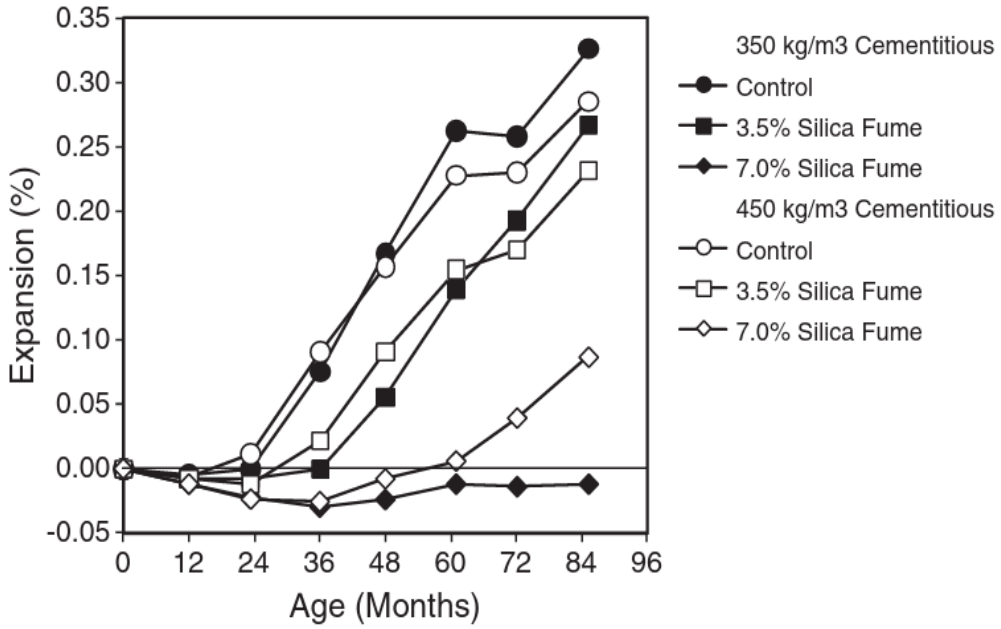

Figure 2.8: Effect of cement alkalis and concrete expansion containing silica fume (Oberholster, 1989).

Figure 2.8 shows the results for different dosages of silica fume in mitigating ASR expansion. Two series of mixes were cast with cementitious content of 350 and 450 kg/m^3. In each series, they substituted part of the Portland cement with 3.5% and 7.0% silica fume by mass. As shown in the figure, 3.5% or 7% of silica fume usage delayed the expansion in all cases. However, only the mixture at the lower cement content with 7% silica fume failed to expand after just over seven years of field exposure. These results clearly show that the efficacy of silica fume in controlling expansion is affected by alkali content. 7% silica fume replacement level appears sufficient to provide long-term prevention of expansion when the "active alkalis" of the mix were just less than 4 kg/m^3 Na_2O_{eq} but not at the higher alkali content of 5 kg/m^3 Na_2O_{eq} (Oberholster, 1989). The unique properties of silica fume, such as its fine particle size and high reactivity, contribute to its ability to fill the pore spaces in concrete and chemically bind with alkalis, thereby reducing the potential for ASR. Furthermore, silica fume enhances concrete's overall strength and durability, making it an excellent strategy for mitigating ASR and improving the long-term performance of concrete structures.

2.7.2.2.3 Ground Granulated Blast-Furnace Slag (GGBFS)

Ground granulated blast-furnace slag (GGBFS), a by-product of the iron and steel industry, has gained significant attention as a supplementary cementitious material for mitigating alkali-silica reaction (ASR) in concrete.

Khan and Sarker (2019) conducted a study to evaluate the effectiveness of GGBFS in reducing ASR expansion in concrete. Their findings demonstrated a noteworthy expansion reduction due to incorporating GGBFS, thereby underscoring its potential as an ASR mitigation strategy. Figure 2.9 shows AMBT's result for mortar bars with GGBFS, fly ash, and a combination of GGBFS and fly ash. The combination of GGBFS and fly ash replaced 100% of OPC. The results showed a reduction in expansion at 28 days from 0.6 to 0.35%. The combination of GGBFS and fly ash showed more effective results. AAM2 mortar bars represent a replacement of cement with 80% GGBFS and 20% fly ash and showed more mitigation in expansion with about 0.25%. With the same sequence, increasing fly ash more than GGBFS showed more effective results in mitigating ASR. As a result, GGBFS showed a mitigation effect of ASR but was still less effective than fly ash. Similarly, Nausherwan (2020) studied the influence of GGBFS proportions on ASR mitigation. The study highlighted

the ability of GGBFS to curtail ASR expansion and enhance overall concrete performance and durability. Moreover, it elucidated the role of GGBFS in impeding the availability of alkalis for ASR by forming stable compounds and inhibiting the reaction.

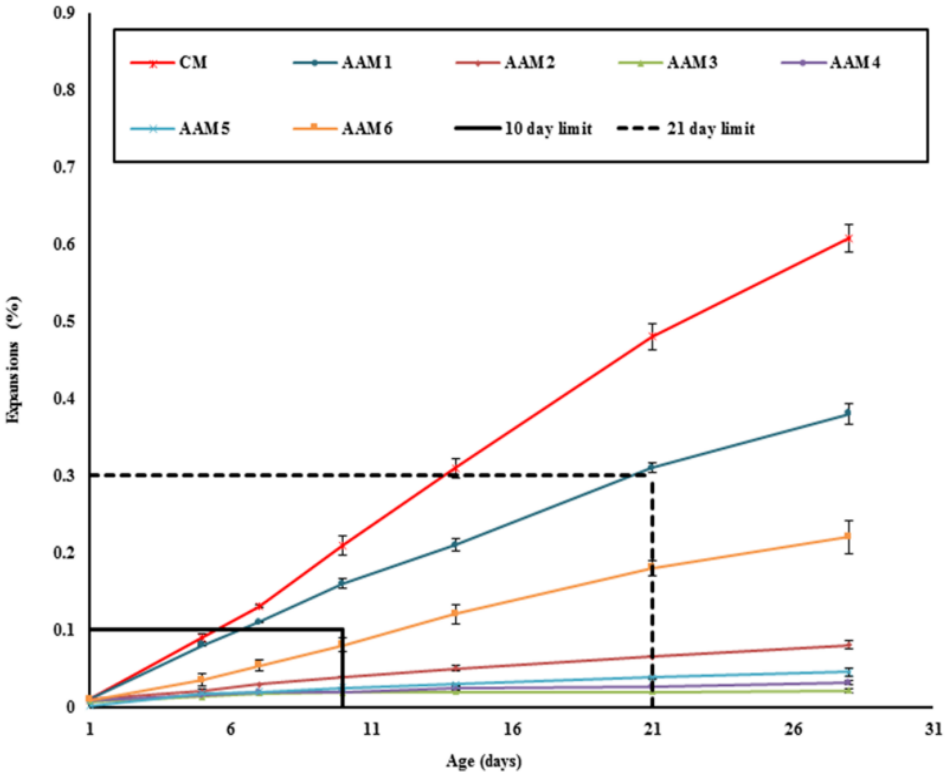

Figure 2.9: ASR expansion in mortars with GGBFS and fly ash (Sarker, 2019).

The collective body of research, including these seminal studies, substantiates the effectiveness of GGBFS in mitigating ASR in concrete. Incorporating GGBFS as a supplementary cementitious material diminishes the potential for ASR expansion and enhances concrete structures' strength, durability, and long-term performance.

2.8 Waste glass powder (WGP)

Nowadays, waste glass is one of the most common solid waste materials around the globe, imposing a substantial environmental problem and thereby needing an urgent solution. Because of that, many researchers turned to recycling waste powder to reuse it in other industries. Waste glass can be used as an aggregate and cementitious replacement in construction.

2.8.1 Using waste glass as an aggregate

Early attempts at using waste glass in concrete focused on using it as coarse aggregates. Several challenges faced this usage in terms of constitutional strength and durability. These early trials were unsuccessful because of ASR due to amorphous glass powder particles—also, bottle glass limits waste glass particles' size and shape. Using bottle glass limits the size and shape of WG's particles, as the maximum size of the particles cannot be more significant than the thickness of the bottle. Another source of aggregate is crushed waste bottles. They tend to produce massive, flat, elongated aggregates that may negatively affect workability and have been linked to decreases in compressive strength (Johnston, 1974; Topcu, 2004). Another challenge is the contamination and uniformity of glass waste. Most shattered and mixed-color waste glass that cannot be recycled results in diversity in the material's chemical composition. Paper and plastic labels, caps and corks, and sugars left over from the bottles' original use and contents could all cause contamination (Phillips, 1972). In addition, seasonal variations in the waste stream should be anticipated. To overcome these challenges, many chemical and mechanical treatments are done. One of these treatments was crushing waste glass into powder, which opened a light in its pozzolanic reaction. As a result, the ASR also decreased.

2.8.2 Using waste glass in powder form

Waste glass powder mitigates the alkali-silica reaction depending on particle size. WGP can conduct a pozzolanic reaction and dissolve entirely. Figure 2.10 shows the relationship between the particle size of glass powder and mitigating ASR. The bigger the glass particle size, the more expansive the gel formed, even for different contents of glass powder (Liu et al., 2015). The mechanism by which glass powder can mitigate ASR is still under investigation. Some studies presented theories on how glass powder mitigates ASR (Idir et al., 2011; Pereira-de-Oliveira, 2012). The effect of glass powder depends on some physical properties and chemical composition. Physical properties mainly depend on particle size and particle distribution of the glass powder used. Less particle size gives more pozzolanic reaction because of a larger surface area. Regarding chemical composition, glass powder exhibits behavior similar to supplementary cementitious materials (SCMs) despite their distinct chemical

compositions. The main chemical element of glass powder is silica (Si), and different proportions of other elements, such as Na and Ca, with small ratios of Al and K.

Additionally, WGP has a higher level of Ca^{2+}, which is released for pozzolanic reactions and consumed in hydrated products (Shayan and Aimin, 2006). As a result, there may not be enough SiO_2 to produce ASR gel, so the expansion and swelling resulting from ASR will be mitigated. WGP particles surrounding the reactive aggregate dissolve when exposed to water, producing a pozzolanic process that creates C-S-H gel. These small C-S-H gel particles then undergo a second reaction with SiO_2 in glass to produce C-S-H gel with a low Ca/Si ratio.

The ASR expansion rate can also be controlled at safe levels when the WGP content is 10%, 20%, and 30%, with average particle sizes less than 8.2, 16.95, and 144.08 µm, respectively, according to Liu et al. (2015).

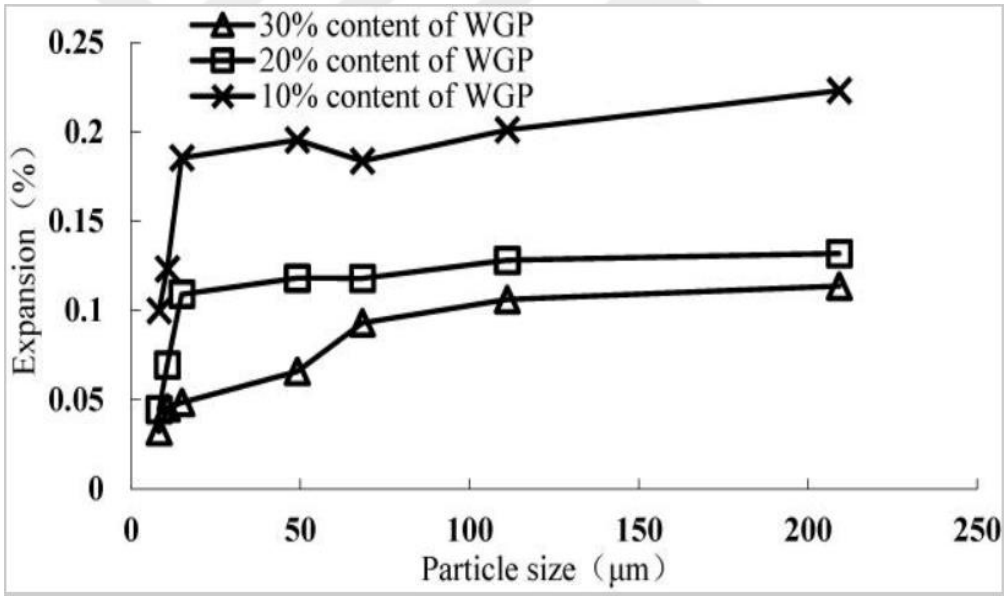

Figure 2.10: ASR expansion of the mortars containing WGPs with different particle sizes (Liu et al., 2015).

Fanijo et. al. (2021) studied WGP as an SCM and compared it with silica fume and slag. WGP was examined as a binary and ternary replacement, and AMBT was applied to investigate ASR mitigation (Fanijo et al., 2021). Figures from 2.11 to 2.14 show the relationships between expansion in mortar bars and WGP content, silica fume (SF) content, slag content (S), and ternary mixtures of WGP, SF and S. The particle size for WGP and SF was 10 µm. They examined how glass powder, slag, and silica fume

affect the ASR expansion in mortar and concrete glass aggregate mixtures. They used two testing methods to assess their effectiveness: AMBT and miniature concrete prism test (MCPT). Among the tested materials, only the mixture with 30% glass powder replacement successfully controlled ASR expansion in both mortar and concrete samples, meeting specified limits. The research attributes this success to reduced Calcium Hydroxide (CH) consumption, resulting in minimal alkali discharge from cementitious materials and the high alkali-binding ability of the glass powder-containing mixture (Fanijo et al., 2021).

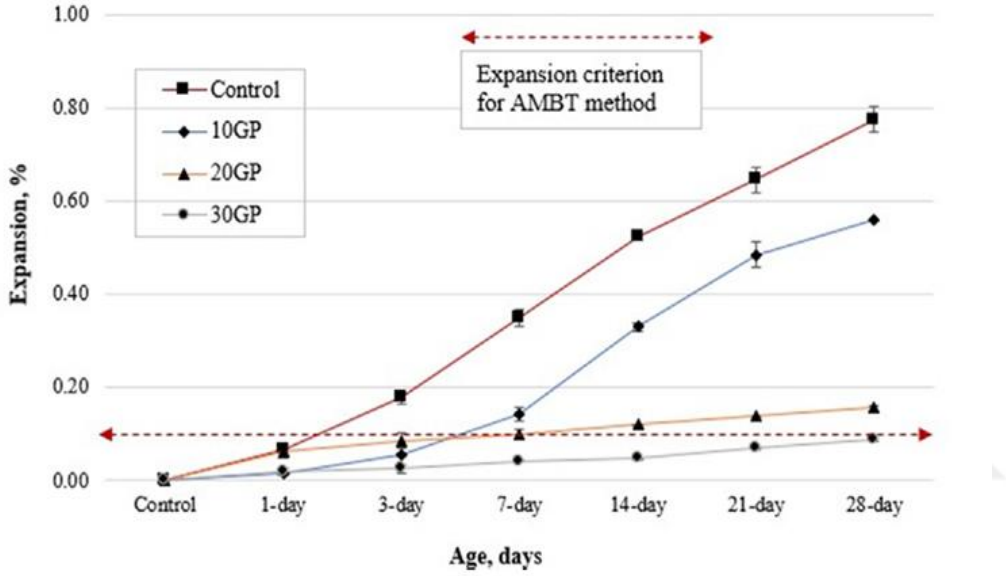

Figure 2.11: Expansion behavior of mortar bar containing glass powder GP (Fanijo et al., 2021).

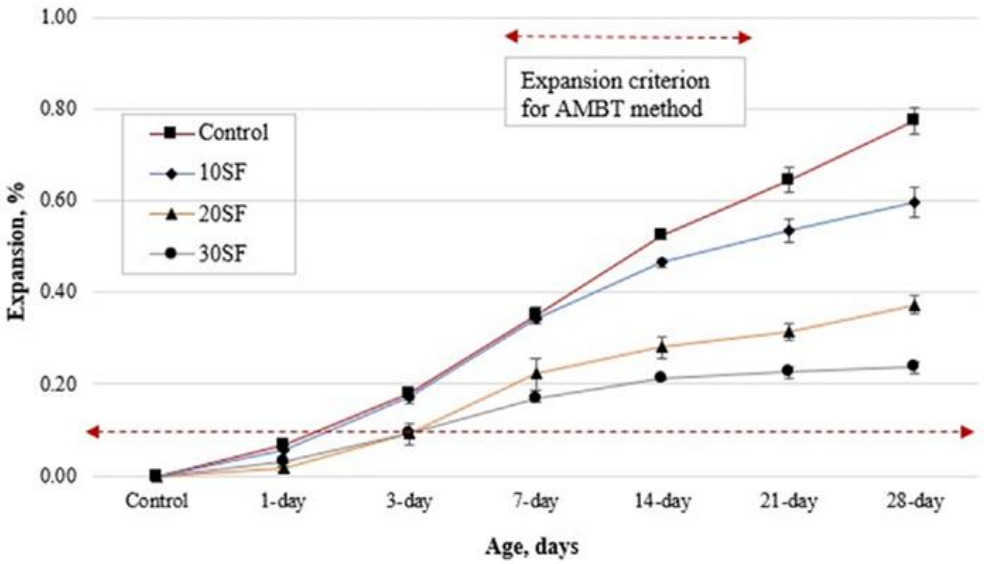

Figure 2.12: Expansion behavior of mortar bar containing silica fume (Fanijo et al., 2021).

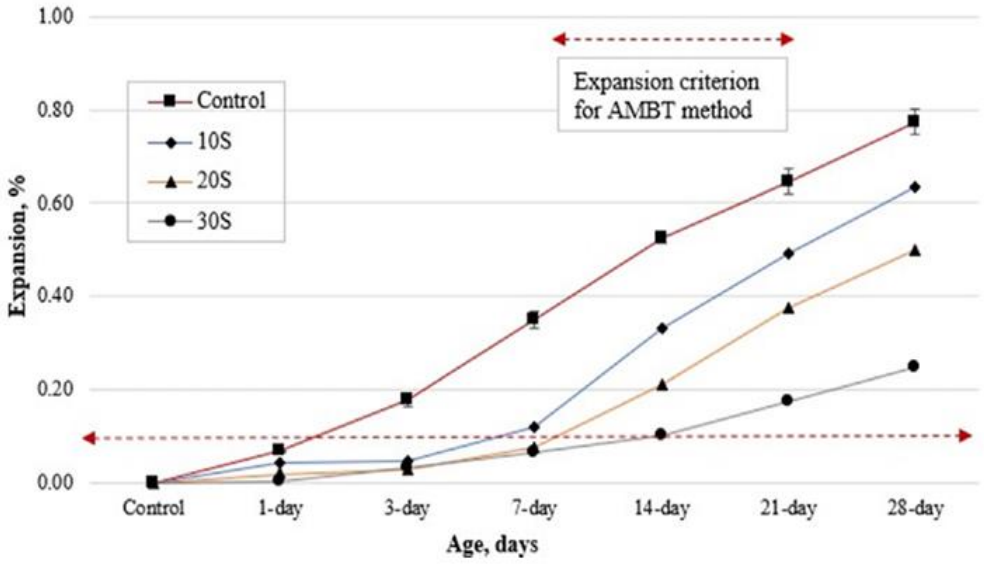

Figure 2.13: Expansion behavior of mortar bar containing slag (Fanijo et al., 2021).

Figure 2.14 shows the effect of ternary replacement on mitigating ASR. Even ternary replacement is not as effective as WGP in mitigating ASR. The most effective mixture was 10% slag and 20% WGP (10S20G) reduced the expansion up to 0.11% at 14 days, followed by 15S15G, 10SF10G, 15SF15G, 10SF20G, and control.

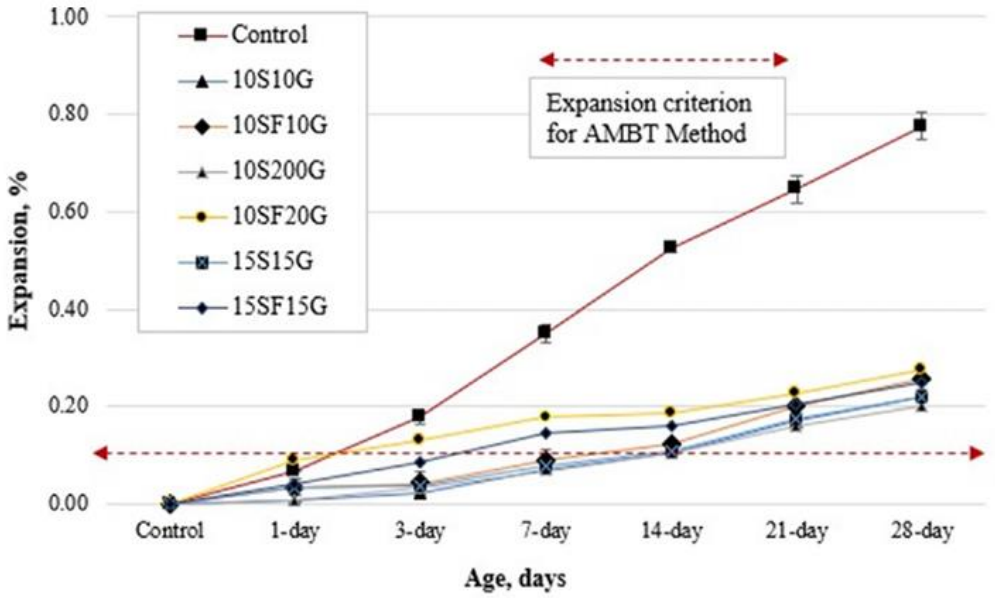

Figure 2.14: Mitigation behavior of mortar bar with ternary mixtures (Fanijo et al., 2021).

Ke et al. (2018) concluded that glass particles smaller than 300 μm reduce ASR expansion effectively. However, a more than 300 μm particle size may increase ASR expansion at 30% of WGP content. The study by Ke et al. (2018) shows that the alkalis (Na^+ and K^+) level utilized in the ASR pore solution was higher in the control mixture than in glass powder mixtures. This is because the C-S-H gel of the control mix reacts rapidly with SiO_2, resulting in more ASR ring formation. At the same time, the fine particles of glass powder dissipate a higher percentage of calcium (Ca^{2+}) in both pozzolanic reaction and hydration products, causing the insufficient presence of reactive SiO_2 to form the ASR gel (Ke et al., 2018).

2.8.3 Effect of waste glass powder on mechanical properties of concrete and mortar

Some studies show that using WGP in cementitious materials such as concrete and mortar decreases the early age strength (Aliabdo et al., 2016). This decrease is attributed to the presence of phosphorous (P) and zinc (Zn) as retarders (Stephan, 1999; Bénard, 2005). We can avoid this retarding in hydration using finer particles of glass powder (< 41 μm), which lead to more surface area and, then, leads to a faster hydration process (Idir et al., 2011). Figure 2.15 shows the effect of waste glass powder as a cementitious replacement on compressive strength at early ages (3 and 7 days).

As shown in the figure, the compressive strength increased slightly at 5 and 10% of WGP content and started decreasing with the increase of WGP content.

Similar results were found by Li et al. (2022), as shown in Figure 2.16. The increase in the WGP content seemed to decrease the compressive strength at 7, 28, and 90 days, respectively (Li et al., 2022).

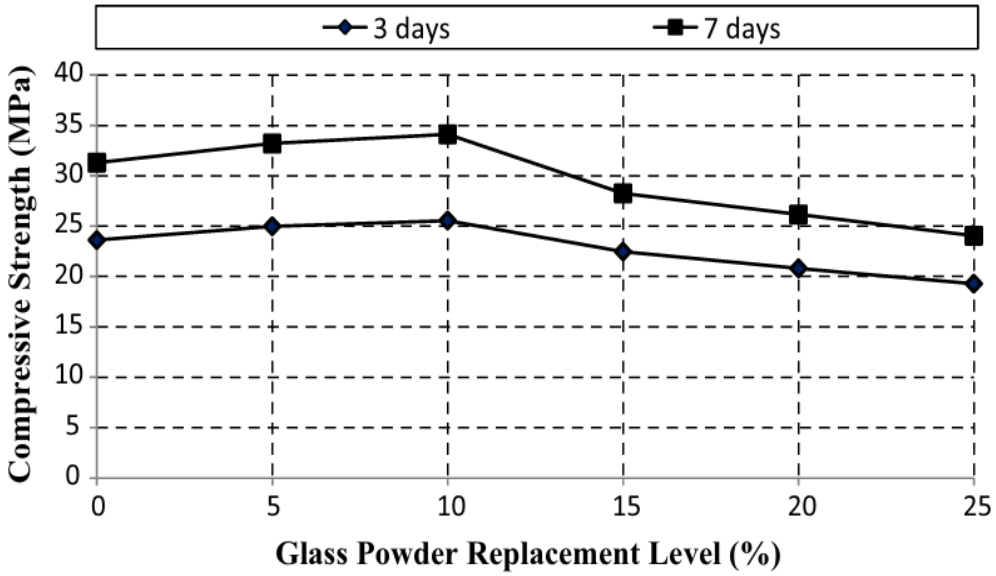

Figure 2.15: Effect of glass powder as cement replacement on compressive strength of mortars (Aliabdo et al., 2016).

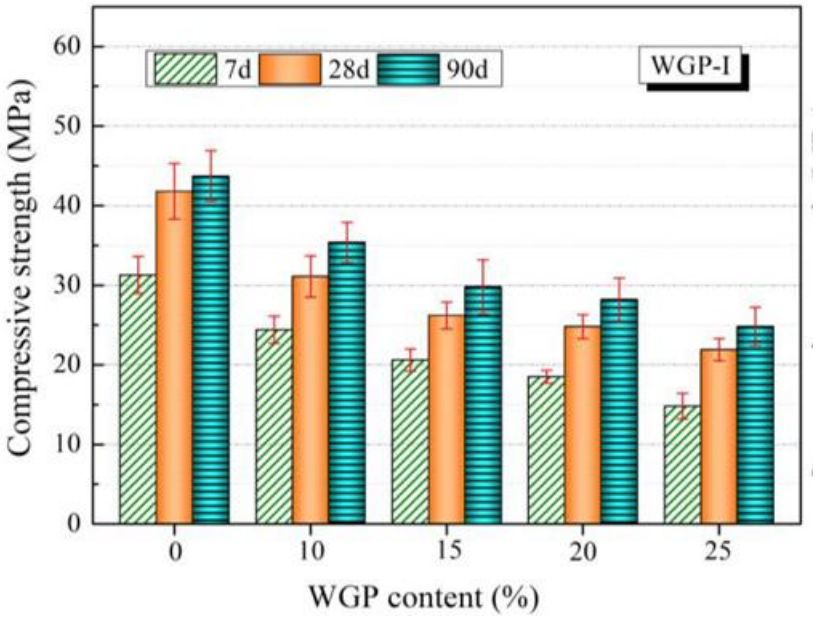

Figure 2.16: Compressive strength development for different WGP content at 7, 28, and 90 days (Li et al., 2022).

Flexural strength seems to follow the same trend as compressive strength. Figure 2.17 shows the development of flexural strength and compressive strength at the same time. Shoaeia et al. (2020) compared adding GP and alkali-activated slag (AAS) in mortars. AAS, produced using ground granulated blast furnace slag (GGBFS), gives almost the same compressive and flexural strength reduction ratio as GP. However, adding 20% of GP seems to increase flexural and compressive strength, possibly due to a sufficient C-S-H formation. Also, similar increases were seen in AAS at 30% replacement (Shoaeia et al., 2020).

Generally, WGP‘s pozzolanic reaction increases with time, and the reduction in strength decreases. Patel et al. (2019) compared the compressive strength of the mortars with and without WGP at 7 and 28 days. A 9% reduction for WGP with 75 μm particle size (WGP75) and a 3% reduction for WGP with 63 μm particle size (WGP63) were observed when the cement replacement ratio was 5%. However, at a 20% replacement level, the reductions increased to 16% for WGP75 and WGP63 mixes. This higher reduction could be attributed to the filler effect of glass powder during this period, along with differences in particle size ratios (Patel et al., 2019). The glass powder-modified mortar exhibited positive outcomes when we looked at the results of extended curing periods and substitution percentages (7 to 90 days). For instance, with a 20% substitution, the rate of compressive strength development at 90 days was only 6% lower than that of the control mix for WGP75, and it was nearly equal to the control mix for WGP63 (Patel et al., 2019). This improvement in strength suggests that the pozzolanic reaction may occur in later stages, the mortar's pozzolanic behavior becoming more prominent with time and contributing to forming a denser microstructure in the mortar. In summary, WGP’s pozzolanic effect becomes more and more noticeable at later ages (Patel et al., 2019).

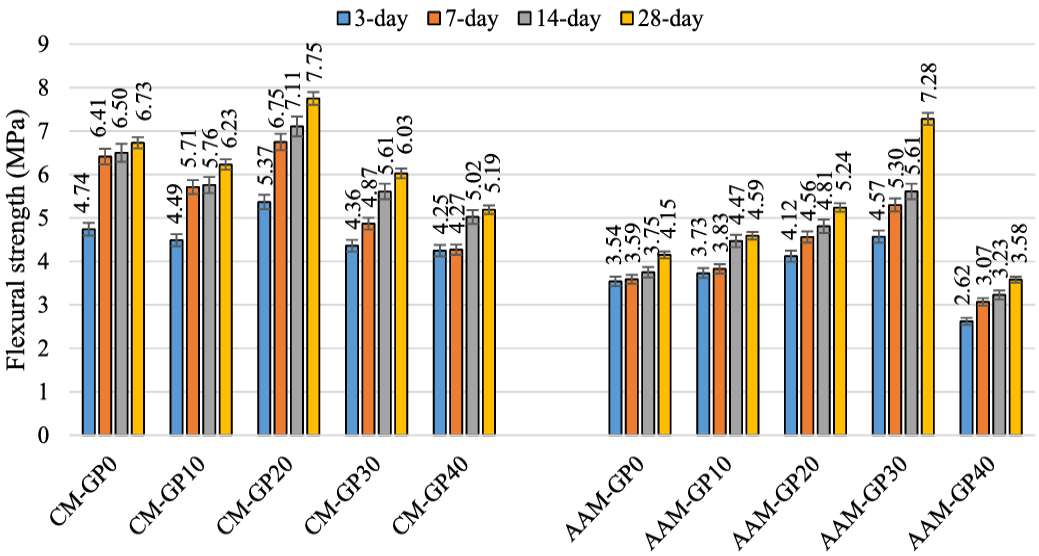

(a)

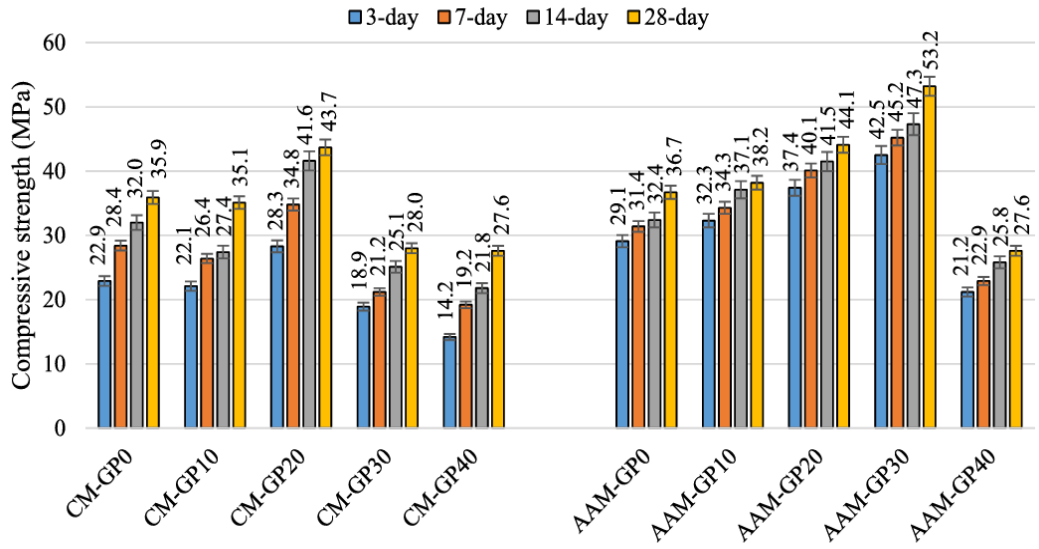

(b)

Figure 2.17: Compressive and flexural strength of mortar with WGP at different ages a) Flexural strength, b) Compressive strength (Shoaeia et al., 2020).

On the other hand, some results showed an increase in compressive and flexural strength with adding GP, as shown in Figures 2.18 a) and b). This contribution in compressive and flexural strength was explained by Parghi et al. (2016) with the higher silica and aluminum dissolution, which led to a better pozzolanic reaction. Also, GP can work as a filling material in voids available between a cement matrix and fine aggregates' interface (Parghi et al., 2016).

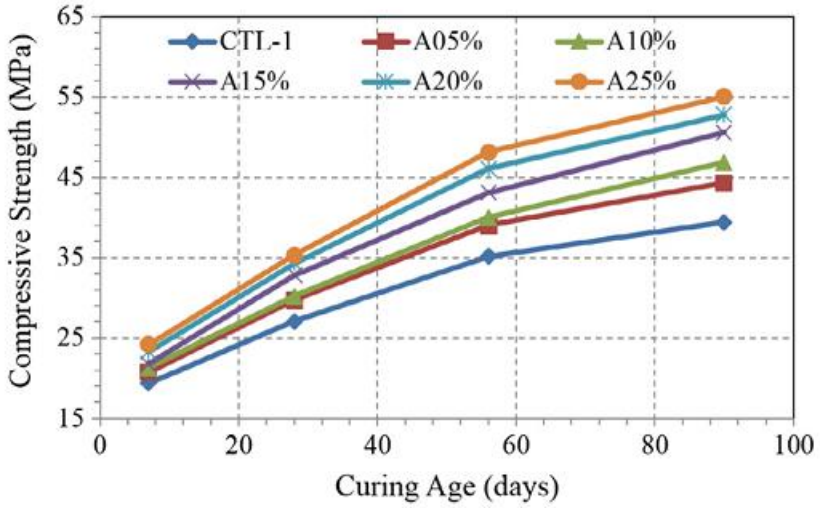

(a)

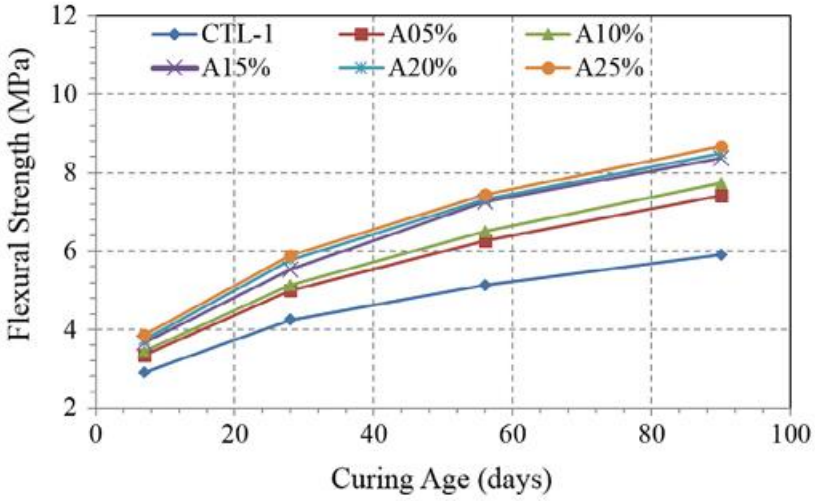

(b)

Figure 2.18: Compressive and flexural strength development of recycled glass powder as a cementitious replacement a) compressive strength, b) flexural strength (Paraghi and Alam, 2016).

Most research used WGP as a cementitious replacement, proving that GP harms mechanical properties. As a result, some studies try to add SCMs and nanoparticles to WGP (Cai et al., 2019; Shoaeia et al., 2020). Although the pozzolanic reaction of WGP and nano-silica can reduce ASR, several studies also found that alkalinity in the pore solution did not decrease with time, particularly at early ages (Zheng, 2016; Guo et al., 2018). Due to the significant alkali release from the reacting glass, the pozzolanic reaction of WGP enhanced the pore solution's alkali content (Idir et al., 2010). The findings demonstrated that NS addition can increase the initial pH value of cement pastes due to the accelerated effect of NS on the dissolution of cement particles (Shayan and Aimin, 2006). However, there was no significant pH value reduction at a

later stage due to the relatively lower level of pozzolanic reaction. After 15 hours of cement hydration, an increase in Ca^{2+} concentration in the pore solution of the C_3S incorporating NS paste started again and gradually got close to that of the pure C_3S paste (Singh et al. 2016).

Idir et al. (2010) suggested that adding WGP mitigates ASR due to the slowed-down dissolution of silica from reactive aggregates by increasing aluminum concentration in the pore solution. However, it is still unknown why WGP can reduce ASR. The process by which NS can improve the strength has not been examined thoroughly. Incorporating NS up to 4% in concrete does not affect ASR but may benefit early strength and mechanical properties.

2.8.4 Effect of waste glass powder on workability

Several studies investigated the effect of WGP on the properties of fresh mortar (Paraghi and Alam, 2016; Fanijo et al., 2021). Paraghi and Alam (2016) concluded that using WGP in mortar and concrete can reduce the workability of the mixture. Figure 2.19 shows the relationship of the flowability with the different replacement levels of recycled glass powder (RGP) in various mixes. Series A expresses adding only RGP, while series B to D expresses adding RGP to FA, FA + SF, and FA + SF + styrene butadiene rubber (SBR), respectively. In all series, including series A, adding RGP reduces the workability of mortar. We can say that the more glass powder there is, the drier the mixture.

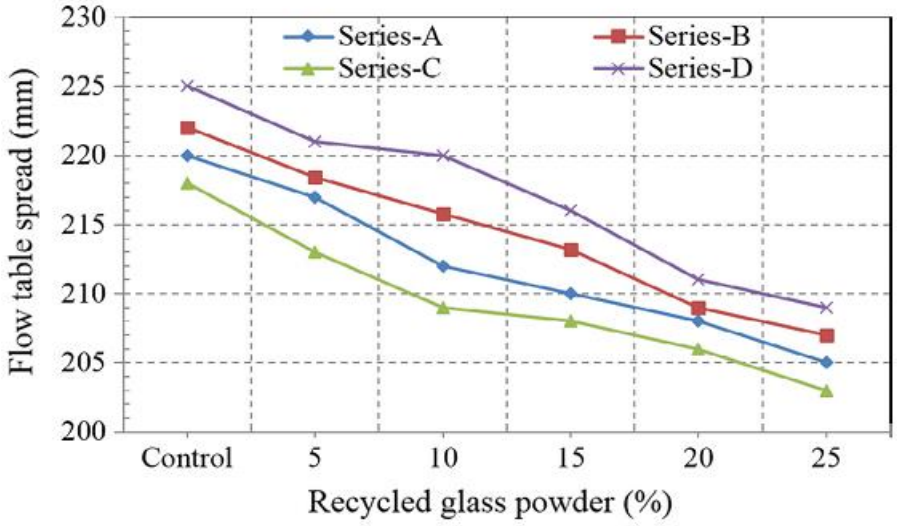

Figure 2.19: Flow table spread value of recycled glass mortar (Paraghi and Alam, 2016).

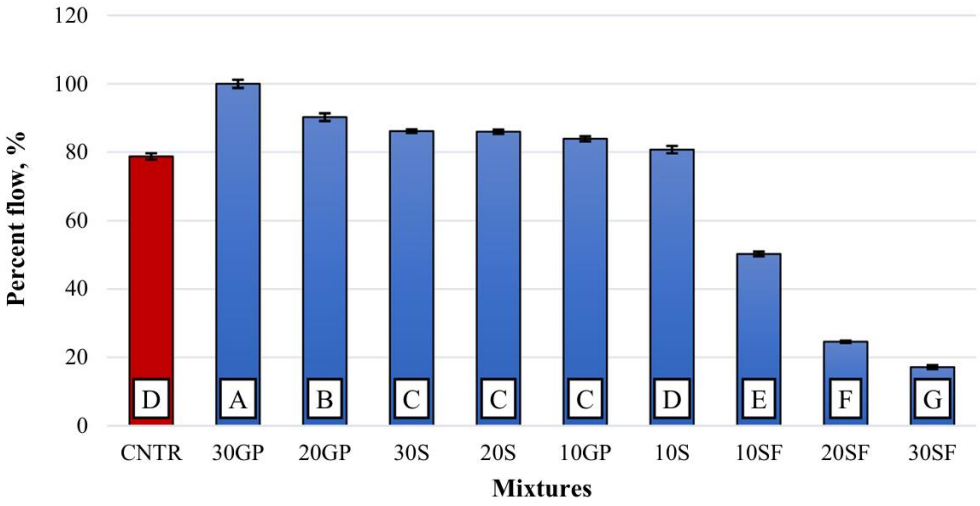

Figure 2.20: Flow percentage of mortar samples at binary replacement (Fanijo et al., 2021).

Figure 2.20 also presents workability results as a flow percentage of mortar samples at binary replacement. It shows increases in the flowability of mortars with 10, 20, and 30% WGP replacements. In comparison with other SCMs, WGP presents a more workable mixture and even more than the control specimen. These results contradict other studies, such as Paraghi and Alam (2016).

2.9 Effect of nano silica on concrete and mortar

2.9.1 Effect of NS on workability

A lot of studies have investigated the effect of nano silica on workability. Most studies show that using nano-silica in concrete reduces workability (Kumar et al., 2019; Ghafari et al., 2014; Nattaj and Nematzadeh, 2017). Due to the high surface area of the NS particles and the unsaturated bonds in NS, a portion of the mixing water (water molecules) attracts towards the surface of NS particles and thus produces silanol (Si-OH) groups (Mukharjee and Barai, 2020). However, some studies have reported increased workability with adding nano-silica (Elkady et al., 2013). They claimed that the agglomeration effect is the most significant disadvantage of using nano-silica. This effect makes nano silica's particles agglomerate in specific points, resulting in some free water appearing between particles. That was the reason for the reduced workability and fluctuating results in some mechanical properties. Various techniques have been proposed to overcome the agglomeration effect, including using surfactants

and sonication by Elkady et al. (2013). The fluctuating results in other studies may be attributed to the particle size and dosage of nano silica used.

Another limitation of using nano-silica in concrete is its potential to increase brittleness, which can reduce the toughness and ductility of the concrete (Turkmenoglu et al., 2022). However, nano silica's effect on concrete's brittleness is still under debate, and further research is needed to understand this phenomenon fully.

2.9.2 Effect of NS on mechanical properties of concrete and mortar

Using glass powder shows that it reduces the compressive strength of the concrete because of retarding the hydration resulting from adding more SiO_2 to the solution rather than Ca, unlike OPC. Also, adding glass powder produces C-S-H with low Ca/Si, which is one reason for reducing the compressive strength. To overcome this reduction, nano-silica can be used together with glass powder.

In recent years, nano-silica use in concrete has gained increasing attention due to its unique properties and potential benefits for concrete performance. Many studies tested the effect of using nano silica on the mechanical properties of concrete (Yu et al., 2014; Mukharjee and Barai, 2014; Chithra et al., 2016). Abhilash et al. (2021) conducted a comprehensive review of the effect of nano-silica on concrete, highlighting its potential benefits and limitations. According to their thinking, most studies concluded that using nano-silica in concrete between 1 and 4% can improve mechanical properties, especially at an early age (Yu et al., 2014; Chithra et al., 2016). It was shown that adding nano-silica could significantly improve concrete's compressive strength, flexural strength, and tensile strength (Nigam and Verma, 2023; Yu et al., 2014). The reasons for this improvement are its higher pozzolanic activity and large surface area, which improves the permeability of concrete. NS's pozzolanic reaction is higher than that of silica fume and the other SCMs. NS reacted with CH crystals to reduce their size and amount, resulting in a denser Interfacial Transition Zone (ITZ) microstructure between aggregates and cement paste, resulting in long-term strength development in concrete and durability (Abhilash et al., 2021). Figure 2.21 shows the effect of NS's content on flexural and compressive strength at 3, 7, and 28 days for ultra-high performance concrete (UHPC). It is noticed that the development of flexural and compressive strength took the parabolic trend of increasing up to 4%, and it decreased slightly with more NS content (Yu et al., 2014).

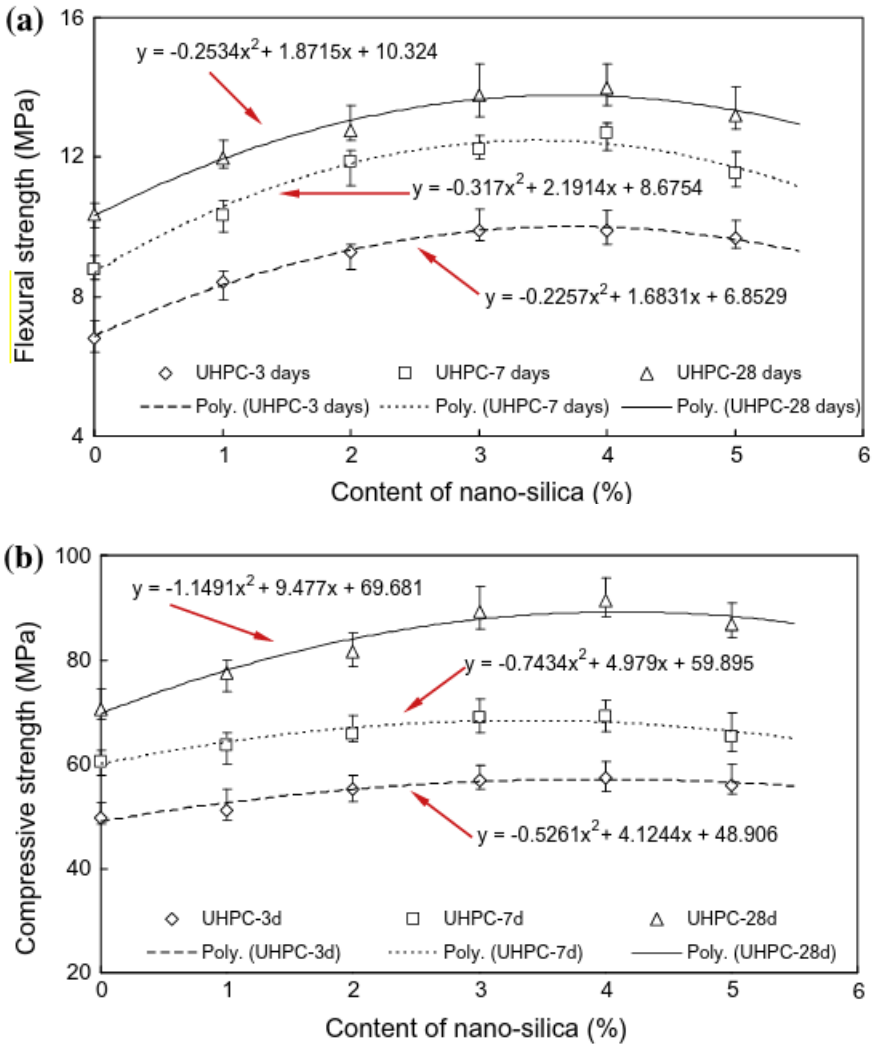

Figure 2.21: Variation of (a) flexural strength and (b) compressive strength of UHPC (Yu et al., 2014).

In addition to enhancing mechanical properties, NS can also improve the durability of concrete. The addition of NS has been shown to increase the resistance of concrete to chemical attack, freeze-thaw cycles, and carbonation (Zhaol, et al., 2021). The improved durability is attributed to the reduced porosity and permeability of concrete, which results from the pozzolanic reaction of nano-silica with the calcium hydroxide produced during cement hydration (Ke et al., 2018).

2.10 Test Methods to Determine ASR

Many test methods have been proposed to determine ASR using different procedures. Comparisons between several techniques used for testing ASR can be seen in Table 2.2.

Table 2.2: Comparison of different methods for assessing ASR for mortars (combination of aggregate and cement) and aggregates.

Test Method	Standard	Procedure	Duration
Mortar bar tests	ASTM C1260	Used to detect the potential deleterious alkali reactivity of an aggregate source. The test involves placing specially prepared mortar bar specimens in a high-alkaline solution bath at a temperature of 80 °C (176 °F) for 14 days. The length is measured over time, and the potential reactivity is determined based on the level of expansion	14 days
	ASTM C1567	Used to detect the potential for harmful alkali-silica reactions of combinations of cementitious materials and aggregate in mortar bars. The test involves placing specially prepared mortar beam specimens in a high alkaline solution bath at a temperature of 80 °C (176 °F) for 16 days. The length is measured over time, and the potential reactivity is determined based on the level of expansion.	16 days
	ASTM C441	They are used to evaluate the effectiveness of pozzolans or GGBSF in preventing excessive concrete expansion due to ASR. The test may be used as a preliminary or screening test to assess the relative effectiveness of different materials being considered to prevent excessive expansion due to alkali-silica reactions. It may also be used to evaluate materials proposed for use on a particular job to avoid excessive expansion due to alkali-silica reactions by testing them with the cement or cement used on the job.	N/A
	ASTM C227	Used to determine the susceptibility of cement-aggregate combinations to expansive reactions involving hydroxyl ions associated with the alkalis by measurement of the increase (or decrease) in the length of mortar bars containing the combination during storage under prescribed conditions of the test.	N/A

Table 2.2 (Cont.): Comparison of different methods for assessing ASR for mortars (combination of aggregate and cement) and aggregates.

Test Method	Standard	Procedure	Duration
Concrete prism test	ASTM C1293	Used to evaluate the potential of an aggregate or combination of an aggregate with pozzolan or slag to expand deleteriously due to any form of ASR. It involves measuring the length change of concrete specimens due to alkali-silica reaction over some time.	1 to 2 years
Petrography test	ASTM C856	Used to perform petrographic examination of hardened concrete samples. The samples examined may be taken from concrete constructions, concrete products or portions thereof, or concrete or mortar specimens exposed to natural environments or simulated service conditions or subjected to laboratory tests.	N/A
	ASTM C295	Used to perform petrographic examination of aggregates for concrete. The guide outlines procedures for the petrographic examination of samples representative of materials proposed for use as aggregates in cementitious mixtures or raw materials for producing such aggregates. I couldn't find any information about the duration of this guide.	N/A
Chemical test	ASTM C289	Used to determine the potential reactivity of an aggregate with alkalis in Portland-cement concrete as indicated by the amount of reaction during 24 hours at 80°C between 1 N sodium hydroxide solution and aggregate that has been crushed and sieved to pass a 300-µm sieve and be retained on a 150-µm sieve.	24 hours

In this study, ASTM C1576 is used to measure the reactivity of used sand, and the expansion formation resulted in a control specimen using accelerated mortar bar test AMBT. The Accelerated Mortar Bar Test (AMBT) is a rapid method used to assess the reactivity of aggregates, particularly in the context of alkali-silica reaction (ASR). This test is used in almost all studies investigating ASR as it gives accepted results relatively quickly. The AMBT provides results within a relatively short testing duration, making it a practical choice for assessing aggregate reactivity. It allows for the early identification of potentially deleterious ASR in combinations of cementitious materials and aggregates, providing a timely warning. Despite its speed, the AMBT's reliability is a concern. It may not always accurately predict long-term ASR behavior. While the AMBT is quick, the Concrete Prism Test (CPT) is considered more accurate for determining potential aggregate reactivity, but AMBT is still acceptable in determining the reactivity of aggregates.

In this study, the expansion in the control specimen to the other specimens with WGP and nano silica was compared to investigate their effect on mitigating ASR gel formation.

3. TESTING PROCEDURES

3.1 Introduction

This study used WGP and NS as cementitious replacements to mitigate ASR. The ratios of glass powder replacement were 10%, 15%, 20%, and 25% of cement weight. At the same time, the percentages of nano silica were 1%, 1.5%, and 2%. That makes 20 different combinations, as shown in Table 3.1.

A list of performed tests in this study is given below:

- Accelerated mortar bar test. (AMBT) according to ASTM C1576.
- 3-point flexural strength test according to EN 196-1.
- Compressive strength test according to EN 196-1.
- Capillary water absorption test according to ASTM C1585.
- Scanning electronic microscope (SEM).
- Thermogravimetric Analysis (TGA).

Table 3.1: Combinations used in the study.

Control	0%GP 1%NS	0%GP 1.5%NS	0%GP 2%NS
10%GP 0%NS	10%GP 1%NS	10%GP 1.5%NS	10%GP 2%NS
15%GP 0%NS	15%GP 1%NS	15%GP 1.5%NS	15%GP 2%NS
20%GP 0%NS	20%GP 1%NS	20%GP 1.5%NS	20%GP 2%NS
25%GP 0%NS	25%GP 1%NS	25%GP 1.5%NS	25%GP 2%NS

3.2 Materials

3.2.1 Fine aggregate (sand)

The sand used in this study was examined once before in terms of causing expansions under severe AMBT conditions. It was found that this sand was the resource of reactive silica. Figure 3.1 shows that the expansion in mortar bar produced using this sand has an average expansion of 0.35% at 14 days. According to ASTM C 1778, if mortar bars in this test expand less than 0.10% after 14 days' immersion, the aggregate is usually

considered non-reactive. If the mortar bars expand 0.10% to 0.30%, they are classified as moderately reactive, 0.30% to 0.45% highly reactive, and more than 0.45% highly reactive. Therefore, the sand used in this study can be considered a highly reactive aggregate. The specific gravity of the sand was found to be 2.69 g/cm^3. The sieve analysis was applied to this sand to determine the particle size distribution (Figure 3.2).

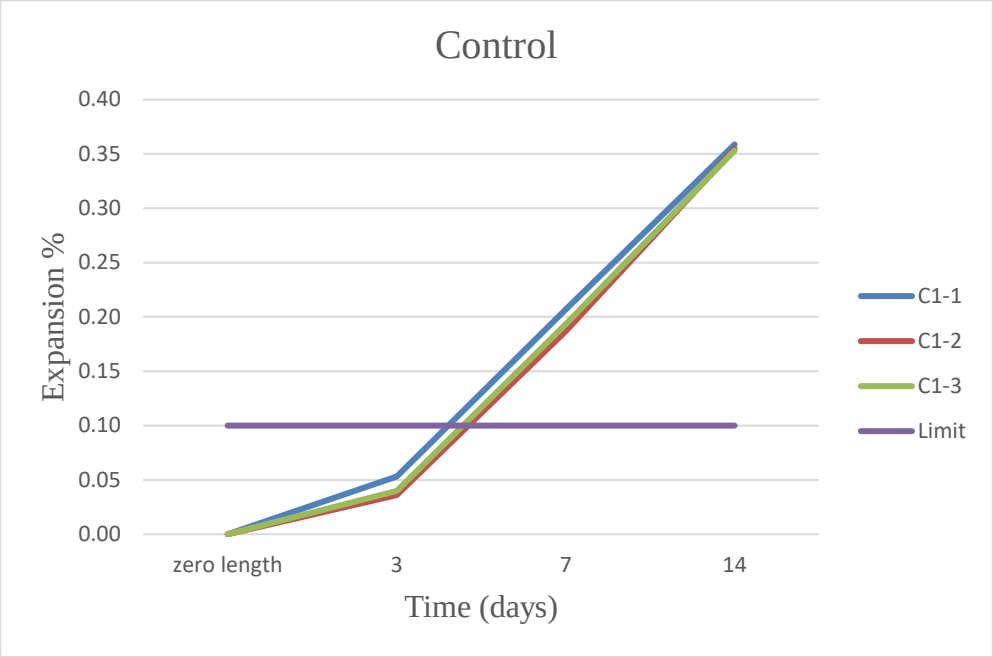

Figure 3.1: AMBT of the sand used in this study.

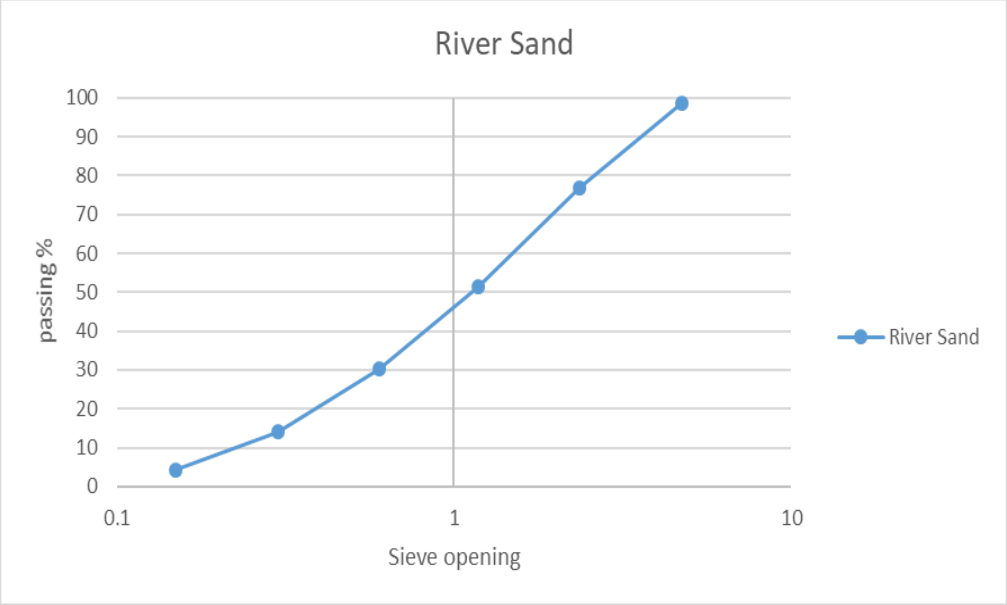

Figure 3.2: Sieve analysis for the sand used in this study.

3.2.2 Cement

In all mortar combinations, Ordinary Portland cement (OPC) was used (CEMI 42.5N). The specific gravity of this cement was measured and found to be 3.14 gm/cm^3. The chemical compositions of cement were analyzed using X-ray fluorescence (XRF) and presented in part 3.2.4. To maintain consistent alkali levels across all mortar bars during the Accelerated Mortar Bar Test (AMBT)**,** it is crucial to employ Ordinary Portland Cement (OPC) with a low alkali content ratio. This ensures that the primary source of alkali reacts exclusively with the mortar bars immersed in the NaOH solution.

3.2.3 Waste glass powder (WGP)

Initially, two types of waste glasses were tested in this study to find the most suitable waste glass powder. Type 1 was a waste glass with a relatively more significant size and distinct colors (green, white, etc.). This one was crashed in the Los Angeles machine in the Building Materials Laboratory and sieved from a 0.1 mm sieve before use. AMBT, compressive, and flexural strength were applied as trial tests. Because of impurities found in the first type and, at the same time, the hardness of separating the glass from other materials in the mix, the trial test conducted with this type showed contradictory results. As a result, we concentrated on the second WGP, which showed promising results.

Type 2 was white, with an average particle size of 0.1 mm. The origin of this glass was E-glass fiber, which is the reason for its purity and homogeneity. According to literature reviews, a particle size of less than 100 µm effectively mitigates ASR expansion (Ke et al., 2018). For this reason, WGP was sieved through 60 µm and 45 µm sieves before using in the production. The amount retained when wet-sieved on 45 µm was lower than 5%, specified as a maximum ratio in ASTM C 1866/1866M.

Figure 3.3 shows waste glass powder (type 2) after the preparation for mixing. The specific gravity of WGP was 2.47 g/cm³. The chemical compositions of waste glass powder were analyzed using X-ray fluorescence (XRF) and presented in part 3.2.4.

Figure 3.3: Used waste glass powder.

3.2.4 XRF results of cement and waste glass powder

X-ray fluorescence is a non-destructive analytical technique used to determine the elemental composition of a material. In an XRF test, a sample is irradiated with high-energy X-rays, which causes the atoms in the model to emit characteristic fluorescent X-rays. These fluorescent X-rays have energies specific to the elements present in the sample. By measuring the power and intensity of the emitted X-rays, the XRF instrument can identify and quantify the elements in the sample. XRF analysis can determine a wide range of elements, from low atomic number elements (such as carbon and oxygen) to high atomic number elements (such as uranium and lead). XRF is capable of analyzing both solid and liquid samples, as well as thin films and coatings (Wagatsuma, 2021). To know the chemical oxides in our raw materials, two samples of cement and glass powder were sent to the Geochemistry Research Laboratory to apply the XRF test. Table 3.2 shows the different oxide ratios in waste glass powder and cement. As can be seen, more than 50% of waste glass has SiO_2 (56%). Total equivalent alkalis, $Na2O_{eq}$, = (Na_2O + 0.658K_2O = 0.08+0.658x0.68 = 0.53%) and the max. Required $Na2O_{eq}$ is (4%) according to (ASTM C 1866/1866 M). As a result, the used waste glass powder can be classified as GE glass (ASTM C 1866/1866 M).

For cement, almost 1% of total equivalent alkalis is recorded (Na_2O + 0.658K_2O = 0.32+0.658x1.1 = 1.04%). The Loss on ignition of cement is 3.07%, which is close to the ratio mentioned in ASTM C150-07 (3.0%).

Table 3.2: Chemical composition for glass powder and cement.

	SiO_2	Al_2O_3	Fe_2O_3	MgO	CaO	Na_2O
Glass powder	55.87	16.42	0.63	8.47	13.15	0.08
Cement	16.83	3.84	3.7	1.06	64.51	0.32

Table 3.2 (Cont.): Chemical composition for glass powder and cement.

	K_2O	TiO_2	P_2O_5	SO_3	Cr_2O_3	LOI
Glass powder	0.68	0.5	0.04	0.01	0.01	3.29
Cement	1.1	0.25	0.2	4.73	0.12	3.07

3.2.5 XRD results of cement and waste glass powder

X-ray diffraction is a scientific technique that can be used to analyse materials' atomic and molecular structures. The XRD test involves shining X-rays onto a crystalline material and measuring the resulting diffraction pattern. When X-rays interact with the atoms in a crystal, they scatter in specific directions due to the arrangement of atoms within the crystal lattice. By analysing the angles and intensities of the diffracted X-rays, researchers can determine the positions of atoms within the crystal structure.

The XRD test provides valuable information about the crystal structure, lattice parameters, crystal symmetry, and the presence of impurities or defects within a material by comparing the output with the database they have. It can identify the types of crystalline phases present in a sample, determine the degree of crystallinity, and reveal changes in the crystal structure due to factors like temperature, pressure, or chemical reactions (Gilbert, 2016). Figure 3.4 shows the XRD results of cement and waste glass powder used in this study. We can notice that cement has a crystalline structure referring to some components such as Alite ($Ca_3(SiO_4)O$), Hydrotalcite ($Mg_6Al_2(OH)16CO_3{\cdot}4H_2O$) and Gypsum ($CaSO_4{\cdot}2H_2O$). On the other hand, for WGP, the used software (Malvern Panalytical ver. 5.2) could not recognize any peak referred to as any crystalline structure. As a result, the glass powder particles can be considered amorphous. Also, the physical requirement was achieved.

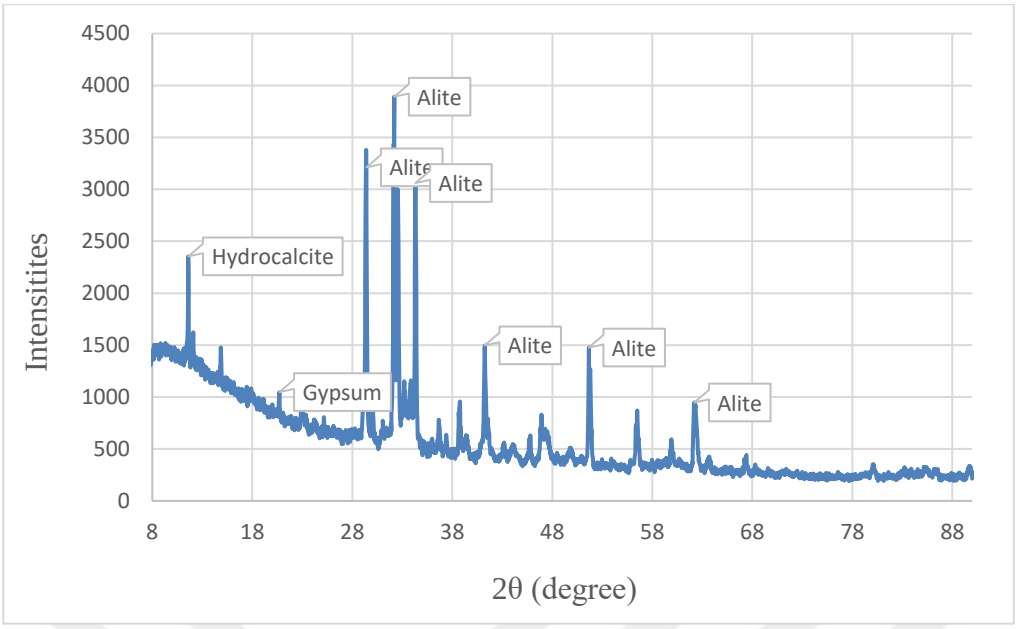

(a)

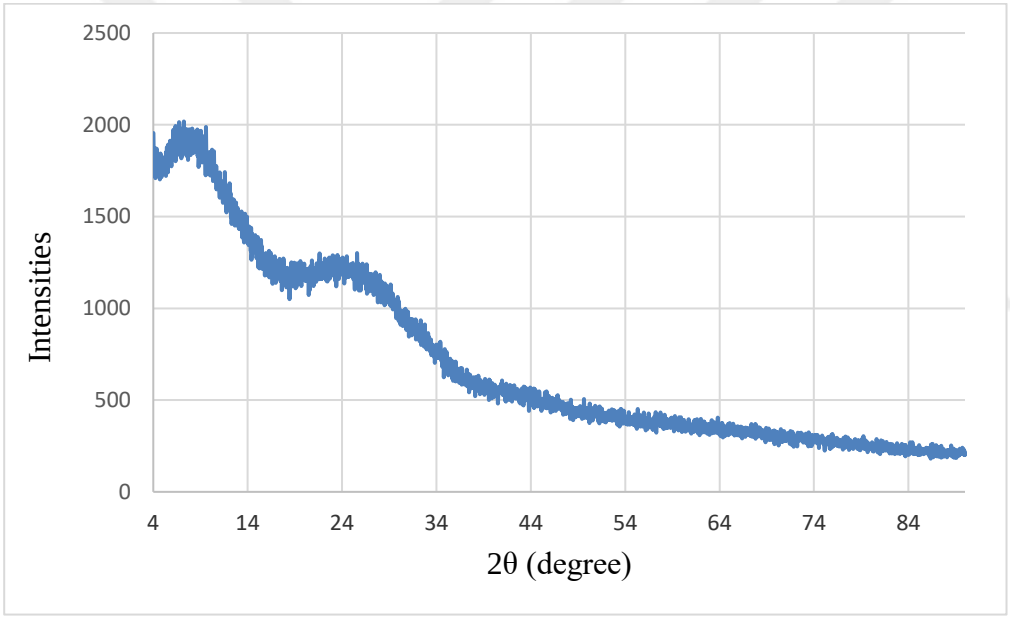

(b)

Figure 3.4: XRD results for a) cement and b) glass powder.

3.2.6 Nano silica

A commercial aqueous colloidal nano-silica (Levasil Colloidal Silica, CB8 produced by AkzoNobel) is used in this study. It is an alkaline, aqueous dispersion of colloidal silica with approximately 50% solids by weight. The silica dispersion is sodium stabilized, and the amorphous silica particles carry a negative surface charge. The SiO_2 particles are discrete, have a smooth, spherical shape, and are present in a broad particle size distribution. The physical appearance of the dispersion is a white liquid, slightly more viscous than water (Nouryon et al.).

The typical Properties of Levasil CB8 are mentioned in Table 3.3.

Table 3.3: Typical Properties of Levasil CB8.

Silica, wt.%	50
pH	9.5
Viscosity, cP	8
Density	1.4 g/cm^3

3.2.7 Superplasticizer

A water reducer was used to increase the mortars' flowability. MasterGlenium 51 can be used with ratios between 0.5% and 1.5%, the most significant percentage mentioned in the technical conditions. Some properties of the MasterGlenium 51 are given in the company's datasheet (Master Builders Solution), shown in Table 3.4.

Table 3.4: Properties of MasterGlanium 51.

Appearance	Brown liquid
Specific gravity at 20°C	1.10 ± 0.03 g/cm³
pH-value	6.0 ± 1
Alkali content (%)	≤ 5.00 by mass
Chloride content (%):	≤ 0.10 by mass
Corrosion behavior	Contains only components according to BS EN 934-1:2008, Annex A.1.
Air Content	Fulfilled
Water reduction	≥ 112% of Reference mix
Increase in consistency	Increase of ≥ 120mm from initial slump or ≥ 160mm from initial flow
Retention of consistency	At 30 min ≥ Reference mix at initial

3.3 Mix Design

This study aims to check the effect of WGP and NS as cementitious replacements in mitigating ASR and their impact on mortars' mechanical properties. Substitution ratios were taken according to some literature and the trial tests we have done. Most studies used WGP starting from 10% to 50% of cement weight. NS is used at 1% to 4% of cement weight (Yu et al., 2014; Chithra et al., 2016). In the trial tests, mortars with 10%, 15%, and 20% of WGP were tested as cement replacement ratios with 1% and 2% of NS replacement, according to AMBT, compressive and flexural strengths. For water–cement ratio (w/c), the ASTM C1576 and BS EN 196-1 standards suggested using a w/c ratio of 0.47 and 0.5, respectively.

To maintain a workable flowability, the amount of water reducer was adjusted according to the results from the trial tests. Also, the adjustment of the water reducer considered the variation in workability and air content for fresh mortar with the increase of WGP and NS replacement ratio. The mix design is presented in Tables 3.5 and 3.6 for AMBT and mechanical properties, respectively.

The mix design was considered according to the recommendations mentioned in ASTM C1576 and BS EN 196-1. Figure 3.5 shows mortars poured in molds and covered with plastic cover for 24 hours and then unmolded and cured in a water path.

Figure 3.5: Mortars poured in compressive and strength molds.

Table 3.5: Mix design for AMBT.

	Water	Sand	OPC	GP	NS
Sp.gr (g/cm^3)	**1**	**2.69**	**3.14**	**2.47**	**1.4**
Control	206.8	990	440	0	0
0GP1NS	206.8	990	435.6	0	4.4
0GP1.5NS	206.8	990	433.4	0	6.6
0GP2NS	206.8	990	431.2	0	8.8
10GP0NS	206.8	990	396	44	0
10GP1NS	206.8	990	391.6	44	4.4
10GP1.5NS	206.8	990	389.4	44	6.6
10GP2NS	206.8	990	387.2	44	8.8
15GP0NS	206.8	990	374	66	0
15GP1NS	206.8	990	369.6	66	4.4
15GP1.5NS	206.8	990	367.4	66	6.6
15GP2NS	206.8	990	365.2	66	8.8
20GP0NS	206.8	990	352	88	0
20GP1NS	206.8	990	347.6	88	4.4
20GP1.5NS	206.8	990	345.4	88	6.6
20GP2NS	206.8	990	343.2	88	8.8
25GP0NS	206.8	990	330	110	0
25GP1NS	206.8	990	325.6	110	4.4
25GP1.5NS	206.8	990	323.4	110	6.6
25GP2NS	206.8	990	321.2	110	8.8

Table 3.5 (Cont.): Mix design for AMBT.

	Superplasticizer	W/C	W/B	Poz/Binder
Sp.gr (g/cm^3)	**1.05**			
Control	1.9	0.47	0.47	0
0GP1NS	3	0.474	0.47	0.01
0GP1.5NS	3	0.477	0.47	0.015
0GP2NS	3	0.480	0.47	0.02
10GP0NS	3.4	0.522	0.47	0.1
10GP1NS	3.4	0.528	0.47	0.11
10GP1.5NS	3.4	0.531	0.47	0.115
10GP2NS	3.4	0.534	0.47	0.12
15GP0NS	3.4	0.553	0.47	0.15
15GP1NS	3.4	0.560	0.47	0.16
15GP1.5NS	3.4	0.563	0.47	0.165
15GP2NS	3.4	0.566	0.47	0.17
20GP0NS	3.4	0.588	0.47	0.2
20GP1NS	3.4	0.595	0.47	0.21
20GP1.5NS	3.4	0.599	0.47	0.215
20GP2NS	3.4	0.603	0.47	0.22
25GP0NS	3.4	0.627	0.47	0.25
25GP1NS	3.4	0.635	0.47	0.26
25GP1.5NS	3.4	0.639	0.47	0.265
25GP2NS	3.4	0.644	0.47	0.27

Table 3.6: Mix design for compressive and flexural strength specimens.

	Water	Sand	OPC	GP	NS
Sp.gr (g/cm^3)	**1**	**2.69**	**3.14**	**2.47**	**1.4**
Control	225	1350	450	0	0
0GP1NS	225	1350	445.5	0	4.5
0GP1.5NS	225	1350	443.25	0	6.75
0GP2NS	225	1350	441	0	9
10GP0NS	225	1350	405	45	0
10GP1NS	225	1350	400.5	45	4.5
10GP1.5NS	225	1350	398.25	45	6.75
10GP2NS	225	1350	396	45	9
15GP0NS	225	1350	382.5	67.5	0
15GP1NS	225	1350	378	67.5	4.5
15GP1.5NS	225	1350	375.75	67.5	6.75
15GP2NS	225	1350	373.5	67.5	9
20GP0NS	225	1350	360	90	0
20GP1NS	225	1350	355.5	90	4.5
20GP1.5NS	225	1350	353.25	90	6.75
20GP2NS	225	1350	351	90	9
25GP0NS	225	1350	337.5	112.5	0
25GP1NS	225	1350	333	112.5	4.5
25GP1.5NS	225	1350	330.75	112.5	6.75
25GP2NS	225	1350	328.5	112.5	9

Table 3.6 (Cont.): Mix design for compressive and flexural strength specimens.

	Superplasticizer	W/C	W/B	Poz/Binder
Sp.gr (g/cm^3)	**1.05**			
Control	5	0.5	0.5	0
0GP1NS	5	0.505	0.5	0.01
0GP1.5NS	5	0.508	0.5	0.015
0GP2NS	5	0.510	0.5	0.02
10GP0NS	6.75	0.556	0.5	0.1
10GP1NS	6.75	0.562	0.5	0.11
10GP1.5NS	6.75	0.565	0.5	0.115
10GP2NS	6.75	0.568	0.5	0.12
15GP0NS	6.75	0.588	0.5	0.15
15GP1NS	6.75	0.595	0.5	0.16
15GP1.5NS	6.75	0.599	0.5	0.165
15GP2NS	6.75	0.602	0.5	0.17
20GP0NS	6.525	0.625	0.5	0.2
20GP1NS	6.75	0.633	0.5	0.21
20GP1.5NS	6.75	0.637	0.5	0.215
20GP2NS	6.75	0.641	0.5	0.22
25GP0NS	6.75	0.667	0.5	0.25
25GP1NS	6.75	0.676	0.5	0.26
25GP1.5NS	6.75	0.680	0.5	0.265
25GP2NS	6.75	0.685	0.5	0.27

4. EXPERIMENTAL PROCEDURES

4.1 Fresh Mortar Tests

4.1.1 Workability tests (Flow Table Spread test) FTS

The workability of a mortar is its ability to be easily mixed, placed, and finished, and workability can be determined according to BS EN 1015-3 (1999). This standard describes a procedure for measuring the dispersion of fresh mortar on a flat surface to determine its consistency. Figure 4.1 shows the flow table test done for all mortars.

Figure 4.1: Flowability test.

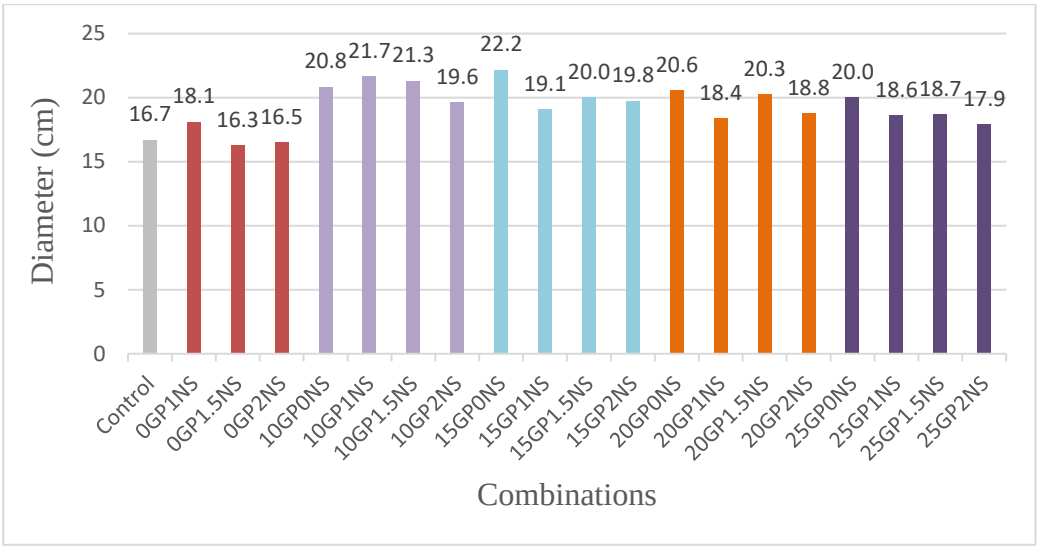

(a)

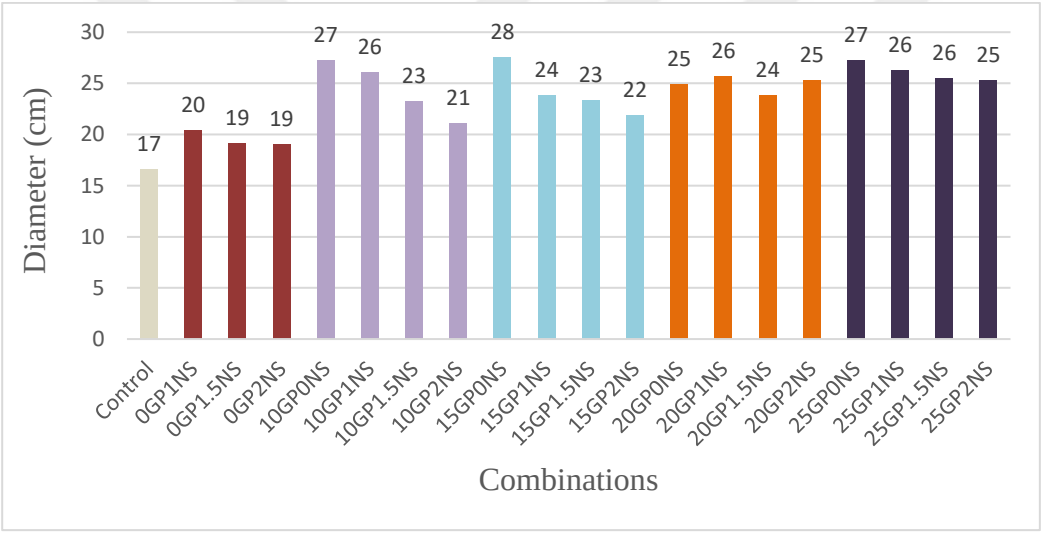

(b)

Figure 4.2: Flowability test in specimens for a) compressive and flexural mortars and b) AMBT mortars.

From the trial production, a water reducer must be used to have mortar with ease and homogeneity with which it can be mixed and placed correctly. MasterGlenium 51 was used in different amounts, from 1.1% to 1.5% of the cement's weight. That was necessary to keep the workability as close as possible to each other for the whole combination. From the literature and the first trial before our study, nano silica was noticed to harm workability, and the ratios of water reducers were decided. These specimens were mixed according to Table 3.5, whose proportions are taken from BS EN 196-1 standard. Figure 4.2 shows the average diameter of the fresh mortars in the

flowability test for different combinations. It was noticed that NS decreased the workability probably because of its tiny particles and large surface area. This result conforms to studies such as (Nigam and Verma, 2023; Güneyisi et al., 2016). According to Nigam and Verma, 2023, slump value and compaction factor tests show a similar graph vs the nano-silica content. The slump value of 0.0% incorporated mix shows 110 mm, but after 3% incorporation, it shows a value of around 20 mm. Güneyisi et al. concluded that the slump flow diameters of Self Compacting Lightweight Concretes were determined in the 680–738mm range. According to the results, the highest diameter was achieved for treated surface lightweight coarse aggregates without NS (LWA-WG-NS0) at a 0.25 w/b ratio. At the same time, the lowest was obtained for lightweight aggregate without treated surface (LWA-NS5.0) at 0.25 and 0.50 w/b ratios.

The literature review for WGP as a cementitious replacement mentioned the effect of WGP in mortars in a fresh state. Some studies claimed that the greater the amount of WGP in mortars, the less workability we get (Aliabdo et al., 2016; Paraghi and Alam, 2016). In our study, the slump test results showed that the workability did not affected much with the WGP replacements in a mortar. The superplasticizer used with the same amount in all mortars contained WGP to determine the effect of WGP on the workability. According to Figure 4.2(a) and (b), the flow spread table test (FST) results for mortars prepared for compressive and flexural strength remained unchanged with an increase in the amount of WGP replacement. This was also observed in the FST results from AMBT, where WGP showed the same results, as per Figure 4.2(c).

4.1.2 Measurement of Air Content

One of the most essential fresh mortar tests is air content. In this study, the air contents for fresh mortars were calculated to understand the effect of GP and NS on mortar density. Air contents were calculated for both mortars produced for AMBT and flexural–compressive strength tests for 7 and 28 days according to ASTM C185-20.

The apparatus required for this test method are a calibrated vessel, a balance, and a tamping rod.

The steps of the test are specified below:

1. A calibrated vessel was used for all mortars with volume already calibrated by filling the vessel with water and measuring the weight.

2. The specific gravity of water = 1 g / cm^3, which mean the weight in grams = the volume in cm^3
3. The calibrated vessel is then filled with mortars in three layers, each being tamped with 25 blows of the tamping rod.
4. The weight of the calibrated vessel with mortar was measured, and calculations were made.
5. From the specific gravities for each row material used in the mixing, the theoretical unit weights were calculated according to (4.1).
6. The air content was calculated according to equation (4.2):

Theoretical air content = mass of the mortar / total volume of mortar (4.1)

Air content = 100*(1- measured unit weight / theoretical unit weight) (4.2).

Figure 4.3 shows the relationship between air content and different combinations of mortars produced for flexural–compressive strength tests and AMBT. We can conclude that the amount of WGP did not contribute to the percentage of air content, but in most of the specimens, NS's content affects air content in a significant way. The air content ratio increases with the increase of NS's content, which is accommodated with the results of a different study (Senffa et al., 2009).

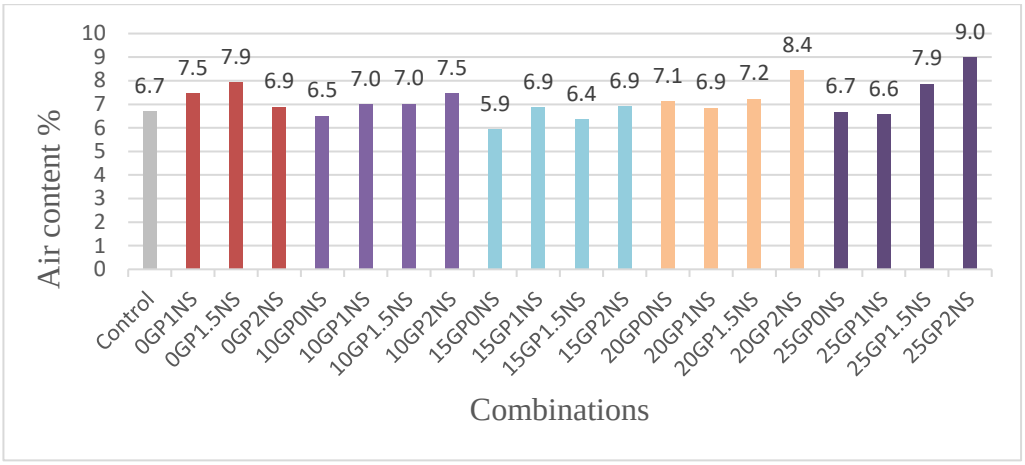

(a)

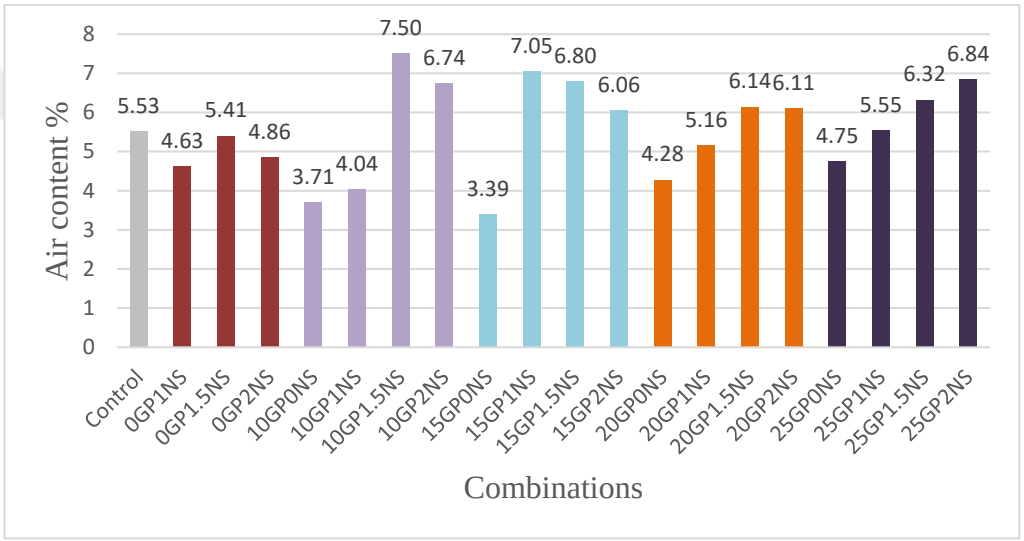

(b)

Figure 4.3: Air content for a) Compressive and flexural strength mortars, b) AMBT mortars.

4.2 Accelerated Mortar Bar Test (AMBT)

The accelerated mortar bar test was performed according to ASTM C1567-23. The used sand is dried and then sieved to obtain the desired particle size distribution. Then, sand is prepared by recombining the portions retained on the various sieves in the grading prescribed in Table 4.1.

Table 4.1: Sieve analysis for accelerated mortar bar test (ASTM C1567-23).

Sieve size (mm)		
Passing	Retained	Mass%
4.75	2.36	10
2.36	1.18	25
1.18	600	25
600	300	25
300	150	15

A mixture of cement, sand, and water was prepared according to specific proportions. The dry materials for the test mortar were proportioned using 1 part of cement to 2.25 parts of graded aggregate by mass. The quantities of dry materials to be mixed at one time in the mortar batches for producing three specimens were 440 g of cement and 990 g of sand. A water-to-binder ratio equal to 0.47 by mass was used.

The mortars were then molded into prismatic bars using molds specially designed for AMBT tests. The bars were typically 25x25x285 mm prisms with a gauge length of 250 mm. The mortar bars were cured in a moist room at 23 ± 2°C and at least 95% relative humidity for 24 hours. After curing, the mortar bars were removed from the mold and stored in water at 23 ± 2°C for 24 hours, and then the initial reading was taken. Then, they transferred to containers with a capacity of 14 liters. The containers were filled with NaOH solution to accelerate the forming of ASR gel during the test duration. The containers were then placed in an oven and stored at 80 ± 1°C for 14 days. Comparator readings were taken at 0, 3, 7, and 14 days. The results of the tests were reported as the percent change in the length of the mortar bars. A change in the length of 0.1% or greater in mortars is considered a reactive and harmful expansion for potential ASR, according to ASTM C1778-22.

4.3 Flexural and Compressive Strength Tests

The samples were prepared twice for the same combination: one for 7-day tests and the other for 28-day tests. Prismatic samples with 40 x 40 x 160 mm dimensions were organized and kept at molds by covering the surfaces with stretch films. After 24 hours, the specimens were placed in water for curing until test days at a temperature of 20 ± 2°C.

4.3.1 Flexural strength

3-point flexural strength tests were conducted according to BS EN. The samples were placed on two supports 100 mm apart from each other. The load was applied at the center of the sample at a rate of 0.5 ± 0.1 MPa/s until the sample fractured and the maximum load was recorded. The failure force was recorded, and the flexural strength was calculated according to equation (4.3) (BS EN 196-1). The test results will discuss the relationship between different combinations and their strength (Chapter 5). Figure 4.4 shows the test setup before and after the failure of specimens in a universal testing machine.

$$\text{Flexural strength } (R_f) = (3/2 * F_f * L)/b \quad (4.3)$$

Where:

R_f is the flexural strength in MPa.

b is the side of the square section of the prism in mm.

F_f is the load applied to the middle of the prism at fracture in N.

L is the distance between the supports in mm.

Figure 4.4: Flexural strength test.

4.3.2 Compressive strength

After breaking the samples into two pieces in the flexural strength test, one of each piece was tested for compressive strength, and the other was kept for the capillary water absorption test. The sample was placed on a flat surface, centered under the

compression machine, and a compressive force was applied at a rate of 0.5 ± 0.1 MPa/s until the sample fractured.

The fracture strength was read from the machine's screen, and the maximum strength at which the sample fractured was recorded as the compressive strength of the mortar. The average of the three individual results, each expressed at least to the nearest 0.1 MPa, was calculated and obtained. Figure 4.5 shows the specimen before testing in the compressive strength machine.

Figure 4.5: Compressive strength test.

4.4 Capillary Water Absorption

The other halves of the prismatic specimens that remained from the flexural and compressive strength test were used for the capillary water absorption test. The test was applied to determine the capillary water absorption ability of the specimens and compare the permeability of different mortars. Calculations were made according to two standards (ASTM C1585 and BS EN 1015-18). First, specimens were cut from one face to smooth the surface, and the other four faces were sealed with an impermeable material (sealing material) to avoid water absorption from all sides except the one from which it was cut. The specimens were stored on a tray with a minimum depth of 20 mm and a plan area large enough to contain the specimens to be

immersed and fitted to maintain a constant water level (BS EN 1015-11). Metal bars with spaces between them to ensure the minimum water contact with the specimen's surface were used to put specimens on it, as shown in Figure 4.6.

The weight was measured in different intervals, as shown in the standards mentioned before. The results will be introduced in Chapter 5 in graphs showing the relationship between the square time in seconds and water absorption.

Figure 4.6: Capillary water absorption test.

4.5 Scanning Electronic Microscope (SEM)

A scanning electron microscope (SEM) is a powerful tool used in various fields of science and engineering to examine materials' surface features at high magnifications. It directs a beam of electrons onto the sample, which interacts with the atoms in the material and produces signals detected by the microscope's sensors. The SEM scans a focused electron beam across the sample's surface, creating extremely high-resolution and magnification images. The images produced by an SEM can reveal the surface topography, morphology, composition, and chemical bonding of materials, making it a valuable tool for characterizing the microstructure of a wide range of materials (Ni, 2013).

Different combinations of mortars were sent to the Membrane Technologies Application-Research Center (MEM-TEK) at Istanbul Technical University after immersing the specimens in NaOH solution for 14 days. Seven mortar combinations are chosen for SEM. These were: Control, (C), 2%NS(2NS), 10%GP+2%NS

(10GP2NS), 15%GP + 2% NS (15GP2NS), 20%GP+2% NS (20GP2NS) and 25% GP+2% NS (25GP2N).

The mortars were crushed to small sizes (1cm * 1 cm). At least four pieces from each combination were sent. Different zoom levels were used: (100X, 500X, 1000X, 1500X, 2000X, 5000X and 10000X).

The aims of SEM are:

1. Indicating microstructure of mortars with waste glass powder and NS.
2. Checking the effect of WGP and NS on the internal structure of mortars and the reduction in pores formed.
3. Checking and indicating that C-S-H gel formed due to hydration and pozzolanic activity.

4.6 X-ray Diffraction (XRD)

X-ray diffraction (XRD), a potential analytical technique, is used in many scientific fields, including materials science, chemistry, and geology, to study the crystalline structure of solid materials. XRD examines the angles at which the crystal lattice disperses the X-rays to create a distinctive diffraction pattern. This is done by directing a monochromatic X-ray beam onto a sample. Using this pattern as a fingerprint of the material's atomic configuration, it is possible to identify crystal phases, calculate lattice parameters, and get information on microstructural characteristics like crystallite size and strain (Chung, 1974).

For this study, various combinations of mortars with WGP+NS were tested. We picked two combinations from each WGP content: WGP with no NS and the highest NS content (2%). This was done to distinguish between the hydration products of each WGP content with and without NS. As the laboratory told us, we had to choose a limited number of mortars. The mortars were sent to Prof.Dr. Adnan Tekin Material Sciences and Production Technologies Application Research Center (ATUM). These combinations were: Control, (C), 1%NS(1NS), 2%NS(2NS), 10%GP+0%NS (10GP0NS),10%GP+2%NS (10GP2NS),15%GP+ 0% NS (15GP0NS), 15%GP + 2% NS (15GP2NS), 20%GP + 0% NS (20GP0NS), 20%GP + 2% NS (20GP2NS), 25% GP + 0% NS (25GP0N), 25% GP + 2% NS (25GP2N).

Table 4.2 shows the chosen combination sent for the XRD test. The specimens were prepared by crushing them and turning them into powder as the laboratory requested.

Table 4.2: Combination chosen for XRD test.

Mortars Picked	0 WGP	10 WGP	15WGP	20WGP	25WGP
0NS	0WGP 0NS (C)	10WGP 0NS	15WGP 0NS	20WGP 0NS	25WGP 0NS
1NS	0WGP 1NS	-	-	-	-
2NS	0WGP 2NS	10WGP 2NS	15WGP 2NS	20WGP 2NS	25WGP 2NS

The aims of the XRD test in this study are:

1. Follow some hydration products resulting in the mortars, such as CH crystals, Ettringite, Quartz, and any notable trend from adding WGP and NS.
2. Investigating pozzolanic reaction by following CH peaks' intensities with different combinations.
3. Compare these results with different literature and other tests in this study, such as SEM and thermogravimetric analysis (TGA).

4.7 Thermogravimetric Analysis (TGA)

Thermogravimetric analysis (TGA) is a technique used to analyze materials' thermal stability and composition. The method involves subjecting a sample to a controlled increase in temperature while measuring its weight change as a function of temperature or time.

During the analysis, the sample is placed in a crucible and heated in a furnace, and its weight is monitored by a sensitive balance (Thermogravimetric analysis (TGA) - types). As the temperature increases, the sample undergoes various thermal processes such as dehydration, decomposition, oxidation, and reduction, which are reflected in the weight change. Figure 4.7 shows TGA's equipment used for thermogravimetric analysis.

Figure 4.7: TGA-55 equipment used-for-thermogravimetric-analysis-TGA.

The TGA instrument provides a thermogram that plots the weight of the sample as a function of temperature or time, which can be used to determine various properties of the sample, such as its thermal stability, composition, purity, and reaction kinetics.

TGA is widely used in various fields, including material science, chemistry, pharmaceuticals, and environmental science, to study the properties of polymers, ceramics, composites, minerals, fuels, and biomaterials. The technique is instrumental in characterizing the thermal behavior of complex materials, such as those with multiple components or impurities, and in studying the effects of temperature on the properties of materials (Thermogravimetric analysis (TGA) – types).

The aim of this test is:

1. Calculating the loss in mass with increasing temperature.
2. Calculating the loss of mass resulting from CH consumption.
3. Comparison between CH consumption of mortars with WGP and mortars without WGP.

5. TEST RESULTS

5.1 AMBT Results

ASTM C1567-23 performed the AMBT tests. Comparator readings were taken on the 3rd, 7th, and 14th days. The mortar bar specimens were stored at a constant temperature of 80°C while submerged in a NaOH solution to facilitate a high-alkaline environment. This was done to ensure that ambient temperatures did not affect the expansion readings (ASTM C1567-23).

5.1.1 Effect of Nano Silica

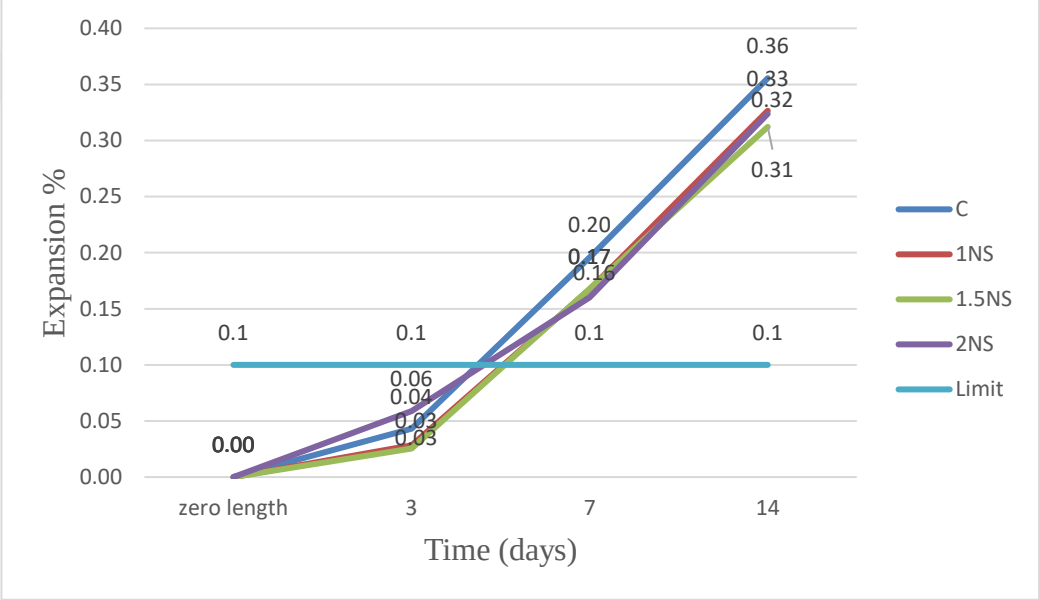

Figure 5.1: Effect of nano-silica on ASR expansion with 1%, 1.5%, and 2% of OPC cement replacement level together with control specimen.

Figure 5.1 shows the relationship between ASR expansion and the specimens with nano silica content. ASR expansion in the control specimen (0% nano-silica) is 0.36%. On the other hand, specimens with 1%, 1.5%, and 2% nano-silica content have 0.32, 0.31, and 0.32%, respectively. We can notice that using nano-silica caused a reduction in expansion compared to the control specimen. The expansion decreases by 9% by adding 1% of nano silica, 14% with 1.5%, and 9% with 2% of nano silica. From these results, we can say that adding nano silica slightly mitigated ASR expansion. This reduction is not gradual with the increase in the amount of nano silica used, and it is not that effective to depend on. The results are accommodated with other research, such as (Cai et al., 2019).

5.1.2 Effect of waste glass powder

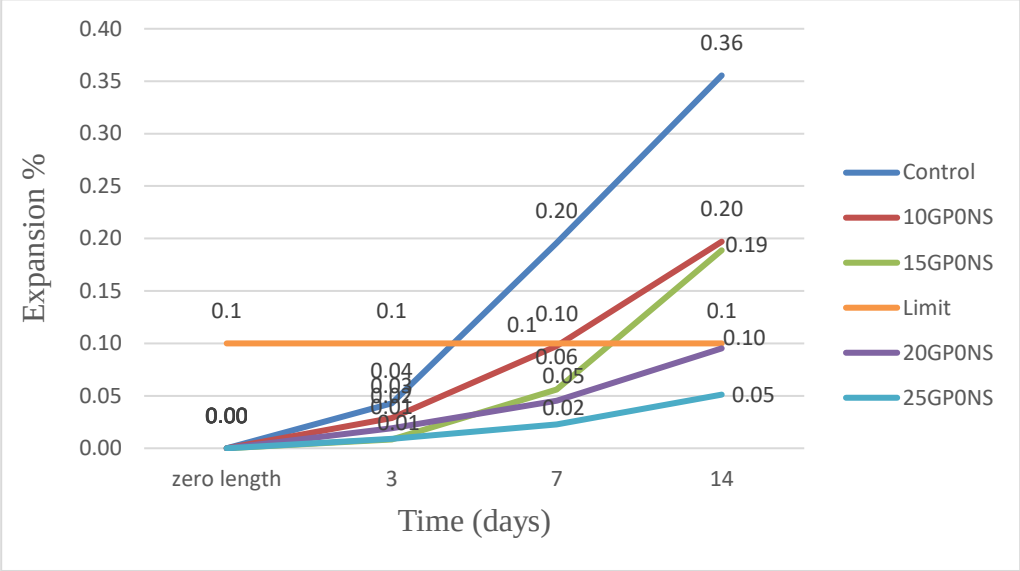

Figure 5.2: Effect of glass powder on ASR expansion with 10%, 15%, 20%, and 25% of OPC cement replacement level.

Figure 5.2 shows the expansion results of mortar bars with different WGP content. The WGP replacement ratios were 10%, 15%, 20% and 25% of cement. We can conclude that WGP showed an effective mitigation level, reaching an 86% reduction in expansion with 25% of WGP. The expansions were 0.2%, 0.19%, 0.10%, and 0.05% for 10GP0NS, 15GP0NS, 20GP0NS, and 25GP0NS, respectively. Only two replacement levels could reduce the expansion to the safe level mentioned in ASTM C 1778. These replacement levels were 20% and 25% of WGP. This effectiveness in mitigating ASR was mentioned in literature reviews (Hadley, 1961; Liu et al., 2015; Ke et al., 2018).

Ke et al. (2018) presented AMBT results for glass powder as a cementitious replacement with a particle size range between 53-75 µm at 3, 7, 14, 28, and 35 days. The glass powder replacement levels were 0%, 10%, 20% and 30%. The expansion decreased at 14 days from 0.085% to 0.025% with 30% of glass powder replacement level with a reduction percentage of 70.6%.

5.1.3 Combined effect of nano silica and waste glass powder

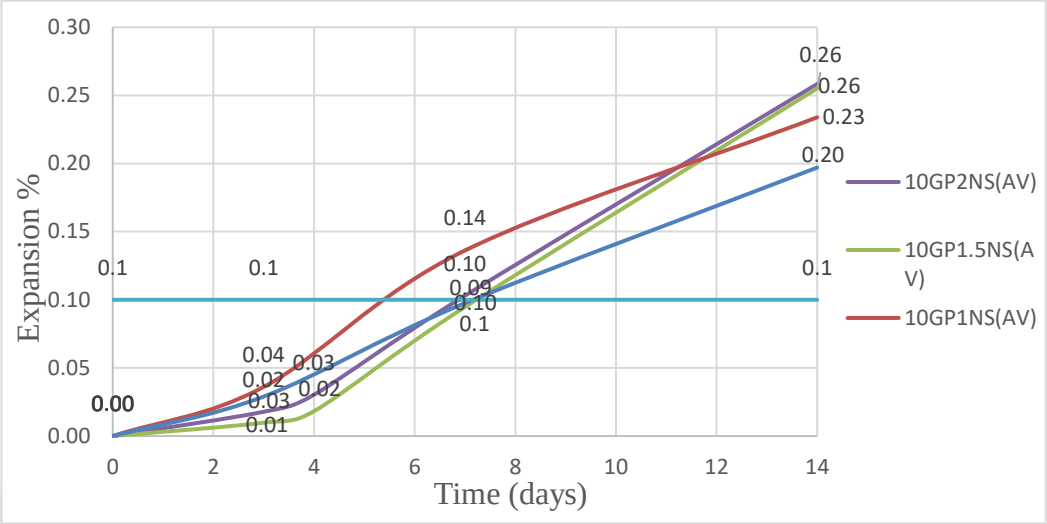

Figure 5.3: Effects of cement replacement with 10% WGP and several amounts of NS on ASR expansion.

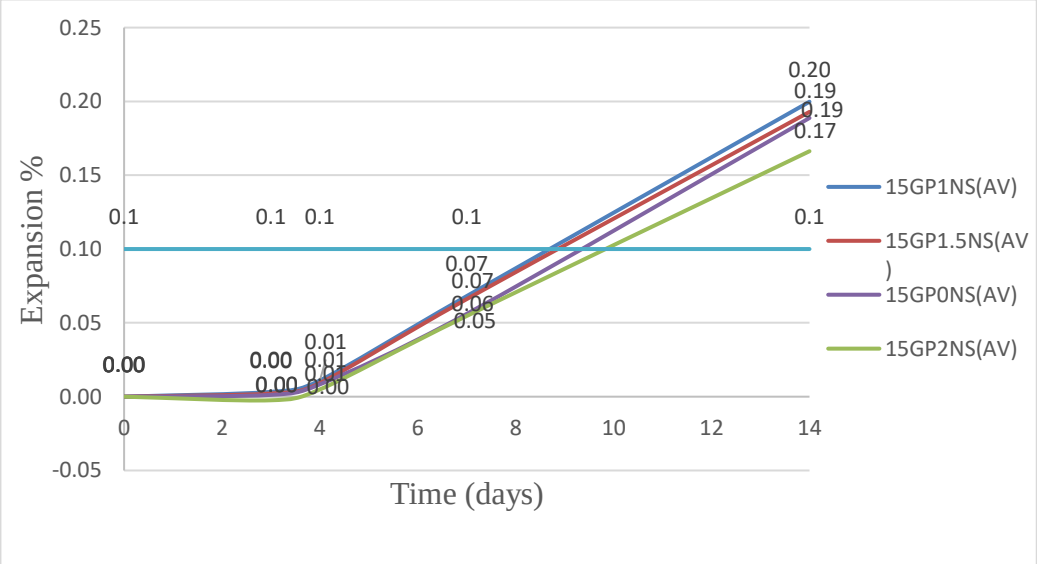

Figure 5.4: Effect of cement replacement with 15% of WGP and several amounts of NS on ASR expansion.

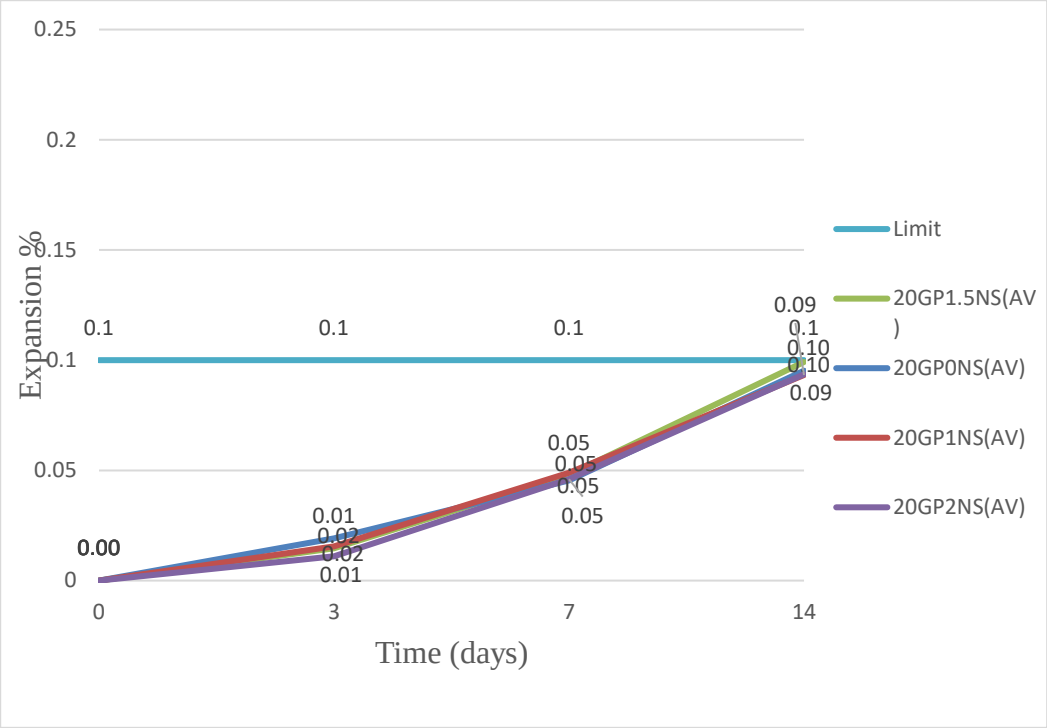

Figure 5.5: Effect of cement replacement with 20% of GP and several amounts of NS on ASR expansion.

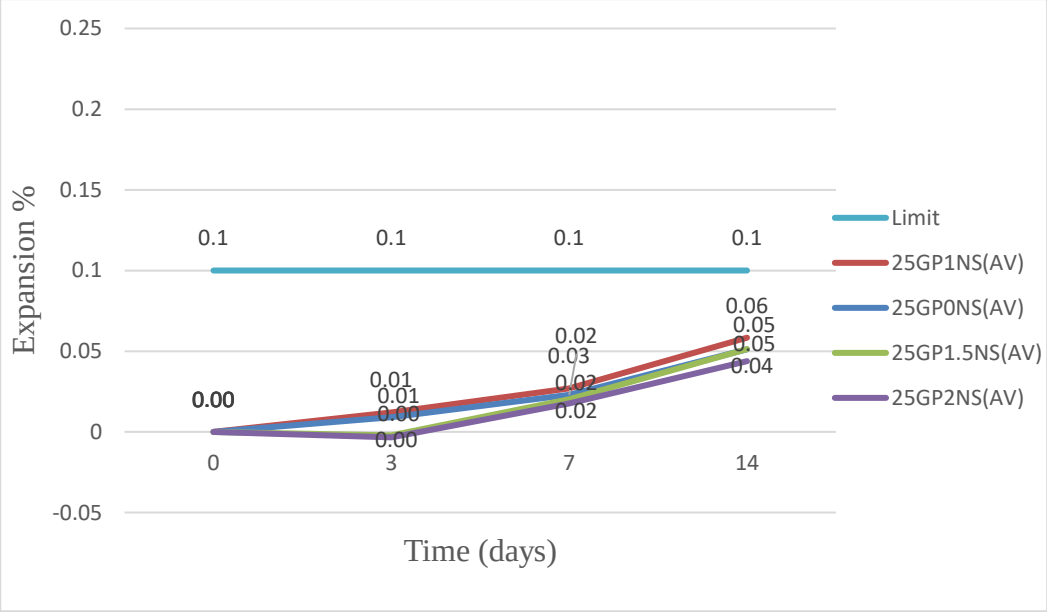

Figure 5.6: Effect of cement replacement with 25% of GP and several amounts of NS on ASR expansion.

Figures 5.3, 5.4, 5.5, and 5.6 show the effects of replacing cement with 10, 15, 20, and 25% WGP together with 0, 1, 1.5, and 2% NS on ASR expansion up to 14 days according to ASTM C1576-23. The figures show that adding glass powder mitigated ASR expansion; increasing the glass powder content decreased ASR expansions. The most effective results are 20% and 25%, decreasing the expansion below 0.1%.

Figure 5.3 shows a 10% replacement of waste glass powder and 1%, 1.5%, and 2% nano-silica with cement. We can conclude that the increased NS content had a negative effect on mitigating ASR at 10% replacement of waste glass powder with cement.

Figure 5.4 shows the results of 15% WGP addition. We noticed here different behavior with gradually increasing nano silica's content. The effect of nano silica on mitigating ASR is almost negligible.

Figure 5.5 expresses a 20% replacement ratio with NS in different percentages. We noticed almost the same reduction ratio for bars with 20% GP replacement with 1%, 1.5%, and 2% NS replacement. The same note at 25% GP replacement in Figure 13.6. The average expansion value of mortars with 10%, 15%, 20%, and 25% GP replacement levels with different NS content was 0.24, 0.19, 0.1, and 0.05%, respectively (shown in Figure 5.7). It is noticeable that, for the same replacement level of GP, NS's effect on expansion can be negligible, especially in high-level replacement of GP (20%, 25%).

Figure 5.8 shows the reduction level of ASR expansion in comparison to control bars. 25% replacement of GP gave the highest reduction level of expansion, reaching 86.1% in 25GP2NS. The expansion in bars reached the unreactive level with 20% GP replacement. Probably because of the small effect of NS on mitigating ASR expansion, as discussed in Figure 5.1, its effect together with GP can't be noticed in comparison with the impact of GP in mitigating.

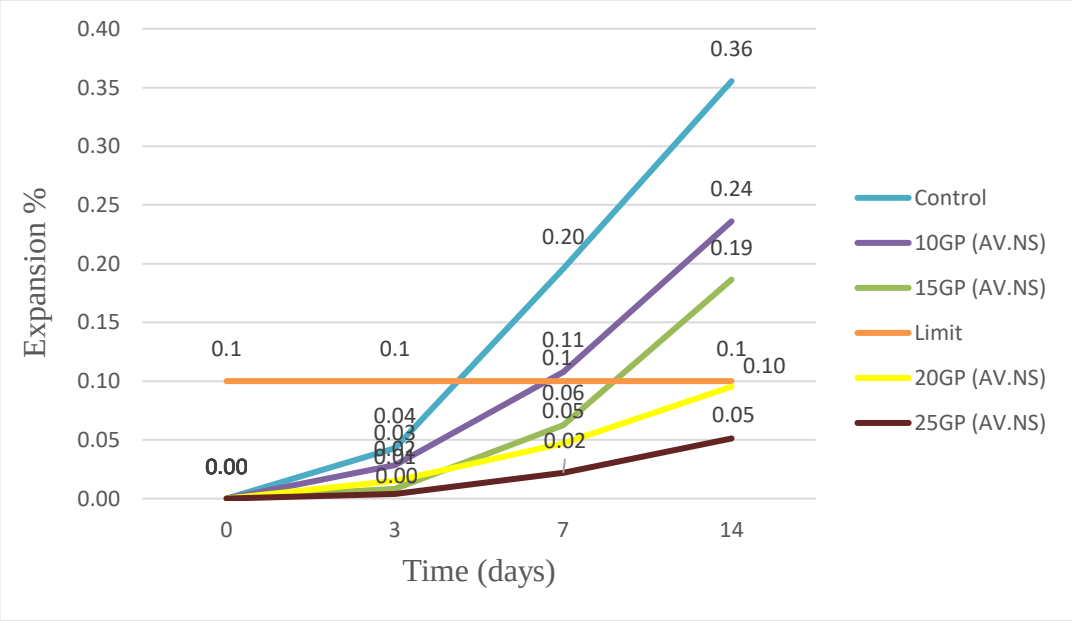

Figure 5.7: The average of 10%, 15%, 20%, and 25% waste glass powder with (0, 1, 1.5, and 2% Nano silica).

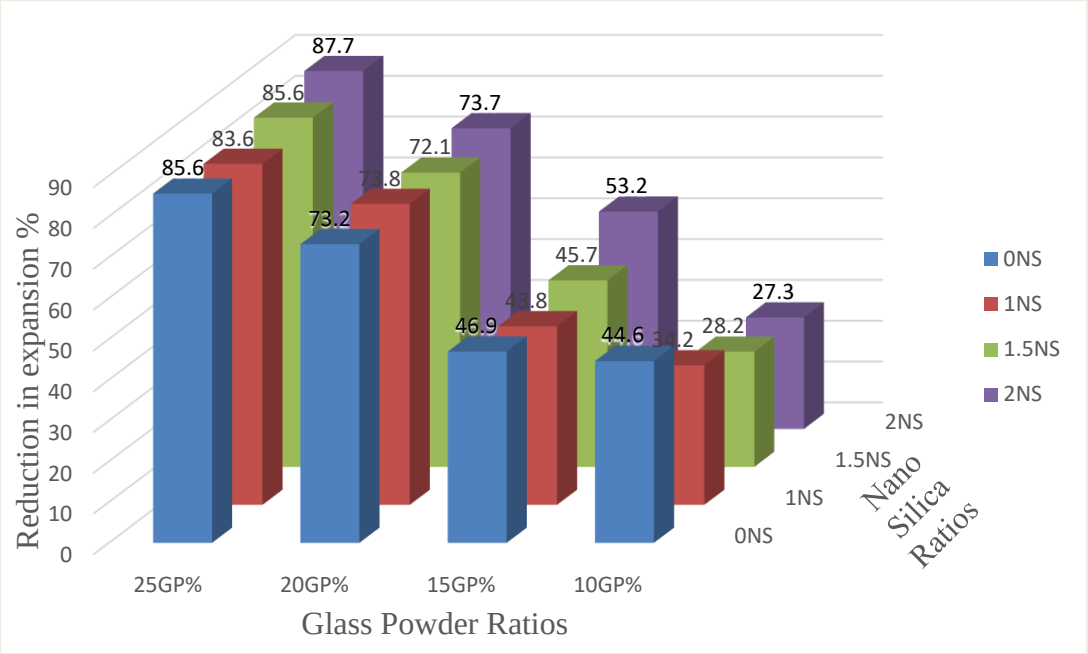

Figure 5.8: The reduction in expansion with different combinations of WGP and NS content.

5.2 Flexural Strength Tests at 7 and 28 Days

5.2.1 Flexural strength at 7 days

The flexural strength was applied to the prismatic specimens according to (BS EN 196-1). The load was applied in the middle of the specimens from the vertical direction. The highest load was recorded, and the flexural strength was calculated, as mentioned in Chapter 4. Figure 5.9 shows the variation of flexural strength at seven days for different combinations of GP and NS used in the study. The overall flexural strength ranges from 6.5 to 8.2 MPa. It shows that increasing the WGP replacement level in mortar has a reduction effect on the flexural strength. At the same time, increasing the NS ratio helped improve flexural strength compared to specimens without NS. For example, for mortars with 20% GP content with 0, 1%, 1.5%, and 2% NS, the results are 7.1 MPa, 7.0 MPa, 7.20 MPa and 7.5 MPa, respectively.

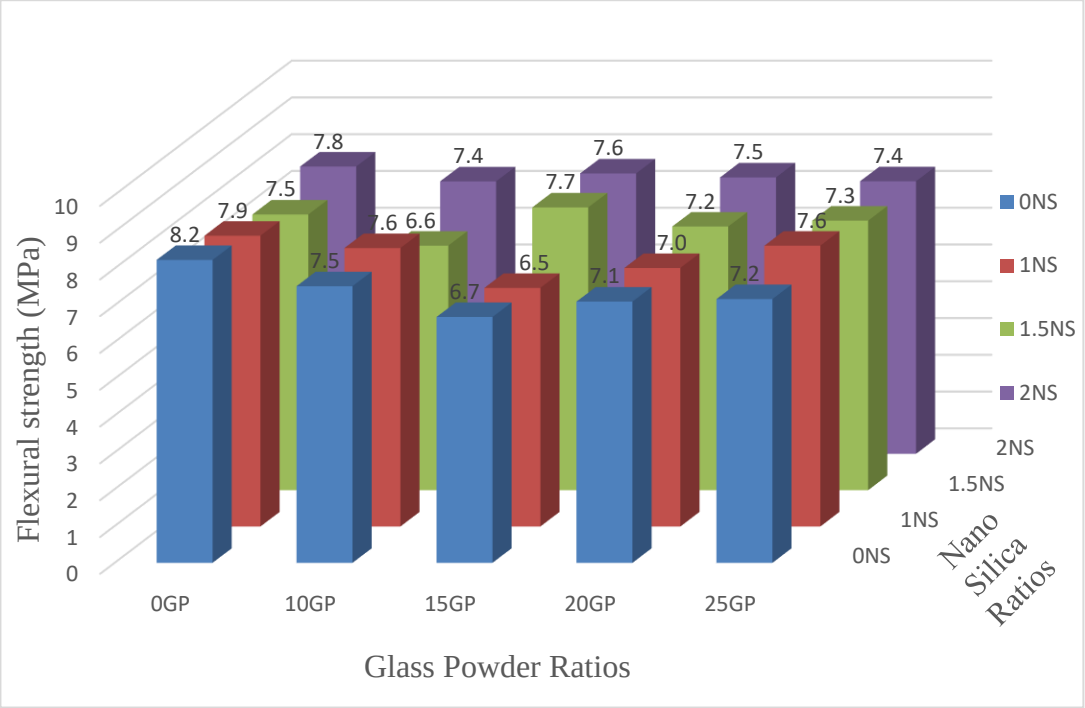

Figure 5.9: Effect of glass powder and nano silica on the 7-days flexural strength.

5.2.2 Flexural strength at 28 days

Figure 5.10 shows the relationship between flexural strength and different mortars with various GP and NS replacement levels at 28 days. At this age, the range of flexural strength is 6.5 MPa to 10 MPa. Adding only GP decreased the flexural strength with the increase in GP content. The role of using NS after an early age was less effective compared to the results from 7 days. That proves NS's fast pozzolanic reaction and seeding effect at an early age, as Hou et al. (2015) and Cai et al. (2019) mention.

These results are accommodated with some literature reviews investigating the effect of NS on the initial setting time and initial hardening process (Güneyisi et al., 2016; Nigam and Verma, 2023). Adding NS forms more H_2SiO_2 in the hydration process, which reacts with more Ca^{+2} ions, generating more C-S-H (Nigam and Verma, 2023).

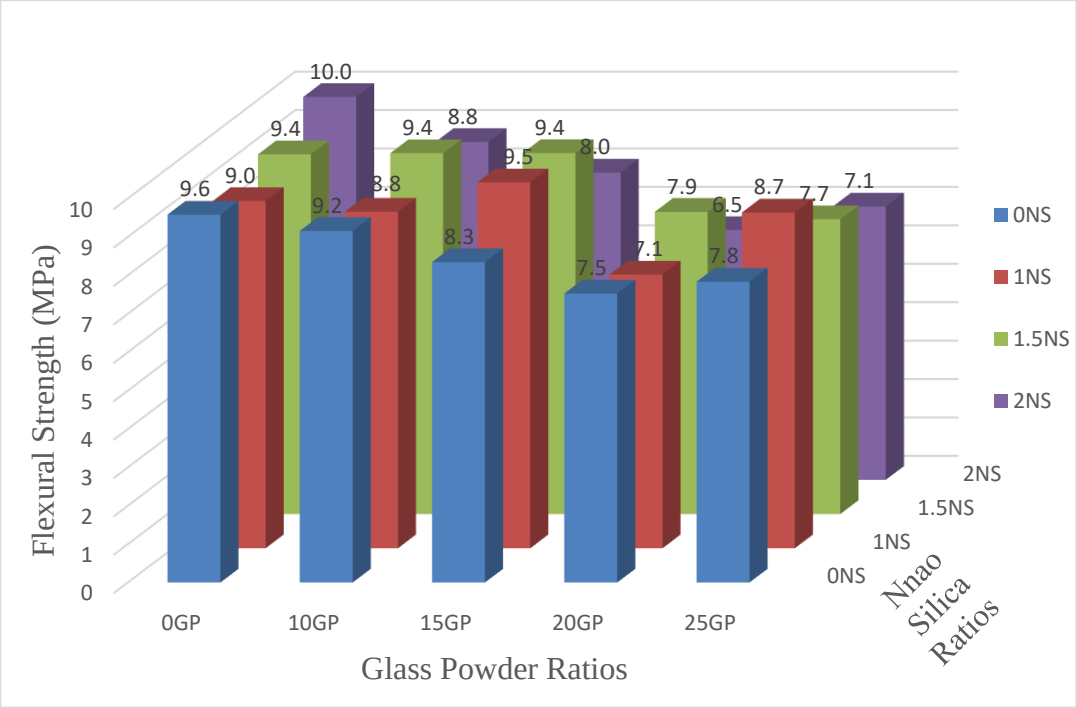

Figure 5.10: Effect of glass powder and nano silica on the flexural strength at 28 days.

5.2.3 Reduction ratios of flexural strength

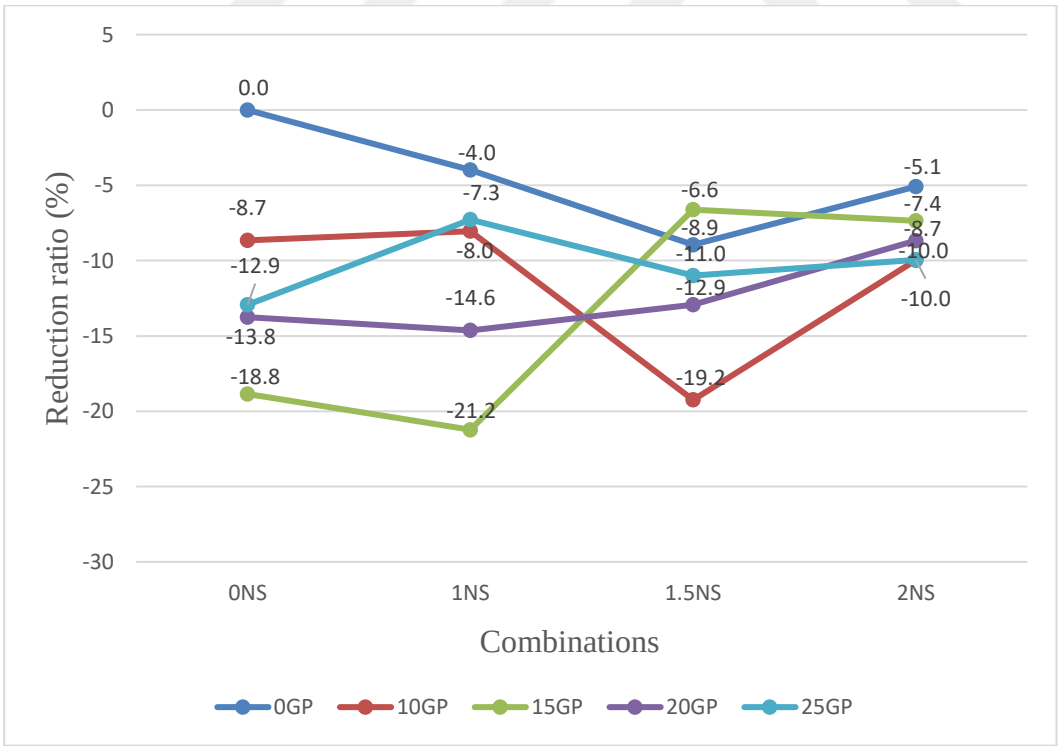

Figure 5.11: Reduction ratios for different combinations of flexural strength at seven days.

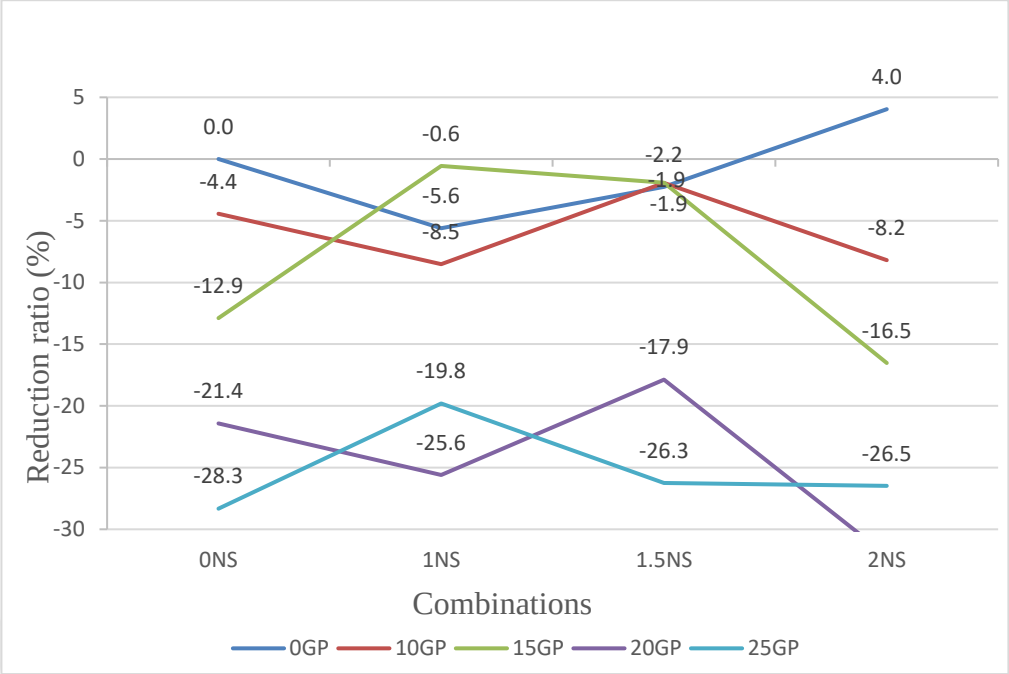

Figure 5.12: Reduction ratios in flexural strength for different combinations at 28 days).

Figures 5.11 and 5.12 show the reduction ratio in flexural strength for all combinations used in this study compared to control mortar at 7 and 28 days, respectively. For seven days of tests, we noticed flexural strength reductions for all GP and NS replacement levels. The highest reduction ratio was 21.2% for 15GP1NS, and there was no recording of an increase in flexural strength. On the other hand, at 28 days results, a reduction in flexural strength with GP replacement level was noticed. The highest decrease was 28.3%, recorded in the 25GP0NS specimen. These results are similar to other studies (Shoaeia et al., 2020).

5.3 Compressive Strength (7 and 28 days)

The compressive strength test was conducted using the compressive machine. Half of the specimens were broken in flexural strength tests used in the compressive strength tests. The test was applied over mortars with 40*40 mm. cross-sectional area of the specimens.

5.3.1 Compressive strength at 7 days

Figure 5.13 shows the variation in compressive strength at 7 days. Compressive strength values ranged from 57.1 MPa in 2NS mortar to 32.5 MPa in 25GP2NS. As shown in Figure 5.13, with the increase of GP's replacement level (without NS), the

compressive strength reduced from 51.8 MPa in the control mortar to 32.6 MPa in the 25GP0NS mortar. The compressive strength in mortars with only NS increased from 51.8 MPa to 57.1 MPa in 2NS mortar. In mortars with combinations between GP and NS, with increasing NS ratio, the compressive strength increased, especially in 10% and 15% GP mortars. With 20 and 25% of GP, the enhancement of NS in compressive strength is not considerable. The results accommodated different studies that mentioned the effect of NS on compressive strength, especially at early ages (Cai et al., 2019). This is because of the fast pozzolanic reaction and seeding effect of NS (Singh, et al., 2016).

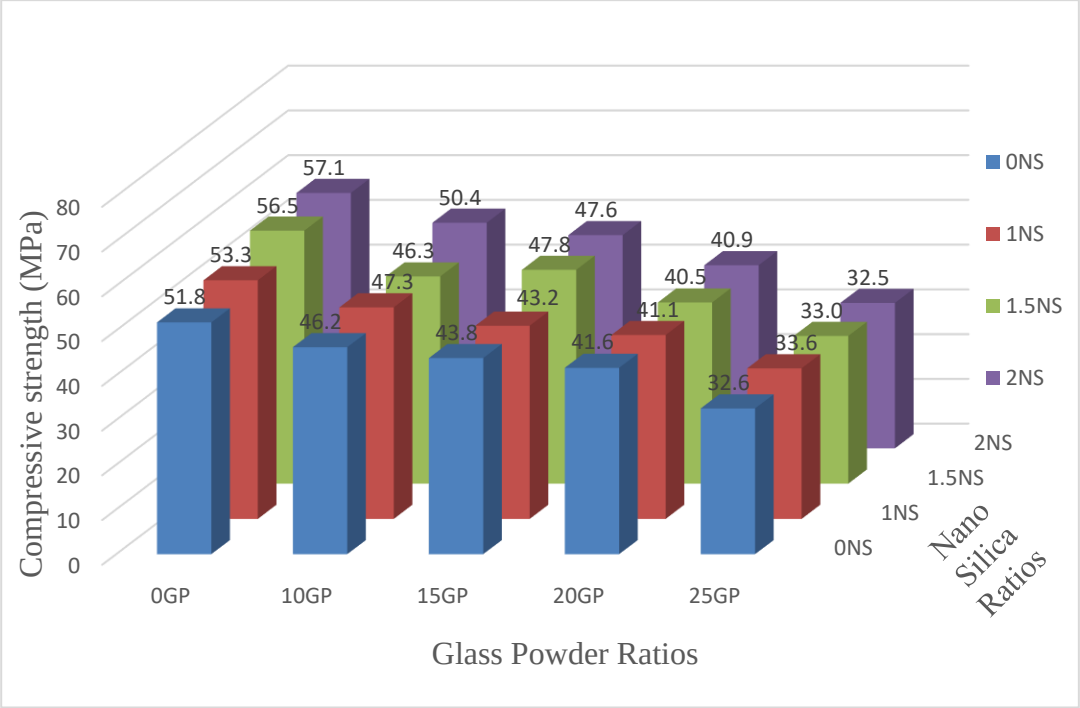

Figure 5.13: Effect of glass powder and nano silica on compressive strength at 7 days.

5.3.2 Compressive strength at 28 days

Figure 5.14 shows the variation in compressive strength at 28 days for different combinations used in this study. Compressive strength values ranged from 72 MPa for 2NS to 49.8 MPa for 25GP0NS. The results show that more GP content results in less compressive strength, which is predicted to be the case after flexural strength results. The role of NS in increasing strength is evident, but the enhancement in strength was less in comparison to early-age results. The increase of compressive strength after 28 days proves again the lower reactivity of GP at early ages, as found in flexural strength. Another study mentioned the same results (Petal et al., 2019).

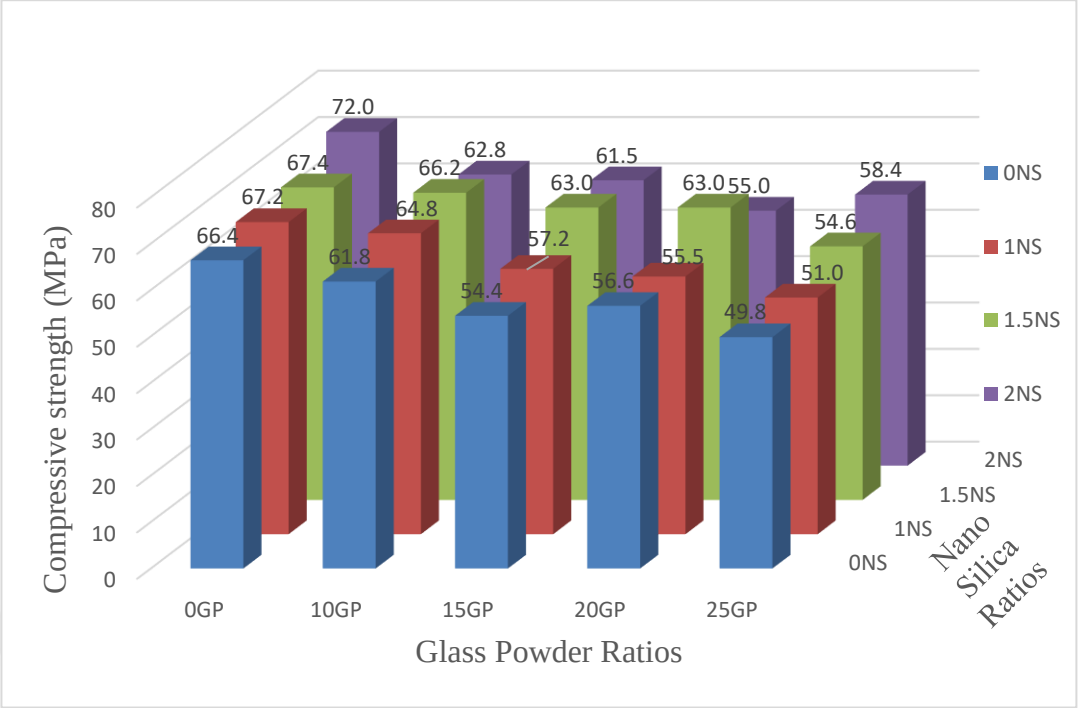

Figure 5.14: Effect of glass powder and nano silica on compressive strength at 28 days.

5.3.3 Reduction ratio of compressive strength

Figures 5.15 and 5.16 show the reduction in compressive strength for 7 and 28 days, respectively. The highest reduction ratio in 7 days' results was 37.2% for 25GP2NS mortar and 25% for 28 days' results for mortar with 25GP0NS. The effect of using NS was more apparent at 7 days; the compressive strength increased to 10.20% in mortar with 2NS in comparison to the control mortar. The increase in compressive strength in mortar with 2% NS at 28 days was 8.4%.

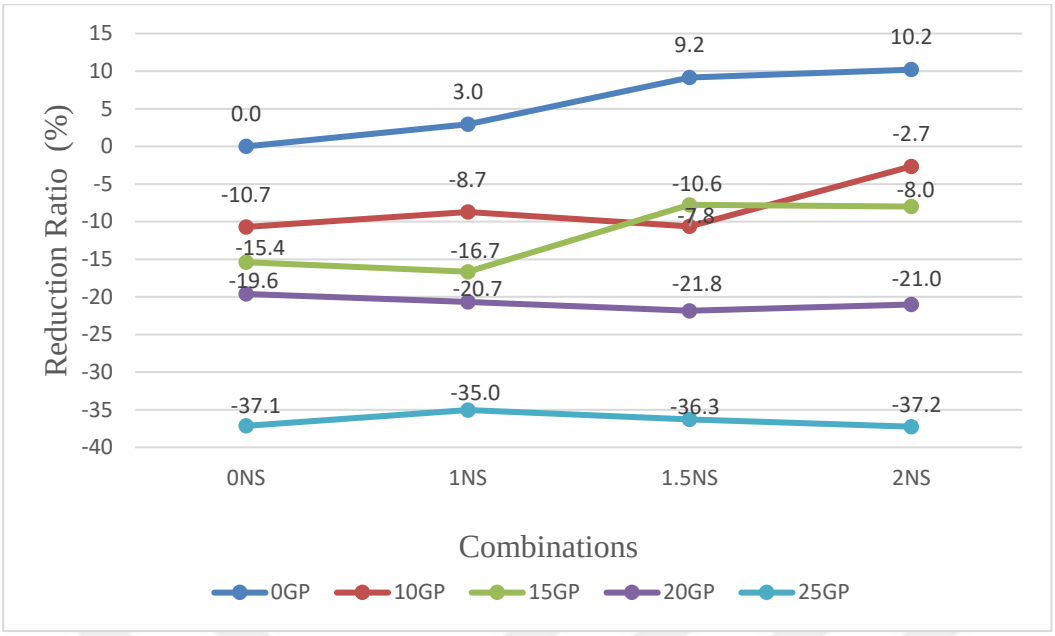

Figure 5.15: Reduction ratio in compressive strength for different combinations at 7 days.

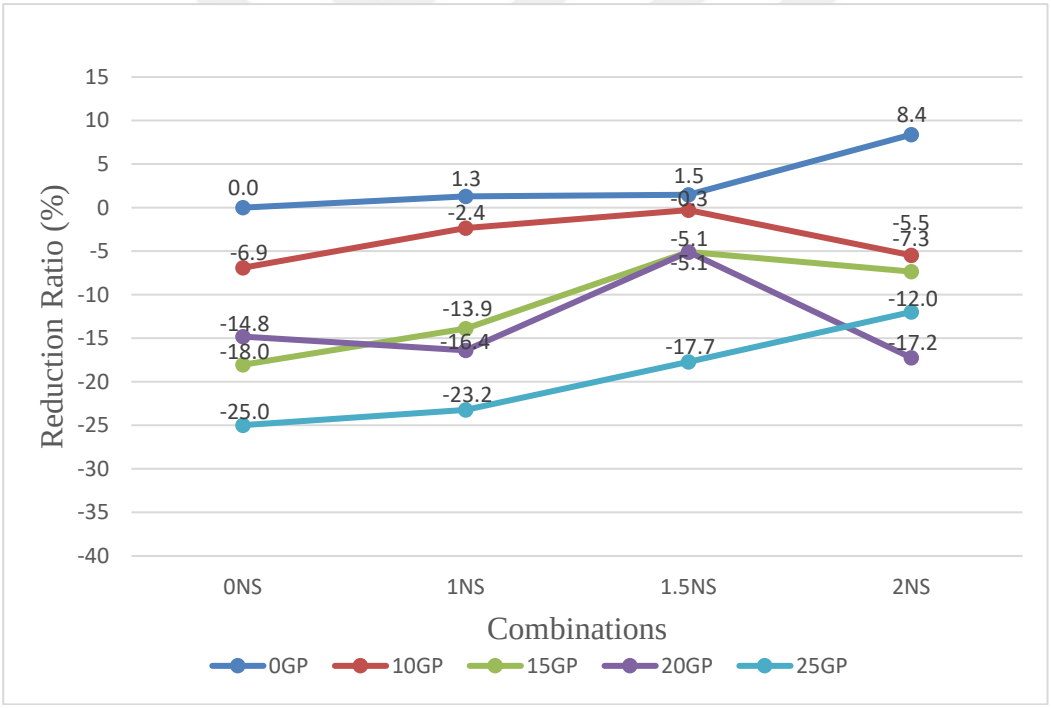

Figure 5.16: Reduction ratio in compressive strength for different combinations at 28 days.

5.4 Capillary Water Absorption

Capillary water absorption refers to the ability of a porous material to absorb water into its pores against the force of gravity. This absorption occurs due to the capillary action of the material's pore structure, which draws water upward through narrow channels.

Capillary water absorption can significantly impact the durability and performance of building materials. When moisture is absorbed into a material's pores, it can cause damage through freeze-thaw cycles, chemical reactions, or simply by increasing the material's weight and reducing its strength. Additionally, excessive moisture absorption can lead to mold growth and other forms of degradation.

To prevent capillary water absorption, building materials can be treated with water-repellent coatings or sealants that block the pores and prevent moisture from entering. Alternatively, materials can be designed with a more closed-pore structure that limits the ability of water to enter. Understanding the characteristics of varied materials' capillary water absorption is essential in building design and maintenance.

According to ASTM C1585 and BS EN 1015-18, the ability of specimens to absorb water through their capillary pores was measured. The measurement for ASTM C1585 was up to 24 hours, and for BS EN 1015-18, the calculations need to be read at 10 and 90 minutes only. Table 5.1 presents the intervals in which the specimens were weighed and recorded for both standards.

Table 5.1: Readings' time for capillary water absorption test.

Time	60s	5min	10min	20 min	30 min	60 min	90 min	Every hour up to 6 h	24 h
Tolerance	2s	10s	2 min	2 min	2 min	5 min	5 min	5 min	Two h

The calculations for BS EN-1015-18 were done in equation (5.1):

$$C = 0.1*(M_2 - M_1)\ kg/(m^2.\ min^{0.5}) \quad (5.1)$$

M_1 and M_2 represent the weight of specimens after 10 min. and 90 min. from the beginning of the test. The water absorption coefficient equals the straight line slope linking the representative points of the measurements carried out at 10 min and 90 min (Considered 0.1) (BS EN-1015-18).

The calculations for ASTM C1585 were done according to equation (5.2):

$$I = m_t / a*d \quad (5.2)$$

I = the absorption,

m_t = the change in specimen mass in grams at the time t.

a = the exposed area of the specimen in mm^2.

d = the density of the water in g/mm^3.

(I) is the absorption calculated by dividing the change in mass by the product of the test specimen's cross-sectional area and the water's density. For this test, the temperature dependence of the water density is ignored, and a value of 0.001 g/mm3 is used. The units of I are mm (ASTM C1585-20).

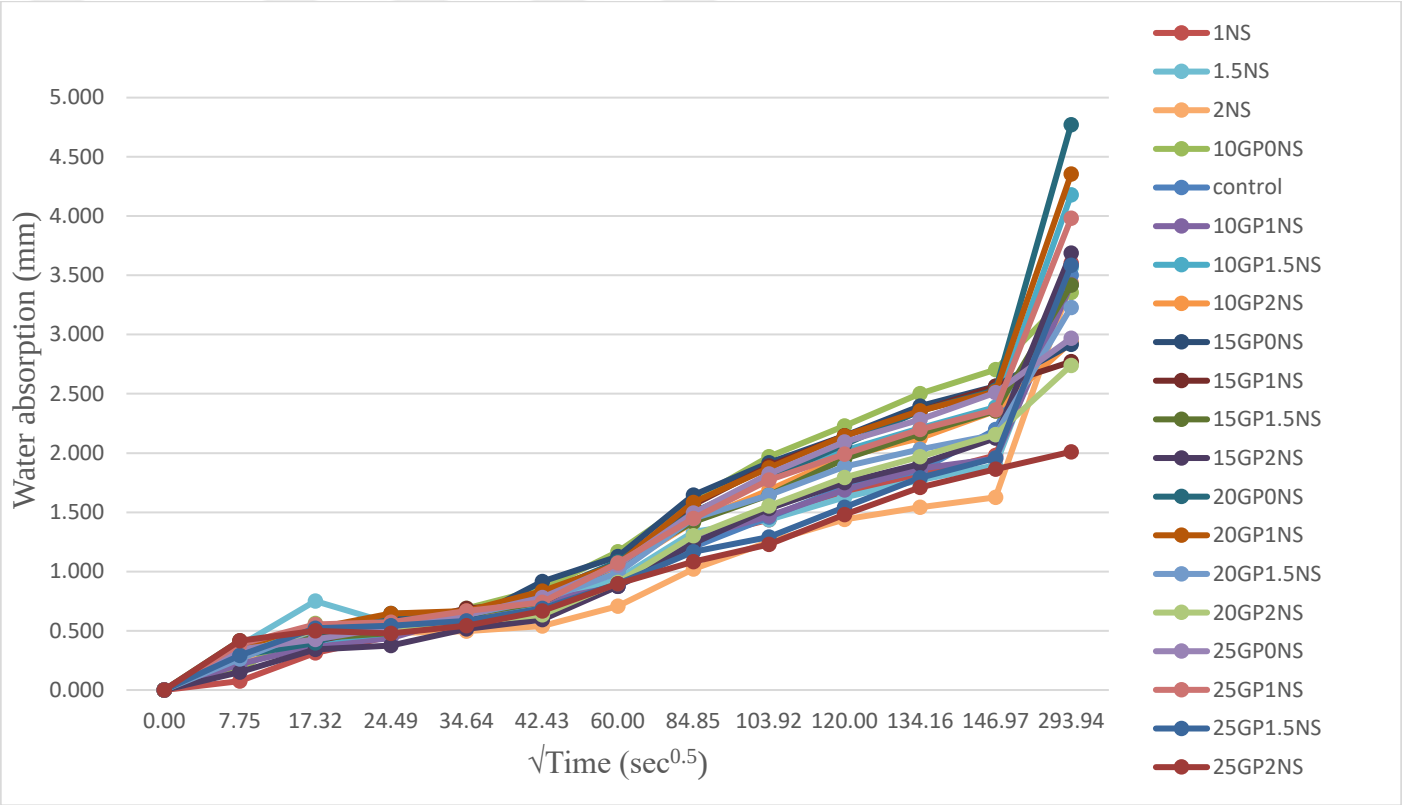

Figure 5.17: Water absorption quantity according to ASTM C1585-20.

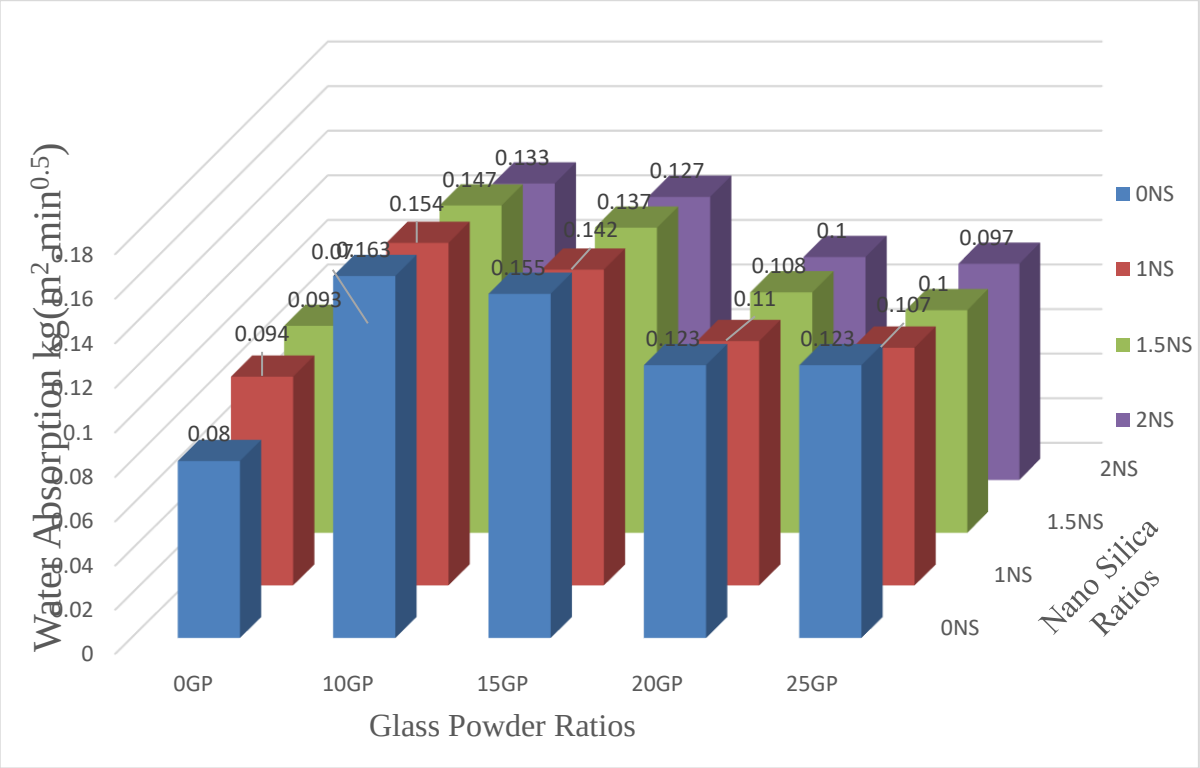

Figure 5.18: Water absorption according to BS-EN 1015-18.

Figures 5.17 and 5.18 show the relationship between water absorption according to ASTM C1585 and BS-EN 1015-18, respectively, and different mortars with different WGP and NS content. They show that the least amount of water to be absorbed is noticed in the control specimen. Adding NS with 1% and 1.5% absorbed more water through the test's time but, at the same time, started to decrease the ability to absorb water with the increase of NS's percentage.

In specimens with WGP content, increasing the percentage of WGP decreases the amount of water absorbed. Also, WGP with NS reduces water absorption more than the specimens with the same amount of WGP but with a lower percentage of NS. We can conclude that waste glass powder can be considered a filling material that reduces the ability of water to get into the pores, especially in early ages before the reaction activity of WGP appears effectively. Also, NS has the same effect, and the best combination of WGP and NS is the highest amount (25GP2NS).

5.5 Thermogravimetric Analysis (TGA)

TGA is often used to study materials' thermal stability, decomposition, oxidation, and moisture content. In this study, TGA is used to determine the percentage of consuming $Ca(OH)_2$, which gives us insight into the pozzolanic effect of WGP.

In TGA, the specimens go through 3 separate phases with the increase in temperature, as mentioned by Jiang et al. (2022):

Phase 1: The weight loss was mainly induced by water evaporation and dehydration of hydrated silicates when the temperature rose to 100˚C–150˚C.

Phase 2: The weight loss was mainly induced by the decomposition of $Ca(OH)_2$ and the formation of CaO when the temperature rose to 400˚C–500˚C.

Phase 3: The weight loss was mainly induced by the decomposition of $CaCO_3$ when the temperature rose to 700˚C–800˚C.

To evaluate the change in CH content, the section of the TGA curve between 400 ˚C and 600˚C was used to calculate the CH by Equation (5.3) (Aliabdo et al., 2016):

$$CH\ (\%) = W_T \times (W_{CH} / W_w) \quad (5.3)$$

Where W_T represents the total weight loss percentage between 400˚C and 600˚C, W_{CH} represents the molecular weight of $Ca(OH)_2$ (-74 g/mol), and W_W represents the molecular weight of water (-18 g/mol).

Two different specimens were chosen to be analyzed: a specimen with zero WGP content (Control) and a specimen with the highest WGP content (25%GP) without nano silica (25GP0NS).

Figure 5.19 shows the relationship between the temperature and the loss in weight in each specimen. Figure 5.20 represents the rate of weight loss in comparison with gradual temperature increases. The rate of weight loss in the control specimen (about 0.07%) is larger than the weight loss in the 25GP0NS specimen (0.03%) in intervals between 400◦C and 600˚C. The loss in weight in this interval is because of CH's content, as mentioned earlier. That proves that the amount of CH still found in the control specimen without hydration is more significant than that in the 25GP0NS specimen.

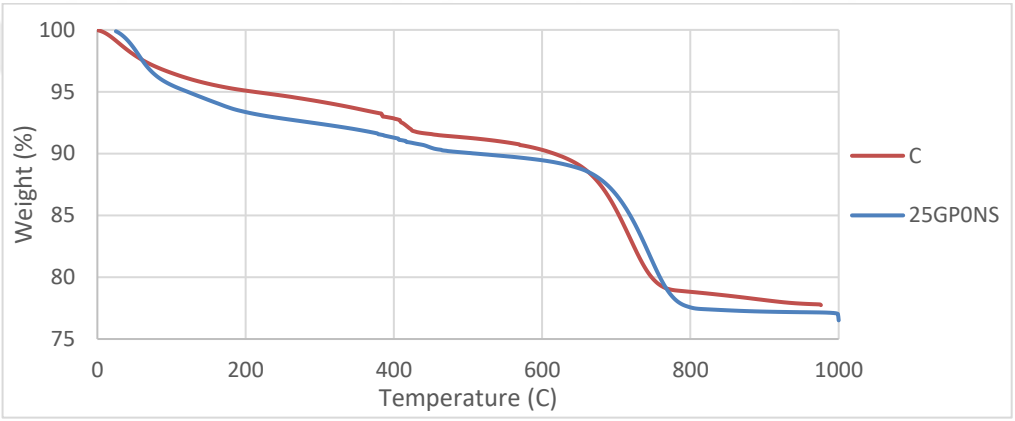

Figure 5.19: TGA curves for control and 25GP0NS specimens.

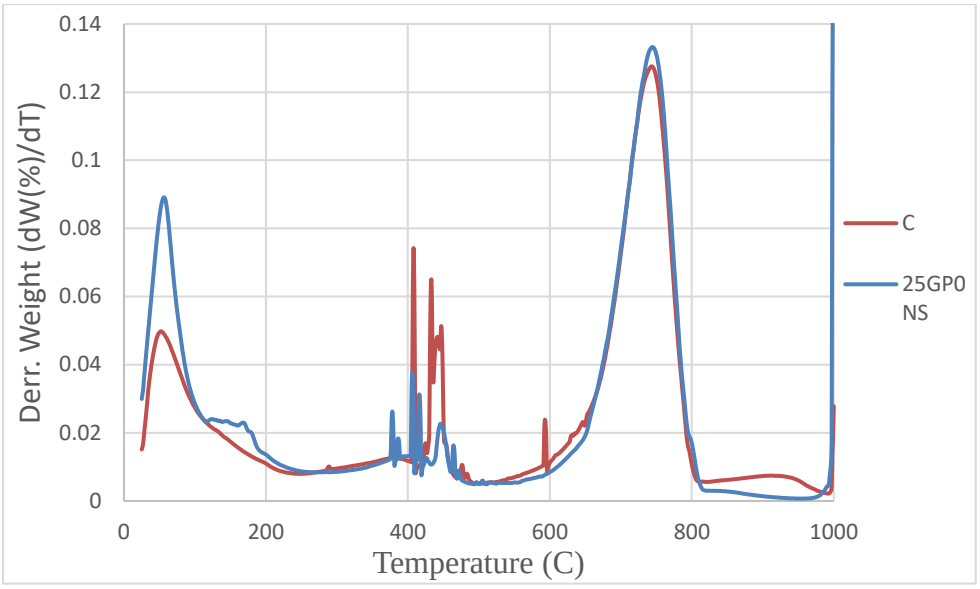

Figure 5.20: Derivative of weight and temperature for control and 25GP0NS.

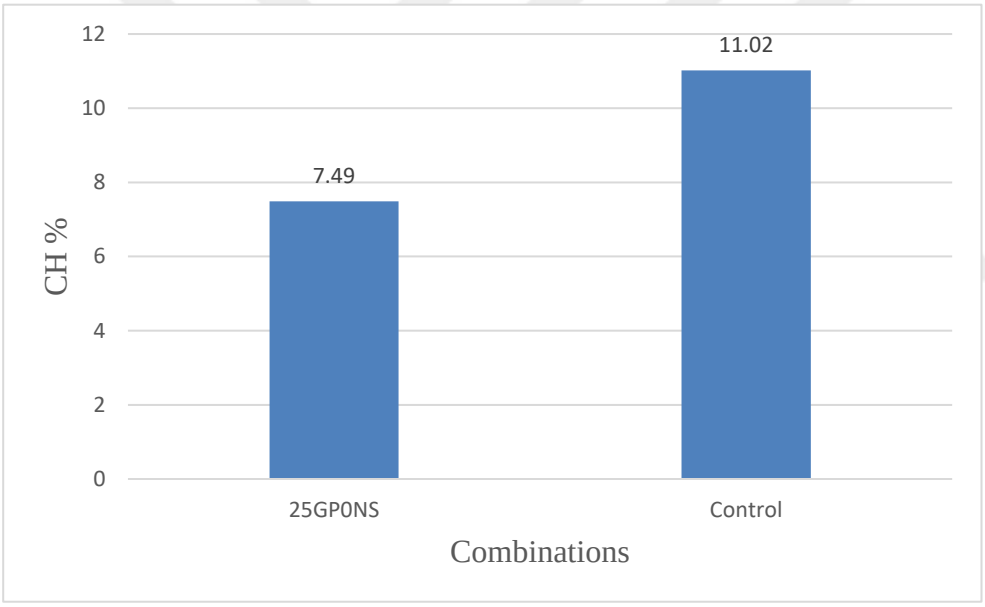

Figure 5.21: Ca $(OH)_2$ content in samples with 25% WGP additions.

To calculate CH content in control and 25GP0NS, the total weight loss percentage between 400˚C and 600˚C was calculated from Figure 5.19, and then equation 5.3 was used.

The total weight loss percentage between 400˚C and 600˚C (W_T) for:

Control = 2.68%

25GP0NS = 1.822%

W_{CH} = -74 gm/mol

Ww = -18 gm/mol

Then, we can calculate the CH percentage as follows:

For Control:

CH % = 2.68 * (-74/-18) = 11.02%

For 25GP0NS:

CH % = 1.822 * (-74/-18) = 7.49%

According to the last calculations, the percentage of consumption in the control specimen was 11.02% and 7.49% in 25GP0NS. The results confirm the pozzolanic effect of WGP, as mentioned before. Figure 5.21 shows the relationship between CH content in control and 25GP0NS specimens. It shows the reduction in CH content in the specimen with 25% GP compared to the control specimen.

5.6 Scanning Electronic Microscope (SEM)

(a)

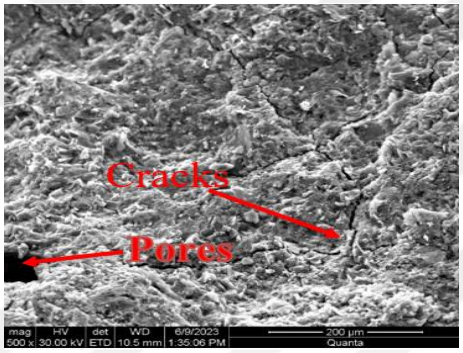

(b)

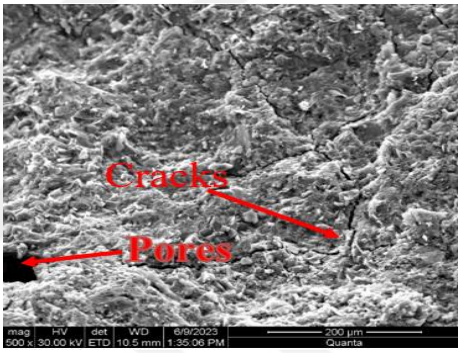

(c)

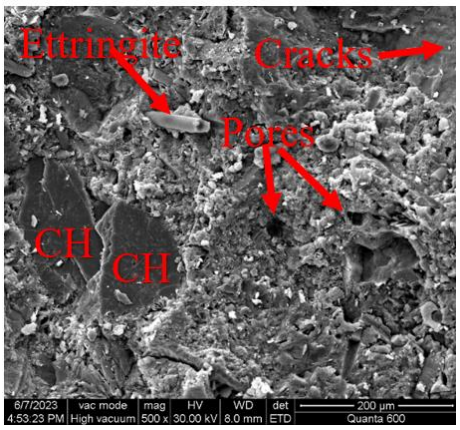

(d)

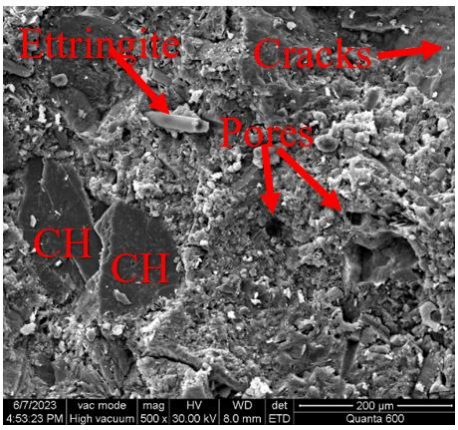

(e) 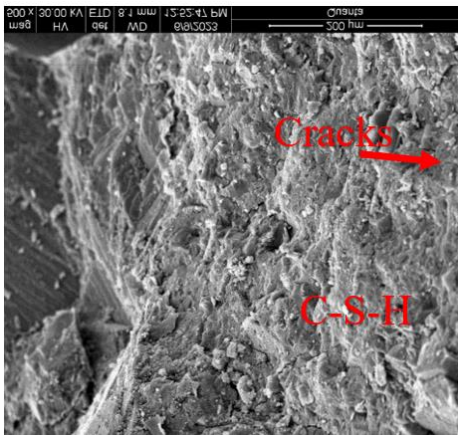

(f) 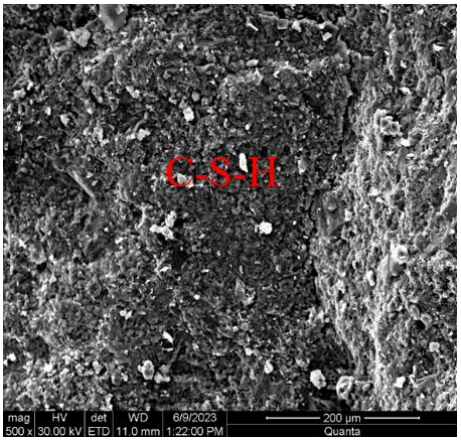

Figure 5.22: Scanning Electronic Microscope (a) SEM for control specimen (b) SEM for 2NS specimen. (c) SEM for 10GP2NS specimen. (d) SEM for 15GP2NS specimen. (e) SEM for 20GP2NS specimen. 22 SEM for 10GP2NS specimen.

Figures from 5.22 (a) to 5.22 (f) show the microstructure of different mortars after being immersed in NaOH solution for 14 days to accelerate ASR gel formation. These specimens are controlled, 2NS, 10GP2NS, 15GP2NS, 20GP2NS, and 25GP2NS, respectively. From these figures, we can notice an improvement in permeability by adding waste glass powder and nano silica. Also, ASR gel appears in control and 2NS specimens and starts to disappear by adding waste glass powder, which accommodated with results from AMBT.

The SEM images in Figures 5.22 (a) to 5.22 (b) present the control specimen and specimens with varying WGP and NS content at the age of 90 days. In Figure 5.22 (a), the cracks appeared in the control sample as evidence of forming ASR gel. Mortar with 2% NS presented a denser structure with more C-S-H formation, but the cracks were still found. Compared to the control specimen, the blended mortar with 10% WGP + 2% NS shows a little increase in hydration products and a relatively dense internal structure with the appearance of CH lamellar (Figure 5.22 (c)). When the WGP content reaches 15%, the internal structure becomes denser, and fewer CH crystals were found with more C-S-H formation Figure 5.22 (d). Figure 5.22 (e) shows that the ettringite in the hydration products of mortar with 20% WGP + 2%NS has transformed from fine to coarse, creating a three-dimensional C–S–H gel, which contributes to higher strength. Additionally, the number of pores and cracks has decreased, indicating improved compactness in the cement mortar, and an increase in WGP content promotes cement hydration. However, in the hydration product of mortar with 25% WGP (Figure 5.22 (f)), the content of C–S–H gel has increased

significantly, and the structure exhibits relatively more porosity. The SEM images affirm that the cement slurry is densest when the WGP content is 25% and 2% NS. The number of hydration products has significantly increased, with the presence of three-dimensional C–S–H gel, lamellar CH crystals, and needle-like ettringite. These hydration products overlap, and there is a substantial reduction in the number of holes and cracks, resulting in a dense network structure. That proves how effective WGP+NS in different contents is in mitigating ASR gel formation.

Despite the pozzolanic activity that WGP+NS does, the formation of C-S-H gel doesn't necessarily mean high strength in the result. It was discussed in some literature, such as Zheng (2016). According to Zheng, SCMs produce C-S-H gel with a low Ca/Si ratio, negatively affecting compressive and flexural strength.

5.7 X-ray Diffraction (XRD)

XRD results for mortars mentioned in chapter 4.8 are mentioned in this chapter. The main aim is to follow some hydration products such as CH and quartz. Figure 5.23 shows the CH content of different mortars according to the XRD test. The results will be discussed in 2 stages: first mortars with only waste glass powder and second mortars with WGP and NS. The main peaks of CH in the XRD spectra were found at 18.00° 2Θ. (d = 4.9092 A), 34.10° 2θ (d = 2.6270 A) and 47.12° 2θ (d = 1.9268 A) (Li et al., 2022). The main peaks of quartz were noticed to be at 26.6° 2θ.

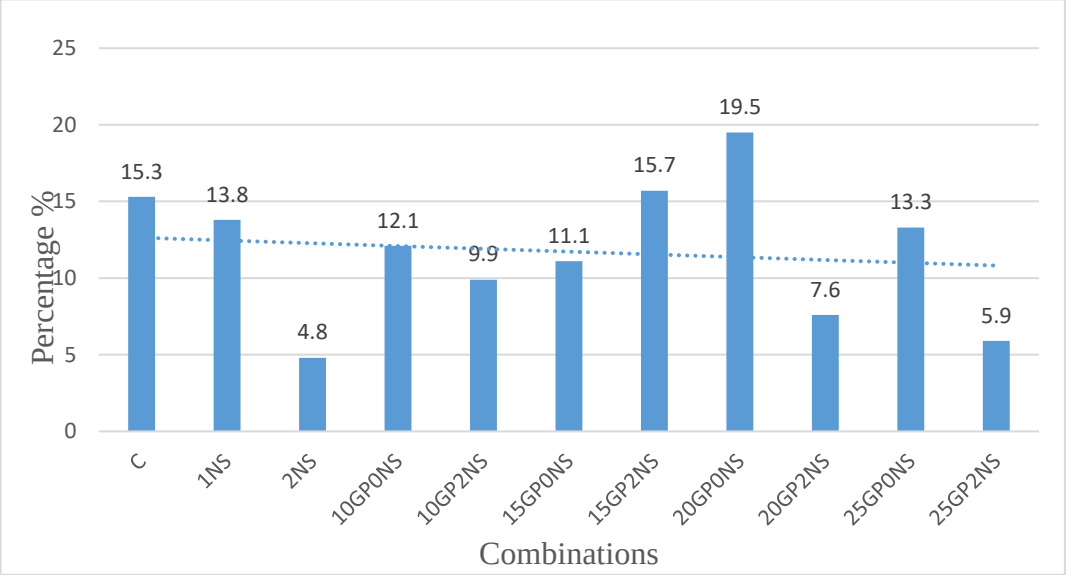

Figure 5.23: CH's percentage in mortars.

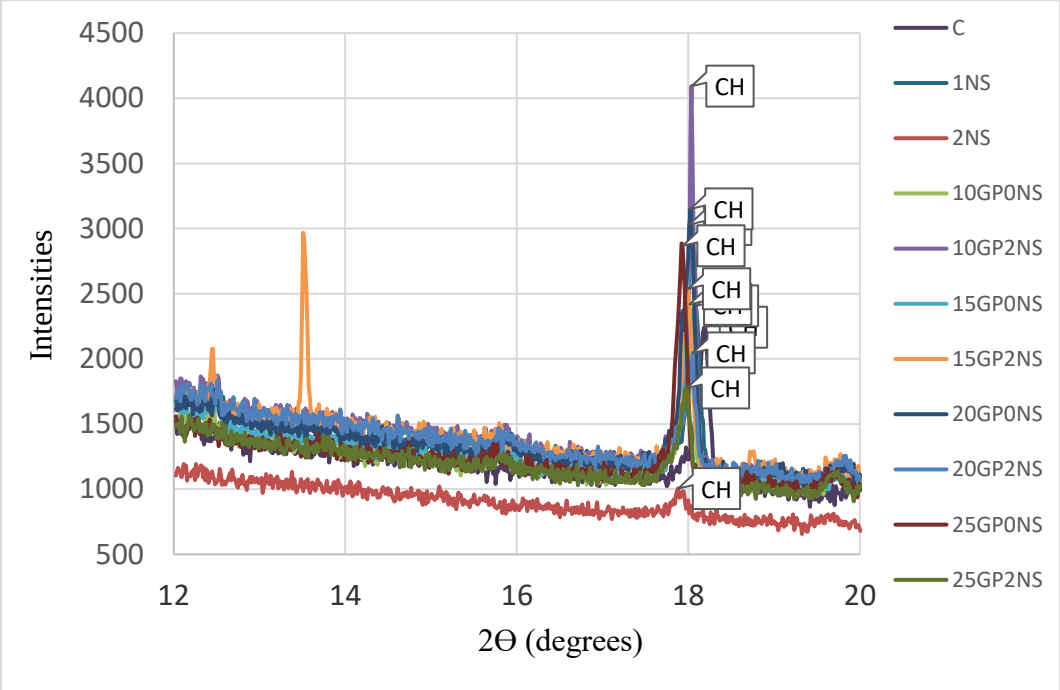

Figure 5.24: X-ray diffraction for different mortars from 12 to 20° 2θ.

5.7.1 Mortars with WGP

With a general look at all mortars, we can figure out a descending trend of CH's crystal content from control mortars up to 25% GP without NS, which is introduced in Figure 5.23. CH's crystal content was 15.3% of mortars in the control specimen, reduced to 12.1% and 11.1% with 10% GP replacement. The exception of these results was at 20%GP replacement, which may have been related to a laboratory mistake; CH's crystals were 19.5%. Finally, at 25% of GP, CH's crystal content was 13.3%. The reduction in CH's crystal content is proof of a pozzolanic activity enhancement with GP's content, which accommodated TGA's results. The same results were found in another research (Li et al., 2022).

The other deduction from XRD's results was quartz formation. In the specimens with only GP, the quartz's formation increased from 46.9% in the control specimen and reached its maximum at 20%GP replacement level to be 69.9% of the total specimen's structure. Figure 5.25 shows the formation of quartz for different combinations used in this study. Quartz's content is presented in Figure 5.25 and accommodated with results (Li et al., 2022).

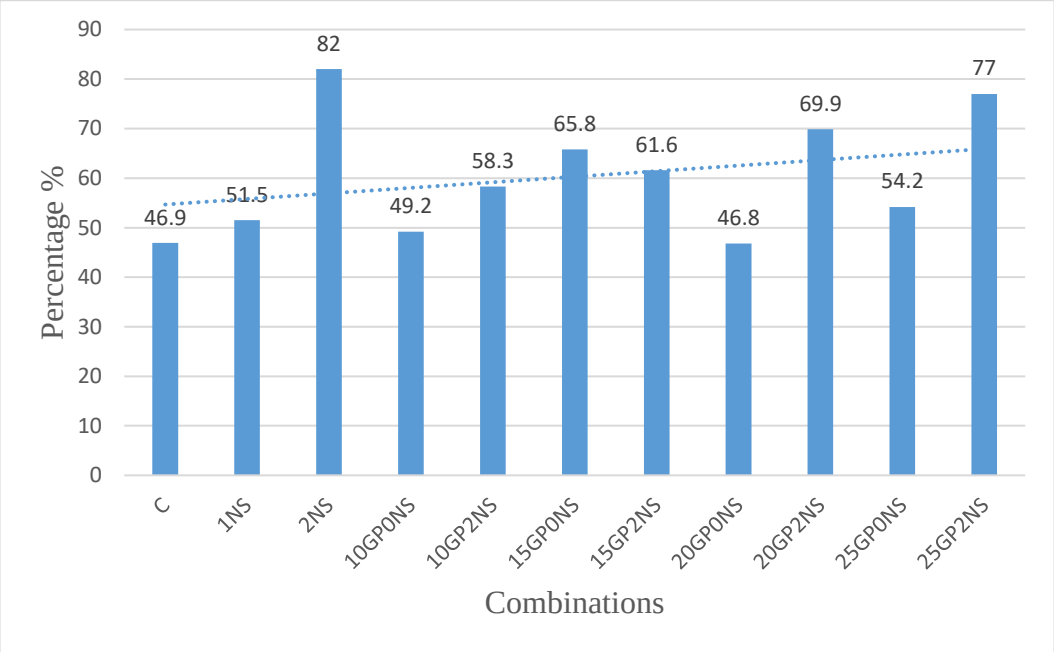

Figure 5.25: Quartz's percentage in mortars.

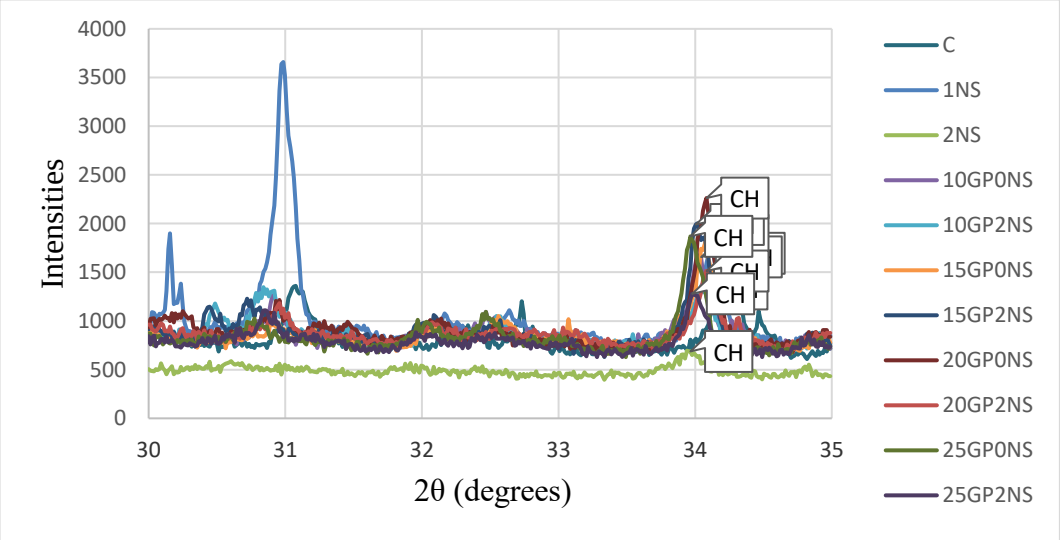

Figure 5.26: X-ray diffraction for different mortars from 30 to 35° 2θ.

5.7.2 Mortars with GP + NS

From Figure 5.23, we can see that, in comparison with control mortar, specimens with 1% and 2% NS had a reduction in CH's crystals content gradually from 15.3 to 13.8 and 4.8%, respectively. Also, except in 15GP2NS mortar, NS and GP content in mortars effectively reduced the CH's crystals content. CH's crystal content was reduced from 15.3% in the control specimen to 5.9% in the specimen with 25GP2NS. We can conclude that NS helped to increase the pozzolanic reactivity in specimens containing GP.

Figures 5.24 and 5.26 show the results of the XRD test in the intervals between (12-20) and (30-35) of 2Θ in degrees, respectively. The results showed a noticeable reduction in CH's peaks' intensities with specimens containing NS, which proves NS's role in the pozzolanic reaction.

The effect of NS in increasing the quartz formation as a primary and secondary cementitious replacement appeared in Figure 5.30. In specimens with 1 and 2% of NS, the quartz formation increased from 46.9% in the control specimen to 51.1 and 82%, respectively. In specimens with GP and NS, the formation level of quartz increased in 10GP2NS, 20GP2NS, and 25GP2NS compared to specimens with the same replacement level of GP only.

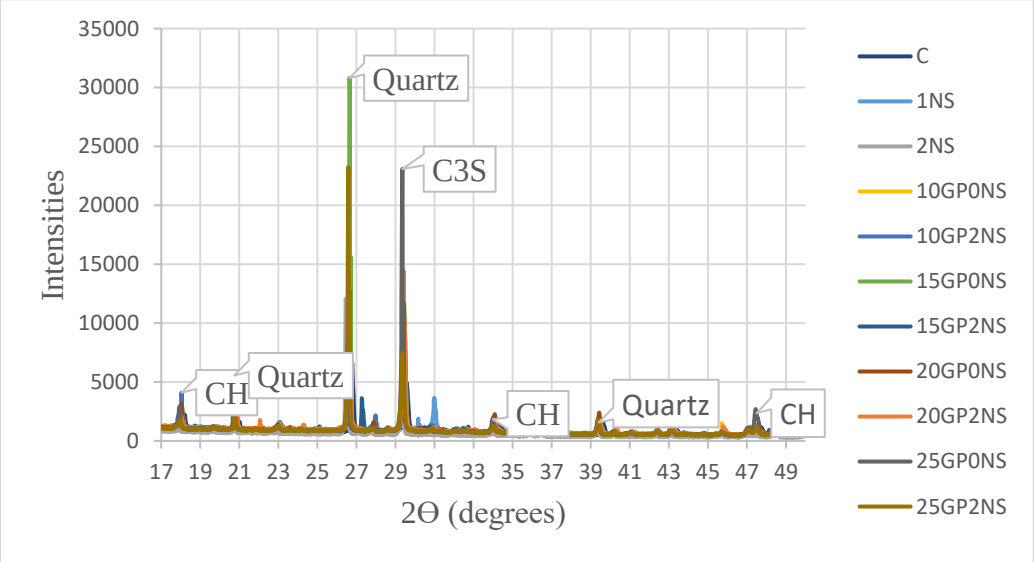

Figure 5.27: X-ray diffraction for different mortars from 17 to 50° 2θ.

Figure 5.27 shows the different peaks introduced in the XRD test. It is noticed that the most intense peak was found to be the quartz and, followed by C_3S (Alite).

6. DISCUSSION

The level of ASR expansion was affected by different proportions of glass powder added. The mechanical properties, such as compressive and flexural strength, are also affected. In this chapter, I will try to explain the mechanism by which WGP and NS mitigated ASR and affected compressive and flexural strength using the findings from TGA, SEM, and XRD tests.

6.1 AMBT Test

Accelerated mortar bar test results show how effective glass powder was in reducing ASR expansion. 10%, 15%, 20%, and 25% glass powder replacement gave 33%, 47%, 72%, and 86% reduction percent in expansion, respectively. It is more effective than other studies that used glass powder as a cement replacement (Jani and Hogland, 2014; Zheng, 2016). As mentioned in ASTM C1778-22, the expansion ratio target to consider these aggregates are not reactive or the ASR will not cause a damage expansion in concrete is 0.1%. According to our results, 20% and 25% replacements achieve 0.1% and 0.05% expansion, respectively.

Different studies tried to explain why glass powder mitigates ASR, mainly when waste glass is used as an aggregate. It is considered to achieve ASR risk. One of these studies was conducted by Zheng (2016). According to his study, glass powder has a pozzolanic reaction like SCM when it reacts with portlandite to form C-S-H gel. The primary responsibility for the pozzolanic reaction was the Si content in glass powder, which is the main element in glass in terms of chemical composition. The amorphous nature of silica in the glass helps accelerate the reaction with Ca^{+2} in the solution to form more C-S-H and reduce free Ca^{+2} in the pore solution. Glass powder and CH react to produce more C-S-H and improve the pozzolanic reactivity of GP (Ke. et al., 2018) The pozzolanic reaction was confirmed in our study by XRD and TGA results. According to Zheng (2016), two types of C-S-H are formed: the outer and inner layers. The inner layer is noticed to be around glass particles directly in SEM images. The outer layer has a low Ca/Si ratio in the appearance of glass powder, which will affect the mechanical properties as discussed. The Ca/Si ratio reduction makes the formed ASR gel have properties close to the C-S-H gel and affects its swelling and expansion properties.

According to Zheng, (2016) Al ratios in specimens with glass powder content tend to increase over time. It is known that Al ratios in glass are limited. So, the increase of Al in the solution is not from glass. The other two compounds that have high Al ratios are ettrengite and monosulfate. From the XRD test that Zheng made, the level of ettringite stays constant; on the other hand, the level of mono sulfate decreases with time. We can conclude that monosulfate is the primary source of Al in the pore solution. Al has an essential role in mitigating ASR expansion. Al reduces silica dissolving by incorporating it into silica surfaces according to the field of geology and chemistry (Zheng, 2016).

Mortars with WGP showed a remarkably denser structure even after being exposed to temperature and moisture for 14 days, which helped to prevent the forming of ASR gel. This denser structure was because of the filling effect of WGP. From our study, the XRD test showed an increase in forming quartz, which is a well-organized crystal. The increase in quartz formation is because of the increase in Si content by adding more WGP. The stable form of quartz prevents excessive amounts of Si from reacting with alkalis and forming ASR gel.

6.2 Compressive Strength (7-28 days)

Compressive test results show a reduction in compressive strength by the waste glass powder replacement level at 7 and 28 days. Figure 5.15 showed a reduction in compressive strength by 10.7%, 15.4%, 19.6%, and 37.1% in mortars with 10%, 15%, 20%, and 25% of GP at 7 days, respectively. As shown in Figure 5.16, compressive strength decreases by 6.9%, 14.8%, 18%, and 25% in mortars with 10%, 15%, 20%, and 25% of glass powder, respectively (with 0% of nano silica). By increasing the percentage of nano silica, the reduction percentage in compressive strength starts to decrease. At 7 days, the reduction in compressive strength was 2.7%, 8%, 21%, and 37.2% for 10GP2NS, 15GP1.5NS, 20GP2NS, and 25GP2NS, respectively. For 28 days, the reduction percent was 5.5%, 7.3%, 12%, and 17.2% at 28 days for 10GP2NS, 15GP1.5NS, 20GP2NS, and 25GP2NS, respectively. Mortars with only NS increased the compressive strength by 10.8% at 7 days. At 28 days, the mortars with NS increased the compressive strength by 8.4% in comparison to the control mortar. These results confirm the effect of NS at an early age. Also, the

results confirm the delay of hydration in mortars with GP as the results at 28 days were much better than 7 days.

We can find some inconsistent results by increasing nano silica's content. This is because of some reasons. Colloidal nano-silica has an agglomeration effect, especially in 2% and more. This phenomenon makes nano silica particles collected in points rather than dispersed in the whole mortar, creating weak points in the mortars. This phenomenon was mentioned in some studies (Elkady et al., 2013). the agglomeration of nano silica was evident during the production process. Some leftover nano silica was noticed to be collected at the bottom of the bottle while adding it to the bowl. This is the other reason that affected the results slightly.

According to ASTM C618, the strength index needed to accept any material as a pozzolanic material was 75% and 85% of the control sample for 7 and 28 days, respectively. For 7 days, all mortars achieved the strength index requirement except mortars with 25GP0NS, 25GP1NS, 25GP1.5NS, and 25GP2NS.

At 28 days, all mortars achieved the requirements except 25GP0NS, 25GP1NS, 25GP1.5NS, and 20GP2NS. The main note in recording these results was the reduction in compressive strength, although the pozzolanic reaction was noticed by TGA results and in mitigating ASR expansion, as discussed earlier. That may return to the leak of Portlandite in the mortars, and the C-S-H gel formed from the mix between glass powder and Portland cement has a lower Ca/Si ratio, affecting the gel's stiffness properties.

6.3 Flexural Strength (7-28 days)

The results of flexural strength show a little reduction compared to compressive strength. The strength is almost the same with increasing of glass powder. Unlike compressive strength, adding nano silica didn't affect flexural strength. Some studies observed these results (Turkmenoglu et al., 2022). This study investigated the synergistic effect of nano and micro silica and their combination. They found that nano silica had a negative effect on the brittleness of the concrete. They recorded that effect by calculating the ratio between flexural strength and compressive strength. The reduction in ratio means increasing in the brittleness of the concrete. Identical

results were found in our study. Figures 6.1 and 6.2 show the percentage of flexural to compressive strength for 7 and 28-day results.

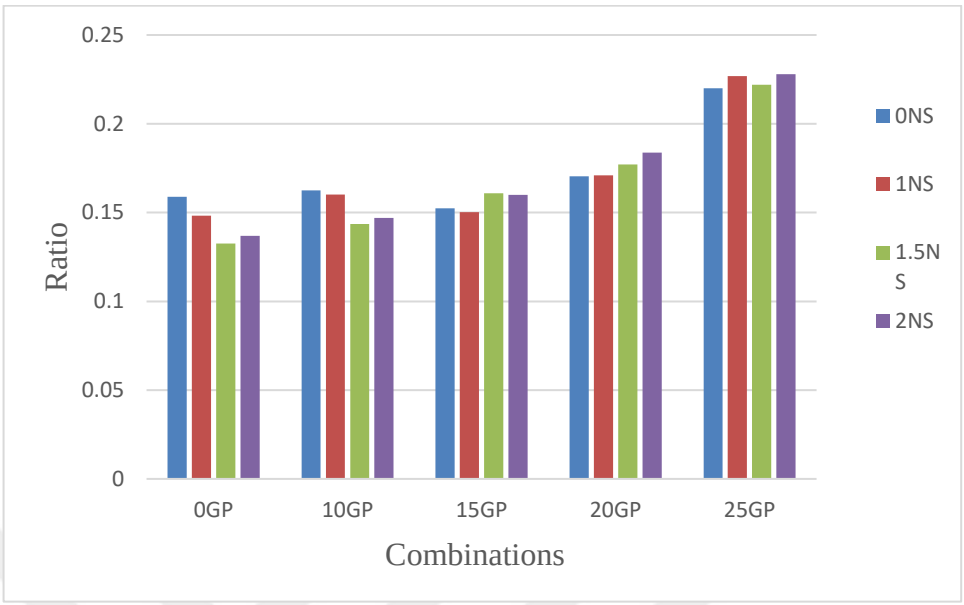

Figure 6.1: Ratio between flexural and compressive strength (7 days).

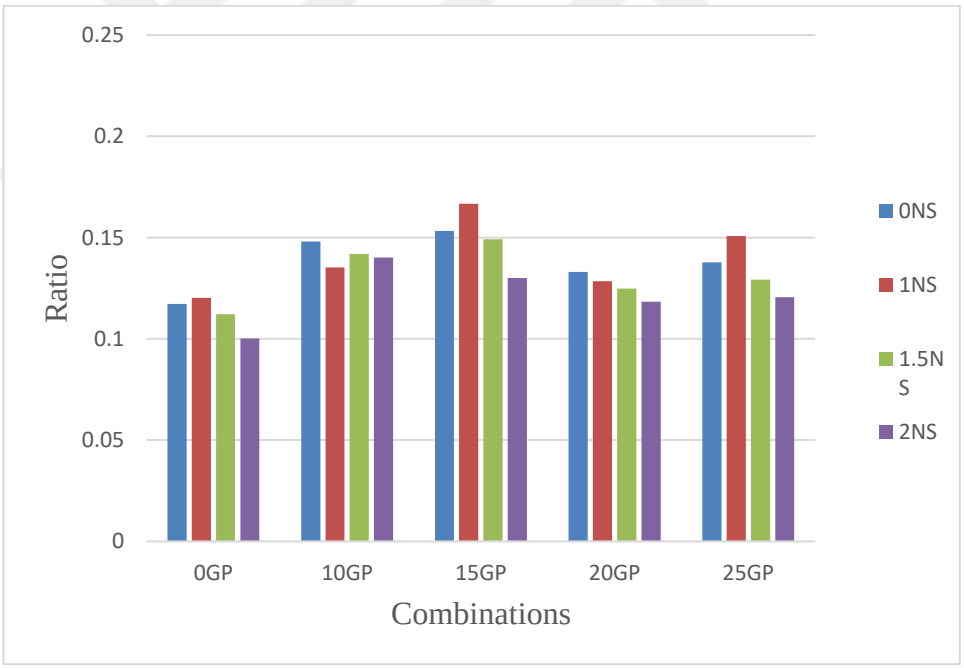

Figure 6.2: Ratio between flexural and compressive strength (28 days).

We can notice that adding nano silica slightly affected the brittleness. At 7 days' results, this ratio increased with the glass powder replacement ratio. That means glass powder can increase the flexural strength slightly. So, we can conclude that this type of glass powder from E glass positively affects ductility. Nano silica has a negative impact. This effect has nothing to do with the hydration process. It is related to the physical composition of this type of glass.

6.4 Water Absorption

The results of water absorption showed how GP and NS affected the durability. Figure 5.18 showed exciting results; adding 10% glass powder increased the water absorption ability of mortar in comparison with the control specimen. However, increasing this percentage showed a reduction in water absorption ability and improved durability. The same was found with nano silica; adding 1%, 1.5%, and 2% of nano silica first increased water absorption (at 1% replacement) and started decreasing with 1.5% and 2% of Nano silica (improving durability). Figure 6.3 shows a relative change in water absorbency compared to the control specimen.

The observed variations in water absorption with increasing amounts of glass powder and Nano silica, despite using particles with identical size and porosity, can be attributed to several influencing factors. The impact of glass powder on water absorption is multifaceted. It relies on variables such as the proportion of glass powder, particle size distribution, and the overall composition of the mortar mixture.

The initial addition of 10% glass powder as a cement replacement presented particles with different water absorption characteristics than the original cement. It is plausible that the glass powder particles exhibited higher porosity or increased water absorbency; glass powder started to fill the voids, forming a pathway to transport water through, thereby contributing to the elevated water absorption observed in the specimens containing 10% glass powder.

However, as the proportion of glass powder was further increased beyond 10%, the effects on water absorption altered (at 15%,20%, and 25%). This phenomenon can be attributed to the filling effect of additional glass powder particles within the mortar matrix. Consequently, these particles contributed to reduced pore size and increased compaction, resulting in diminished water absorption. Moreover, higher proportions of glass powder may have improved particle packing and interfacial bonding, further reducing water ingress. Also, the pozzolanic effect of glass powder and nano silica added more C-S-H gel, which caused denser mortar and helped reduce water absorbency. The same explanation is valid with nano silica and the combination between them. A similar result was found in another powder type, such as marble. Priyadarshini et al. (2023) found a sudden reduction in water absorbency at 10% of marble powder replacement.

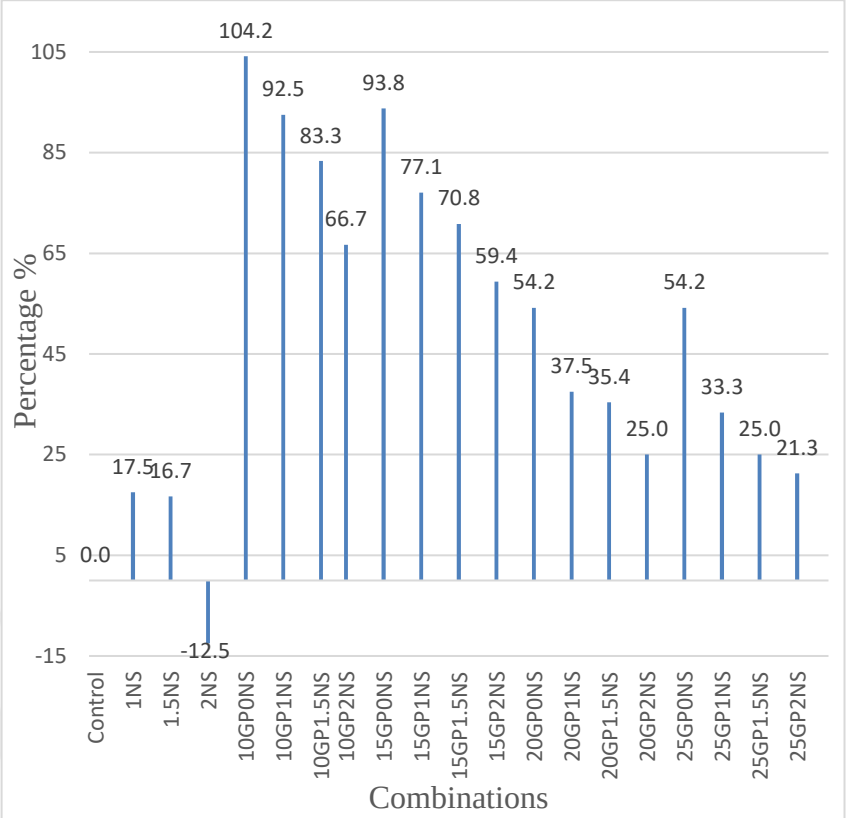

Figure 6.3: Relative change in water absorption.

7. CONCLUSIONS

This study investigated the effectiveness of glass powder (GP) and nano silica (NS) as cementitious replacements in mitigating alkali-silica reaction (ASR) in mortars. Twenty mortar mixtures were formulated with varying combinations of GP and NS, and their mechanical properties, ASR mitigation potential, and pozzolanic reactivity were systematically evaluated. The following key findings and conclusions emerged from this research:

- **ASR mitigation with glass powder**: Glass powder (GP) demonstrated significant effectiveness in mitigating ASR-induced expansion. Mortars incorporating GP at replacement levels of 20% and 25% exhibited a notable reduction in expansion from 0.36% to 0.1% and 0.05%, respectively.
- **Nano silica effects**: While nano silica (NS) did not exhibit a direct mitigation effect on ASR gel formation, it accelerated the pozzolanic reaction in the early ages. This suggests its potential for enhancing early-age strength development in concrete mixes.
- **Mechanical properties**: Mortars with GP replacements showed lower pozzolanic reactivity at early ages, as evidenced by the difference between compressive and flexural strength results at 7 and 28 days. Increasing the GP replacement level tended to reduce flexural and compressive strength, particularly evident in the 7-day test results. Conversely, NS incorporation led to increased compressive and flexural strength at both 7 and 28 days.
- **Pozzolanic reactivity and microstructure**: Thermal gravimetric analysis (TGA) and X-ray diffraction (XRD) confirmed the pozzolanic reaction of GP, as indicated by the reduction in calcium hydroxide (CH) content and the appearance of GP-related compounds. Scanning electron microscopy (SEM) analysis revealed a reduction in cracks in mortars containing GP and showed denser structure in mortars with GP replacement, highlighting its potential for enhancing durability. The pozzolanic activity of GP is the main reason why GP can mitigate ASR.
- **Optimal combination**: The recommended combination of 20% GP and 1.5% NS (20GP1.5NS) demonstrated effective ASR mitigation while maintaining acceptable compressive and flexural strength properties. Further research is needed to investigate potential agglomeration effects, especially with smaller

GP particle sizes, and to explore variations in particle sizes in E-fiber glass powder.

This study utilizes waste materials to contribute to the development of sustainable and circular solutions in construction. Future research should focus on optimizing the sourcing, processing, and application of waste materials in construction and evaluating their long-term performance and environmental impacts.

REFERENCES

Abhilash P.P., Nayak, D. K., Sangoju, B., Kumar, R., Kumar, V. (2021). Effect of nano-silica in concrete; a review. Construction and Building Materials, 278, 122347. https://doi.org/10.1016/j.conbuildmat.2021.122347.

Afshinnia, K., Rangaraju, P. R. (2015). Influence of fineness of ground recycled glass on mitigation of alkali–silica reaction in mortars. Construction and Building Materials, 81, 257–267. https://doi.org/10.1016/j.conbuildmat.2015.02.041.

Aliabdo, A. A., Abd Elmoaty, A. E. M., Aboshama, A. Y. (2016). Utilization of waste glass powder in the production of cement and concrete. Construction and Building Materials, 124, 866–877. https://doi.org/10.1016/j.conbuildmat.2016.08.016.

American Concrete Institute. (2016). ACI 318-14: Building code requirements for structural concrete and commentary. Farmington Hills, MI: ACI. (https://www.concrete.org/store/productdetail.aspx?ItemID=ACI318_14andFormat=DOWNLOAD).

Aquino, W., Lange, D., Olek, J. (2001). The influence of metakaolin and silica fume on the chemistry of alkali–silica reaction products. Cement and Concrete Composites, 23(6), 485–493. https://doi.org/10.1016/s0958-9465(00)00096-2.

ASTM C289-20, Standard Test Method for Potential Alkali-Silica Reactivity of Aggregates (Chemical Method), ASTM International, West Conshohocken, PA, 2020, www.astm.org/cgi-bin/resolver.cgi?C289.

ASTM C1260-20, Standard Test Method for Potential Alkali Reactivity of Aggregates (Mortar-Bar Method), ASTM International, West Conshohocken, PA, 2020, www.astm.org/cgi-bin/resolver.cgi?C1260.

ASTM C1293-20, Standard Test Method for Concrete Aggregates by Determination of Length Change of Concrete Due to Alkali-Silica Reaction, ASTM International, West Conshohocken, PA, 2020, www.astm.org/cgi-bin/resolver.cgi?C1293.

ASTM C856-19, Standard Practice for Petrographic Examination of Hardened Concrete, ASTM International, West Conshohocken, PA, 2019, www.astm.org/cgi-bin/resolver.cgi?C856.

ASTM C441-19, Standard Test Method for Effectiveness of Pozzolans or Ground Blast-Furnace Slag in Preventing Excessive Expansion of Concrete Due to the Alkali-Silica Reaction, ASTM International, West Conshohocken, PA, 2019, www.astm.org/cgi-bin/resolver.cgi?C441.

ASTM C227-20, Standard Test Method for Potential Alkali Reactivity of Cement-Aggregate Combinations (Mortar-Bar Method), ASTM International, West Conshohocken, PA, 2020, www.astm.org/cgi-bin/resolver.cgi?C227.

ASTM C1567-23, Standard Test Method for Determining the Potential Alkali-Silica Reactivity of Combinations of Cementitious Materials and Aggregate (Accelerated Mortar-Bar Method), ASTM International, West Conshohocken, PA, 2020, www.astm.org/cgi-bin/resolver.cgi?C1567.

ASTM C295-20, Standard Guide for Petrographic Examination of Aggregates for Concrete, ASTM International, West Conshohocken, PA, 2020, www.astm.org/cgi-bin/resolver.cgi?C295.

ASTM C618, Standard Specification for Coal Fly Ash and Raw or Calcined Natural Pozzolan for Use in Concrete.

ASTM C1585, Standard Test Method for Measurement of Rate of Absorption of Water by Hydraulic-Cement Concretes.

ASTM C150-22, Standard Specification for Portland Cement.

Awal, A., Hussin, M. (1997). The effectiveness of palm oil fuel ash in preventing expansion due to alkali-silica reaction. Cement and Concrete Composites, 19(4), 367–372. https://doi.org/10.1016/s0958-9465(97)00034-6.

Bénard, P., Garrault, S., Nonat, A., Cau-Dit-Coumes, C. (2005). Hydration process and rheological properties of cement pastes modified by orthophosphate addition. Journal of the European Ceramic Society, 25(11), 1877–1883. https://doi.org/10.1016/j.jeurceramsoc.2004.06.017.

Bérubé, M. A. (2002a). ASR: a critical review of the basic concepts. Cement and Concrete Composites, 24(2), 133-147.

Binal, A. (2015). The Pessimum Ratio and Aggregate Size Effects on Alkali-Silica Reaction. Procedia Earth and Planetary Science, 15, 725–731. https://doi.org/10.1016/j.proeps.2015.08.103.

Bleszynski, R. F., Thomas, M. D. A. (1998). Microstructural Studies of alkali-silica reaction in fly ash concrete immersed in alkaline solution, Advanced Cement Based Materials, 7, 66-78.

BS EN 196-1 British Standards Institution. (2016). Methods of testing cement. Determination of strength. London: BSI.

BS-EN 1015-18, British Standards Institution. Methods of test for mortar for masonry- Part 18: Determination of water absorption coefficient due to capillary action of hardened mortar.

Cai, Y., Xuan, D., Poon, C. S. (2019). Effects of nano-SiO2 and glass powder on mitigating alkali-silica reaction of cement glass mortars. Construction and Building Materials, 201, 295–302. https://doi.org/10.1016/j.conbuildmat.2018.12.186.

Chatterji, S. (1989). Mechanisms of Alkali-Silica Reaction and Expansion, Proceeding of the 8th International Conference on Alkali-Aggregate Reaction (ICAAR), Kyoto, Japan, 101-105.

Chithra, S., Senthil Kumar, S., Chinnaraju, K. (2016). The effect of Colloidal Nano-silica on workability, mechanical and durability properties of High-Performance Concrete with Copper slag as partial fine aggregate. Construction and Building Materials, 113, 794–804. https://doi.org/10.1016/j.conbuildmat.2016.03.119.

Choi, Y. C., Choi, S. (2015). Alkali–silica reactivity of cementitious materials using ferro-nickel slag fine aggregates produced in different cooling conditions. Construction and Building Materials, 99, 279–287. https://doi.org/10.1016/j.conbuildmat.2015.09.039.

Chung, F. H. (1974). Quantitative interpretation of X-ray diffraction patterns of mixtures. II. Adiabatic principle of X-ray diffraction analysis of mixtures. Journal of Applied Crystallography, 7(6), 526–531. https://doi.org/10.1107/s0021889874010387.

Dhir, R. K., Jones, M. R., McCarthy, M. J. (1996). Alkali-silica reaction in concrete. Thomas Telford, https://www.icevirtuallibrary.com/doi/book/10.1680/asric.24625.

Diamond, S. (1989). ASR—Another look at mechanisms, Proceeding of the 8th International Conference on Alkali-Aggregate Reaction (ICAAR), Kyoto, Japan, 83–94.

Diamond, S. (1999). Alkali-aggregate reactions in concrete. Materials and Structures, 32(5), 371-375. (https://link.springer.com/article/10.1007/BF02480599).

Elkady H., Serag M., Elfeky M. (2013). Effect of Nano Silica De-agglomeration, and Methods of Adding Super-plasticizer on the Compressive Strength, and Workability of Nano Silica Concrete., Civ. Environ. 3, 21–35.

Esteves, T., Rajamma, R., Soares, D., Silva, A., Ferreira, V., Labrincha, J. (2012). Use of biomass fly ash for mitigation of alkali-silica reaction of cement mortars. Construction and Building Materials, 26(1), 687–693. https://doi.org/10.1016/j.conbuildmat.2011.06.075.

Fanijo, E. O., Kassem, E., Ibrahim, A. (2021). ASR mitigation using binary and ternary blends with waste glass powder. Construction and Building Materials, 280, 122425. https://doi.org/10.1016/j.conbuildmat.2021.122425.

Feng, X., Thomas, M., Bremner, T., Balcom, B., Folliard, K. (2005). Studies on lithium salts to mitigate ASR-induced expansion in new concrete: a critical review.

Cement and Concrete Research, 35(9), 1789–1796. https://doi.org/10.1016/j.cemconres.2004.10.013.

Ghafari, E., Costa, H., Júlio, E., Portugal, A., Durães, L. (2014). The effect of nano silica addition on flowability, strength, and transport properties of ultra-high performance concrete. Materials and Design, 59, 1–9. https://doi.org/10.1016/j.matdes.2014.02.051.

García-Lodeiro, I., Palomo, A., and Fernández-Jiménez, A. (2007). Alkali–aggregate reaction in activated fly ash systems. Cement and Concrete Research, 37(2), 175–183. https://doi.org/10.1016/j.cemconres.2006.11.002.

Gilbert, A. S. (2016). Encyclopedia of Geoarchaeology. Springer. http://books.google.ie/books?id=tk0knQEACAAJanddq=Gilberto+Artioli,+(2016),++X-ray+Diffraction+(XRD),+Encyclopedia+of+Geoarchaeology+pp+1019%E2%80%931025.andhl=andcd=1andsource=gbs_api.

Guo, S., Dai, Q., Sun, X., Xiao, X., Si, R., Wang, J. (2018). Reduced alkali-silica reaction damage in recycled glass mortar samples with supplementary cementitious materials. Journal of Cleaner Production, 172, 3621–3633. https://doi.org/10.1016/j.jclepro.2017.11.119.

Güneyisi, E., Gesoglu, M., Azez, O. A., Öz, H. Z. (2016). Effect of nano silica on the workability of self-compacting concretes having untreated and surface treated lightweight aggregates. Construction and Building Materials, 115, 371–380. https://doi.org/10.1016/j.conbuildmat.2016.04.055.

Hadley, D.W. (1961). Alkali reactivity of carbonate rocks; expansion and dedolomitization. Proceedings of the Highway Research Board, 40: 462-474.

Hou, P., Qian, J., Cheng, X., and Shah, S. P. (2015). Effects of the pozzolanic reactivity of nanoSiO 2 on cement-based materials. Cement and Concrete Composites, 55, 250–258. https://doi.org/10.1016/j.cemconcomp.2014.09.014

Helmuth, R., Stark, D., Diamond, S., Moranville-Regourd, M. (1993). Alkali-silica reactivity: and overview of research (SHRP-C-342), Strategic Highway Research Program, National Research Council, Washington, DC. 108 pp.

Idir, R., Cyr, M., Tagnit-Hamou, A. (2010). Use of fine glass as ASR inhibitor in glass aggregate mortars. Construction and Building Materials, 24(7), 1309–1312. https://doi.org/10.1016/j.conbuildmat.2009.12.030.

Idir, R., Cyr, M., Tagnit-Hamou, A. (2011). Pozzolanic properties of fine and coarse color-mixed glass cullet. Cement and Concrete Composites, 33(1), 19–29. https://doi.org/10.1016/j.cemconcomp.2010.09.013.

Islam, M. S., Ghafoori, N. (2016). Experimental study and empirical modeling of lithium nitrate for alkali-silica reactivity. Construction and Building Materials, 121, 717–726. https://doi.org/10.1016/j.conbuildmat.2016.06.026.

Jani, Y., Hogland, W. (2014). Waste glass in the production of cement and concrete – A review. Journal of Environmental Chemical Engineering, 2(3), 1767–1775. https://doi.org/10.1016/j.jece.2014.03.016.

Johnston, C.D (1974). Waste Glass as Coarse Aggregate for Concrete. Journal of Testing and Evaluation, 2(5), 344. https://doi.org/10.1520/jte10117j.

Jiang, X., Xiao, R., Bai, Y., Huang, B., and Ma, Y. (2022). Influence of waste glass powder as a supplementary cementitious material (SCM) on physical and mechanical properties of cement paste under high temperatures. Journal of Cleaner Production, 340, 130778. https://doi.org/10.1016/j.jclepro.2022.130778.

Ke, G., Li, W., Li, R., Li, Y., Wang, G. (2018). Mitigation Effect of Waste Glass Powders on Alkali–Silica Reaction (ASR) Expansion in Cementitious Composite. International Journal of Concrete Structures and Materials, 12(1). https://doi.org/10.1186/s40069-018-0299-7.

Kumar, S., Kumar, A., Kujur, J. (2019). Influence of nano silica on mechanical and durability properties of concrete. Proceedings of the Institution of Civil Engineers - Structures and Buildings, 172(11), 781–788. https://doi.org/10.1680/jstbu.18.00080.

Khan, M. N. N., Sarker, P. K. (2019). Alkali silica reaction of waste glass aggregate in alkali-activated fly ash and GGBFS mortars. Materials and Structures, 52(5). https://doi.org/10.1617/s11527-019-1392-3.

Lindgård, J., Andiç-Çakır, Z., Fernandes, I., Rønning, T. F., Thomas, M. D. (2012). Alkali–silica reactions (ASR): Literature review on parameters influencing laboratory performance testing. Cement and Concrete Research, 42(2), 223–243. https://doi.org/10.1016/j.cemconres.2011.10.004

Li, Q., Qiao, H., Li, A., and Li, G. (2022). Performance of waste glass powder as a pozzolanic material in blended cement mortar. Construction and Building Materials, 324, 126531. https://doi.org/10.1016/j.conbuildmat.2022.126531.

Liu, S., Wang, S., Tang, W., Hu, N., Wei, J. (2015). Inhibitory Effect of Waste Glass Powder on ASR Expansion Induced by Waste Glass Aggregate. Materials, 8(10), 6849–6862. https://doi.org/10.3390/ma8105344.

Levasil CB8 Colloidal silica. (n.d.). Nouryon. https://www.nouryon.com/product/levasil-cb8/.

Maas, A. J., Ideker, J. H., Juenger, M. C. (2007). Alkali silica reactivity of agglomerated silica fume. Cement and Concrete Research, 37(2), 166–174. https://doi.org/10.1016/j.cemconres.2006.10.011.

Mindess, S., Young, J. F. (1981). Concrete. Prentice-Hall, Englewood Cliffs, NJ. https://www.pearson.com/us/higher-education/product/Mindess-Concrete-2nd-Edition/9780131681177.html.

Mukharjee, B. B., Barai, S. V. (2020). Influence of Incorporation of Colloidal Nano-Silica on Behaviour of Concrete. Iranian Journal of Science and Technology, Transactions of Civil Engineering, 44(2), 657–668. https://doi.org/10.1007/s40996-020-00382-0.

Monteiro, P., Wang, K., Sposito, G., Santos, M., de Andrade, W. (1997). Influence of mineral admixtures on the alkali-aggregate reaction. Cement and Concrete Research, 27(12), 1899–1909. https://doi.org/10.1016/s0008-8846(97)00206-8.

Mukharjee, B. B., Barai, S. V. (2014). Influence of Nano-Silica on the properties of recycled aggregate concrete. Construction and Building Materials, 55, 29–37. https://doi.org/10.1016/j.conbuildmat.2014.01.003.

McCoy, W.J., Caldwell, A.G. (1951). New approach to inhibiting alkali-aggregate expansion, Journal of the American Concrete Institute, 47(5), 693-706. New Approach to Inhibiting Alkali-Aggregate Expansion (concrete.org).

Moser, R. D., Jayapalan, A. R., Garas, V. Y., Kurtis, K. E. (2010). Assessment of binary and ternary blends of metakaolin and Class C fly ash for alkali-silica reaction mitigation in concrete. Cement and Concrete Research, 40(12), 1664–1672. https://doi.org/10.1016/j.cemconres.2010.08.006.

Naik, T.R. (2008). Sustainability of Concrete Construction, Prac. Period. Struct. Des. Constr. 13 98–103.

Nattaj Farid Hasan, Nematzadeh Mahdi, (2017). The effect of forta-ferro and steel fibers on mechanical properties of high-strength concrete with and without silica fume and nano-silica. Construction and Building Materials, 137, 557–572. https://doi.org/10.1016/j.conbuildmat.2017.01.078.

Ni, C. (2013). Scanning Electron Microscopy (SEM). Springer eBooks. https://doi.org/10.1007/978-0-387-92897-5_1217.

Neville, A. M. (2011). Properties of concrete, Fifth Edition. Pearson Education. https://www.pearson.com/us/higher-education/product/Neville-Properties-of-Concrete-5th-Edition/9780273755807.html.

Nigam, M., Verma, M. (2023). Effect of nano-silica on the fresh and mechanical properties of conventional concrete. Forces in Mechanics, 10, 100165. https://doi.org/10.1016/j.finmec.2022.100165.

Oberholster, R.E. (1989). Alkali-aggregate reaction in South Africa. Some recent developments in research, in: K. Okada, S. Nishibayashi, M. Kawamura (Eds.), Proceedings of the 8th International Conference on Alkali-Aggregate Reaction, pp. 77–82, Kyoto.
https://doi.org/10.1016/j.cemconres.2015.05.024.

Ozol M.A., (1994), Alkali carbonate rock reaction, P. Klieger, J.F. Lamond (Eds.), Significance of Tests and Properties of Concrete and

Concrete-making Materials, ASTM STP 169C, West Conshohocken, Pennsylvania, 372-387.

Phillips JC, Cahn DS, (1972). Keller GW Refuse glass aggregate in Portland cement concrete in: Proceeding of the Third Mineral Waste Utilization Symposium Chicago, p. 163.

Priyadarshini, S., Soren, S., Durga, G. (2023). Effect of waste marble dust powder as a filler material on mechanical properties and water uptake capacity of Epoxy/glass fiber composites. Materials Today: Proceedings. https://doi.org/10.1016/j.matpr.2023.02.096.

Pereira-de-Oliveira, L. A., Castro-Gomes, J. P., Santos, P. M. (2012). The potential pozzolanic activity of glass and red-clay ceramic waste as cement mortars components. Construction and Building Materials, 31, 197–203. https://doi.org/10.1016/j.conbuildmat.2011.12.110.

Patel, D., Tiwari, R., Shrivastava, R., Yadav, R. (2019). Effective utilization of waste glass powder as the substitution of cement in making paste and mortar. Construction and Building Materials, 199, 406–415. https://doi.org/10.1016/j.conbuildmat.2018.12.017.

Puertas, F., Palacios, M., Manzano, H. (2000). Alkali-silica reaction in mortars made with different cements. Cement and Concrete Research, 30(9), 1423-1429. https://www.sciencedirect.com/science/article/abs/pii/S0008884600000526.

Prezzi M., Darwin D., Collins M. P. (1997). A probabilistic approach for the evaluation of the alkali-silica reaction in concrete structures. ACI Materials Journal, 94(3), 245-253.
Search. (n.d.). https://www.pearson.com/us/higher-education/product/Mindess-Concrete-2nd-Edition/9780131681177.html.

Powers T.C., Steinour H.H. (1955). An interpretation of some published researches on the alkali–aggregate reaction; part 1 — the chemical reactions and mechanisms of expansion. ACI Journal Proceedings, 51(2) 497–516.

Parghi, A., Shahria Alam, M. (2016). Physical and mechanical properties of cementitious composites containing recycled glass powder (RGP) and styrene butadiene rubber (SBR). Construction and Building Materials, 104, 34–43. https://doi.org/10.1016/j.conbuildmat.2015.12.006.

Rajabipour, F., Giannini, E., Dunant, C., Ideker, J. H., Thomas, M. D. (2015). Alkali–silica reaction: Current understanding of the reaction mechanisms and the knowledge gaps. Cement and Concrete Research, 76, 130–146.

Swenson, E.G. (1957a). A reactive aggregate undetected by ASTM tests, Proceedings of American Society for Testing and Materials, 57: 48-51.

Stanton, T. E. (1942). Expansion of Concrete through Reaction between Cement and Aggregate. Transactions of the American Society of Civil Engineers, 107(1), 54–84. https://doi.org/10.1061/taceat.0005540.

Stanton, T.E, Portep, O.J., Meder, L.C., Nicol, A., (1942), California experience with the expansion of concrete through reaction between cement and aggregates, ACI Journal, 38(3), 209-235.

Shayan, A., Xu, A. (2006). Performance of glass powder as a pozzolanic material in concrete: A field trial on concrete slabs. Cement and Concrete Research, 36(3), 457–468. https://doi.org/10.1016/j.cemconres.2005.12.012.

Singh, L., Bhattacharyya, S., Shah, S., Mishra, G., Sharma, U. (2016). Studies on early stage hydration of tricalcium silicate incorporating silica nanoparticles: Part II. Construction and Building Materials, 102, 943–949. https://doi.org/10.1016/j.conbuildmat.2015.05.084.

Shehata, M. H., Thomas, M. D. (2000). The effect of fly ash composition on the expansion of concrete due to alkali–silica reaction. Cement and Concrete Research, 30(7), 1063–1072. https://doi.org/10.1016/s0008-8846(00)00283-0.

Shehata, M. H., Thomas, M. D. (2002). Use of ternary blends containing silica fume and fly ash to suppress expansion due to alkali–silica reaction in concrete. Cement and Concrete Research, 32(3), 341–349. https://doi.org/10.1016/s0008-8846(01)00680-9.

Shehata, M. H., Thomas, M. D. (2006). Alkali release characteristics of blended cements. Cement and Concrete Research, 36(6), 1166–1175. https://doi.org/10.1016/j.cemconres.2006.02.015.

Saha, A. K., Sarker, P. K. (2016). Expansion due to alkali-silica reaction of ferronickel slag fine aggregate in OPC and blended cement mortars. Construction and Building Materials, 123, 135–142. https://doi.org/10.1016/j.conbuildmat.2016.06.144.

Saha, A. K., Khan, M., Sarker, P. K., Shaikh, F. A., Pramanik, A. (2018). The ASR mechanism of reactive aggregates in concrete and its mitigation by fly ash: A critical review. Construction and Building Materials, 171, 743–758. https://doi.org/10.1016/j.conbuildmat.2018.03.183.

Senff, L., Labrincha, J. A., Ferreira, V. M., Hotza, D., Repette, W. L. (2009). Effect of nano-silica on rheology and fresh properties of cement pastes and mortars. Construction and Building Materials, 23(7), 2487–2491. https://doi.org/10.1016/j.conbuildmat.2009.02.005.

Stephan, D., Maleki, H., Knöfel, D., Eber, B., Härdtl, R. (1999). Influence of Cr, Ni, and Zn on the properties of pure clinker phases. Cement and Concrete Research, 29(5), 651–657. https://doi.org/10.1016/s0008-8846(99)00008-3.

Shon, C. S., Sarkar, S. L., Zollinger, D. G. (2004). Testing the Effectiveness of Class C and Class F Fly Ash in Controlling Expansion due to Alkali-Silica Reaction Using Modified ASTM C 1260 Test Method. Journal of Materials in Civil Engineering, 16(1), 20–27. https://doi.org/10.1061/(asce)0899-1561(2004)16:1(20).

Sweson, E.G. (1957b). "Cement aggregate reaction in concrete of a Canadian bridge". ASTM Proceedings, 57 1043-1056.

Shoaei, P., Ameri, F., Reza Musaeei, H., Ghasemi, T., Cheah, C. B. (2020). Glass powder as a partial precursor in Portland cement and alkali-activated slag mortar: A comprehensive comparative study. Construction and Building Materials, 251, 118991. https://doi.org/10.1016/j.conbuildmat.2020.118991.

Thomas, M. D. A. (2003). Delayed ettringite formation and cracking in concrete. Cement and Concrete Research, 33(8), 1045-1052. (https://www.sciencedirect.com/science/article/abs/pii/S0008884603000578).
Alkali-aggregate reaction. (1992, January). Cement and Concrete Research, 22(1), 197. https://doi.org/10.1016/0008-8846(92)90154-n.

Thomas, M. (2011). The effect of supplementary cementing materials on alkali-silica reaction: A review. Cement and Concrete Research, 41(12), 1224–1231. https://doi.org/10.1016/j.cemconres.2010.11.003.

Thomas, M. D. A., Fournier, B., Folliard, K. J. (2013). Alkali-aggregate Reactivity (AAR) Facts Book. http://books.google.ie/books?id=AiS8vAEACAAJanddq=Alkali+Aggregate+Reactivity+(AAR)+facts+bookandhl=andcd=1andsource=gbs_api.

Thomas M.D.A., Bleszynski R.F., (2001), The use of silica fume to control expansion due to alkali-aggregate reactivity in concrete—a review, in: S. Mindess, J. Skalny (Eds.), Materials Science of Concrete VI, American Ceramics Society, Westerville, OH, pp. 377–434.

Topçu, L. B., Canbaz, M. (2004). Properties of concrete containing waste glass. Cement and Concrete Research, 34(2), 267–274. https://doi.org/10.1016/j.cemconres.2003.07.003.

Tremblay, C., Bérubé, M-A., Fournier, B., Thomas, M.D.A. and Folliard, K.F., (2007). Effectiveness of lithium-based products in concrete made with Canadian reactive aggregates, ACI Materials Journal, 104(2), 195-205, https://doi.org/10.14359/18583.

Turkmenoglu, H. Nuri, Boyaci, B., Baran, S., Nihat Bicakci, S., Nuri Atahan, H. (2022). Micro and/or Nano-Silica modified moderate and high strength concrete: Rheology and synergistic effects on strength, elastic and inelastic behavior, and microstructure. Construction and Building Materials, 333, 127404. https://doi.org/10.1016/j.conbuildmat.2022.127404.

Wang, H., Gillott, J. E. (1991). Mechanism of alkali-silica reaction and the significance of calcium hydroxide, Cement and Concrete Research, 21, 647-654.

W. (2022, February 19). Thermogravimetric Analysis (TGA) - Types, Methods, Materials, Labs, FAQs | Aurigaresearch. Auriga Research | Testing Lab | NABL ISO/IEC 17025 Accredited | FSSAI Approved. (Accessed: 17 October 2023). https://aurigaresearch.com/pharmaceutical-testing/thermogravimetric-analysis-tga/

Wagatsuma, K. (2021). Spectroscopy for Materials Analysis. Springer Nature. http://books.google.ie/books?id=vq1HEAAAQBAJandpg=PR6anddq=Kazuaki+Wagatsuma,+(2021),+Spectrum+in+X-Ray+Fluorescence+Spectroscopy,+Spectroscopy+for+Materials+Analysis+pp+25%E2%80%9329.andhl=andcd=1andsource=gbs_api.

Yu, R., Spiesz, P., Brouwers, H. (2014). Effect of nano-silica on the hydration and microstructure development of Ultra-High Performance Concrete (UHPC) with a low binder amount. Construction and Building Materials, 65, 140–150. https://doi.org/10.1016/j.conbuildmat.2014.04.063.

Zheng, K. (2016). Pozzolanic reaction of glass powder and its role in controlling alkali–silica reaction. Cement and Concrete Composites, 67, 30–38. https://doi.org/10.1016/j.cemconcomp.2015.12.008.

Zhao, Y., Cui, N., Zhao, S., Zhu, Y., Hou, P., Feng, L., Xie, N. (2021). Aggressive Environment Resistance of Concrete Products Modified With Nano Alumina and Nano Silica. Frontiers in Materials, 8. https://doi.org/10.3389/fmats.2021.695624.

APPENDICES

APPENDIX A: Mix design table for ASR test's mortars
APPENDIX B: Mix design table for Flexural and Compressive strength test's mortars.
APPENDIX C: ASR test results.
APPENDIX D: XRD test results.

Appendix A: The mix design for ASR's test mortars.

Table A.1: Mix design of mortars produced for ASR test.

		Sp.gr (g/cm^3)	Control	0GP1NS	0GP1.5NS	0GP2NS
Material	Water	1	206.8	202.4	200.2	198
	Sand	2.69	990	990	990	990
	OPC	3.14	440	435.6	433.4	431.2
	WGP	2.61	0	0	0	0
	NS	1.4	0	4.4	6.6	8.8
	Superplasticizer	1.05	1.9	3	3	3
Total	TOTAL WEIGHT (gm)		1638.7	1639.8	1639.8	1639.8
	TOTAL VOLUME (cm^3)		716.8	715.2	713.8	712.5
Ratios	W/C		0.47	0.465	0.462	0.459
	W/B		0.47	0.47	0.47	0.47
	Poz/Binder		0	0.01	0.015	0.02
	Ns CB 8 in field		0	8.8	13.2	17.6

Table A.2: Continue mix design for ASR's test mortars.

		Sp.gr (g/cm^3)	10GP0NS	10GP1NS	10GP1.5NS	10GP2NS
MATERIALS	Water	1	206.8	202.4	200.2	198
	Sand	2.69	990	990	990	990
	OPC	3.14	396	391.6	389.4	387.2
	WGP	2.61	44	44	44	44
	NS	1.4	0	4.4	6.6	8.8
	Superplasticizer	1.05	3.4	3.4	3.4	3.4
TOTAL	TOTAL WEIGHT (gm)		1640.2	1640.2	1640.2	1640.2
	TOTAL VOLUME (cm^3)		721.0	718.4	717.1	715.7
RATIOS	W/C		0.522	0.517	0.514	0.511
	W/B		0.47	0.47	0.47	0.47
	Poz/Binder		0.1	0.11	0.115	0.12
	Ns CB 8 in field		0	8.8	13.2	17.6

Table A.3: Continue mix design for ASR's test mortars.

		Sp.gr (g/cm^3)	15GP0NS	15GP1NS	15GP1.5NS	15GP2NS
MATERIALS	Water	1	206.8	202.4	200.2	198
	Sand	2.69	990	990	990	990
	OPC	3.14	374	369.6	367.4	365.2
	WGP	2.61	66	66	66	66
	NS	1.4	0	4.4	6.6	8.8
	Superplasticizer	1.05	3.4	3.4	3.4	3.4
TOTAL	TOTAL WEIGHT (gm)		1640.2	1640.2	1640.2	1640.2
	TOTAL VOLUME (cm^3)		722.5	719.8	718.5	717.1
RATIOS	W/C		0.553	0.548	0.545	0.542
	W/B		0.47	0.47	0.47	0.47
	Poz/Binder		0.15	0.16	0.165	0.17
	Ns CB 8 in field		0	8.8	13.2	17.6

Table A.4: Continue Mix design for ASR's test mortars.

		Sp.gr (g/cm^3)	20GP0NS	20GP1NS	20GP1.5NS	20GP2NS
MATERIALS	Water	1	206.8	202.4	200.2	198
	Sand	2.69	990	990	990	990
	OPC	3.14	352	347.6	345.4	343.2
	WGP	2.61	88	88	88	88
	NS	1.4	0	4.4	6.6	8.8
	Superplasticizer	1.05	3.4	3.4	3.4	3.4
TOTAL	TOTAL WEIGHT (gm)		1640.2	1640.2	1640.2	1640.2
	TOTAL VOLUME (cm^3)		723.9	721.2	719.9	718.6
RATIOS	W/C		0.588	0.582	0.580	0.577
	W/B		0.47	0.47	0.47	0.47
	Poz/Binder		0.2	0.21	0.215	0.22
	Ns CB 8 in field		0	8.8	13.2	17.6

Table A.5: Continue Mix design for ASR's test mortars.

		Sp.gr (g/cm^3)	25GP0NS	25GP1NS	25GP1.5NS	25GP2NS
MATERIALS	Water	1	206.8	202.4	200.2	198
	Sand	2.69	990	990	990	990
	OPC	3.14	330	325.6	323.4	321.2
	WGP	2.61	110	110	110	110
	NS	1.4	0	4.4	6.6	8.8
	Superplasticizer	1.05	3.4	3.4	3.4	3.4
TOTAL	TOTAL WEIGHT (gm)		1640.2	1640.2	1640.2	1640.2
	TOTAL VOLUME (cm^3)		725.3	722.7	721.3	719.9
RATIOS	W/C		0.627	0.622	0.619	0.616
	W/B		0.47	0.47	0.47	0.47
	Poz/Binder		0.25	0.26	0.265	0.27
	Ns CB 8 in field		0	8.8	13.2	17.6

Appendix B: The mix design table for flexural and compressive strength.

Table B.1: Mix design table for flexural and compressive strength test mortars.

		Sp.gr (g/cm^3)	Control	0GP1NS	0GP1.5NS	0GP2NS
MATERIALS	Water	1	225	220.5	218.25	216
	Sand	2.69	1350	1350	1350	1350
	OPC	3.14	450	445.5	443.25	441
	GWP	2.61	0	0	0	0
	NS	1.4	0	4.5	6.75	9
	Superplasticizer	1.05	5	5	5	5
TOTAL	TOTAL WEIGHT (gr)		2030	2030	2030	2030
	TOTAL VOLUME (cm^3)		874.93	872.21	870.85	869.50
RATIOS	W/C		0.5	0.495	0.492	0.490
	W/B		0.5	0.5	0.5	0.5
	Poz/Binder		0	0.01	0.015	0.02
	Ns CB 8 in field		0	9	13.5	18
	Theoretical unit weight		2.320	2.327	2.331	2.335
	cup weight		362.6	358.3	351.2	364
	Measured unit weight		2.163	2.137	2.095	2.172
	Air content		6.754	8.146	10.10	6.975
	Workability		19.35	20.2	16.1	17.25

Table B.2: Continue Mix design table for Flexural and Compressive strength test's mortars.

		Sp.gr (g/cm^3)	10GP0NS	10GP1NS	10GP1.5NS	10GP2NS
MATERIALS	Water	1	225	220.5	218.25	216
	Sand	2.69	1350	1350	1350	1350
	OPC	3.14	405	400.5	398.25	396
	GWP	2.61	45	45	45	45
	NS	1.4	0	4.5	6.75	9
	Superplasticizer	1.05	6.75	6.75	6.75	6.75
TOTAL	TOTAL WEIGHT (gr)		2031.75	2031.75	2031.75	2031.75
	TOTAL VOLUME (cm^3)		879.51	876.79	875.43	874.07
RATIOS	W/C		0.556	0.551	0.548	0.545
	W/B		0.5	0.5	0.5	0.5
	Poz/Binder		0.1	0.11	0.115	0.12
	Ns CB 8 in field		0	9	13.5	18
	Theoretical unit weight		2.310	2.317	2.321	2.324
	cup weight		360.6	359.4	359.9	363.4
	Measured unit weight		2.152	2.144	2.147	2.168
	Air content		7.173	7.460	7.475	6.720
	Workability		21.45	23.1	20.75	21.95

Table B.3: Continue Mix design table for Flexural and Compressive strength test's mortars.

		Sp.gr (g/cm^3)	15GP0NS	15GP1NS	15GP1.5NS	15GP2NS
MATERIALS	Water	1	225	220.5	218.25	216
	Sand	2.69	1350	1350	1350	1350
	OPC	3.14	382.5	378	375.75	373.5
	GWP	2.61	67.5	67.5	67.5	67.5
	NS	1.4	0	4.5	6.75	9
	Superplasticizer	1.05	6.75	6.75	6.75	6.75
TOTAL	TOTAL WEIGHT (gr)		2031.75	2031.75	2031.75	2031.75
	TOTAL VOLUME (cm^3)		880.96	878.25	876.89	875.53
RATIOS	W/C		0.588	0.583	0.581	0.578
	W/B		0.5	0.5	0.5	0.5
	Poz/Binder		0.15	0.16	0.165	0.17
	Ns CB 8 in field		0	9	13.5	18
	Theoretical unit weight		2.306	2.313	2.317	2.321
	cup weight		363.2	362.1	364.7	363.3
	Measured unit weight		2.167	2.161	2.176	2.168
	Air content		6.036	6.610	6.085	6.591
	Workability		20.5	18.2	18.85	19.25

Table B.4: Continue mix design table for flexural and compressive strength test's mortar.

		Sp.gr (g/cm^3)	20GP0NS	20GP1NS	20GP1.5NS	20GP2NS
MATERIALS	Water	1	225	220.5	218.25	216
	Sand	2.69	1350	1350	1350	1350
	OPC	3.14	360	355.5	353.25	351
	GWP	2.61	90	90	90	90
	NS	1.4	0	4.5	6.75	9
	Superplasticizer	1.05	6.525	6.75	6.75	6.75
TOTAL	TOTAL WEIGHT (gr)		2031.525	2031.75	2031.75	2031.75
	TOTAL VOLUME (cm^3)		882.205	879.701	878.341	876.982
RATIOS	W/C		0.625	0.620	0.618	0.615
	W/B		0.5	0.5	0.5	0.5
	Poz/Binder		0.2	0.21	0.215	0.22
	Ns CB 8 in field		0	9	13.5	18
	Theoretical unit weight		2.303	2.309	2.313	2.316
	cup weight		362.7	360.5	360.3	359.3
	Measured unit weight		2.164	2.151	2.150	2.144
	Air content		6.023	6.868	7.064	7.465
	Workability		20.9	16.75	19.5	19.95

Table B.5: Continue Mix design table for Flexural and Compressive strength test's mortars.

		Sp.gr (g/cm^3)	25GP0NS	25GP1NS	25GP1.5NS	25GP2NS
MATERIALS	Water	1	225	220.5	218.25	216
	Sand	2.69	1350	1350	1350	1350
	OPC	3.14	337.5	333	330.75	328.5
	GWP	2.61	112.5	112.5	112.5	112.5
	NS	1.4	0	4.5	6.75	9
	Superplasticizer	1.05	6.75	6.75	6.75	6.75
TOTAL	TOTAL WEIGHT (gr)		2031.75	2031.75	2031.75	2031.75
	TOTAL VOLUME (cm^3)		883.87	881.16	879.80	878.44
RATIOS	W/C		0.667	0.662	0.660	0.658
	W/B		0.5	0.5	0.5	0.5
	Poz/Binder		0.25	0.26	0.265	0.27
	Ns CB 8 in field		0	9	13.5	18
	Theoretical unit weight		2.299	2.306	2.309	2.312
	cup weight		361.9	366	353.7	354.3
	Measured unit weight		2.159	2.184	2.110	2.114
	Air content		6.063	5.291	8.615	8.602
	Workability		20.2	20	17.45	16.65

Appendix C: AMBT results for the whole combinations between WGP and NS.

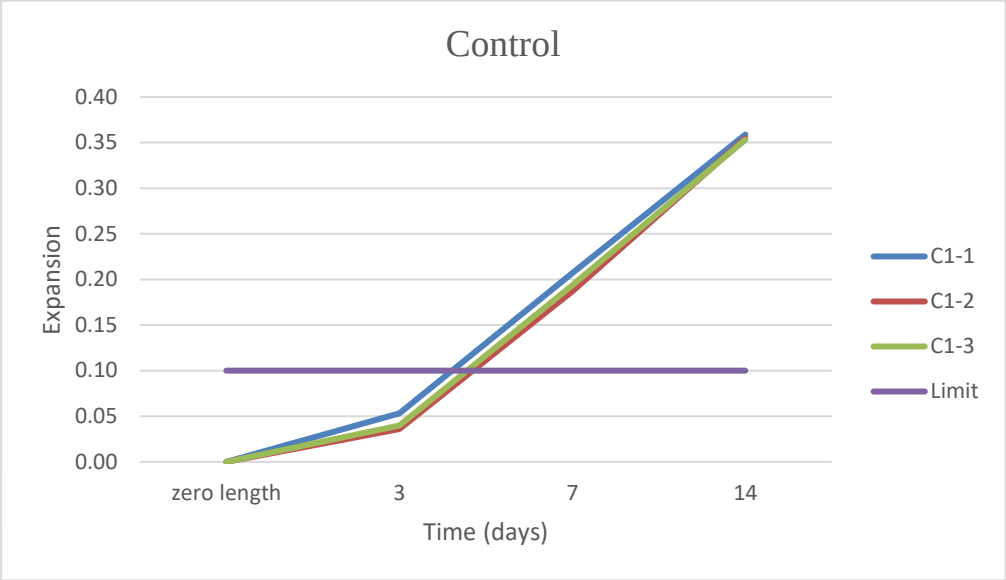

Figure C.1: ASR results for control paste.

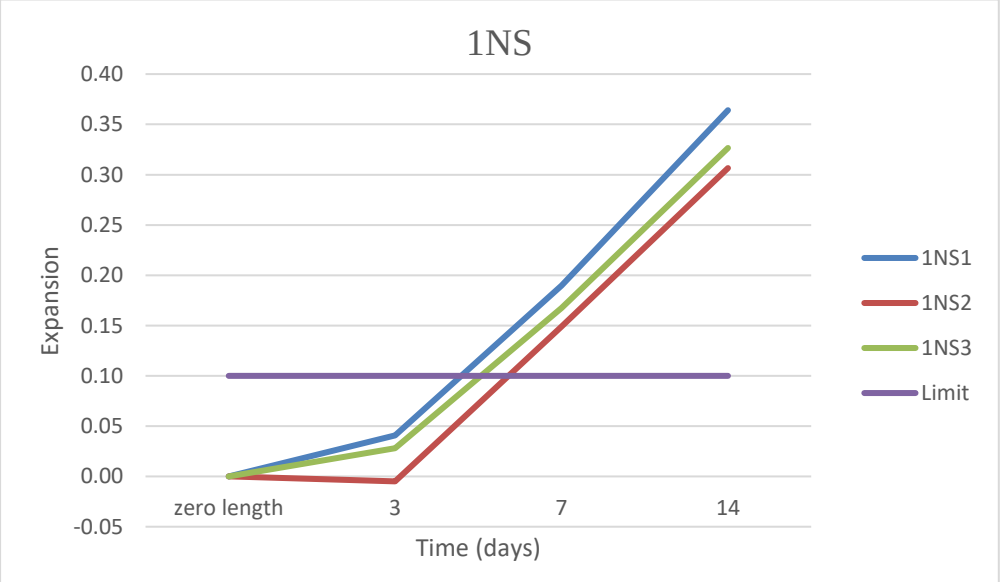

Figure C.2: ASR results for 1%NS paste.

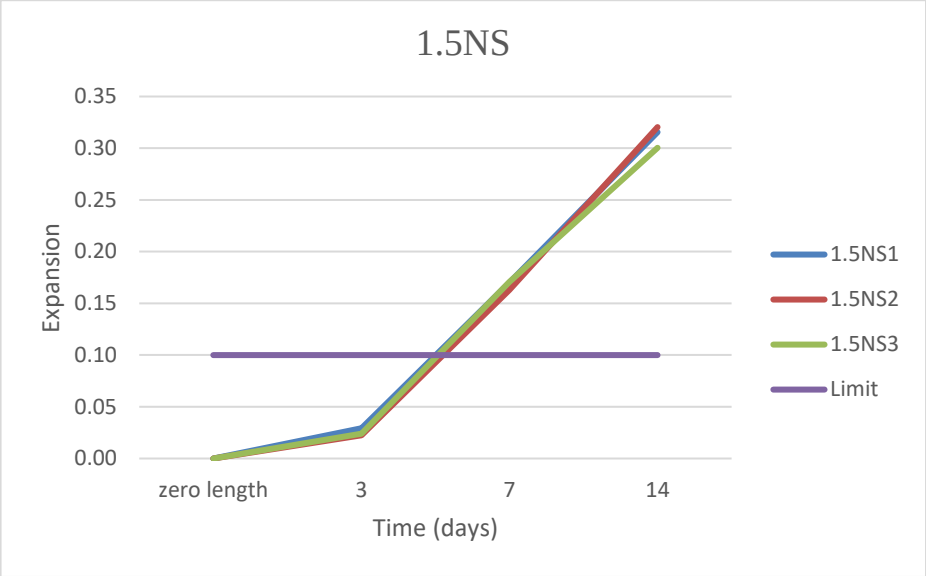

Figure C.3: ASR results for 1.5% NS.

Figure C.4: ASR results for 2% NS.

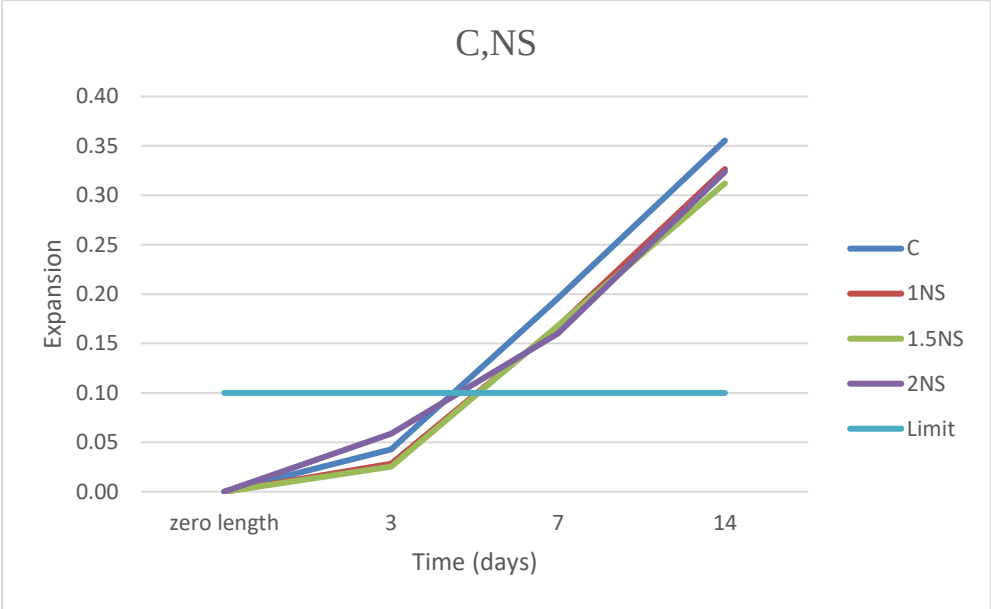

Figure C.5: Average ASR results for control, 1%NS, 1.5%NS, and 2%NS mortars.

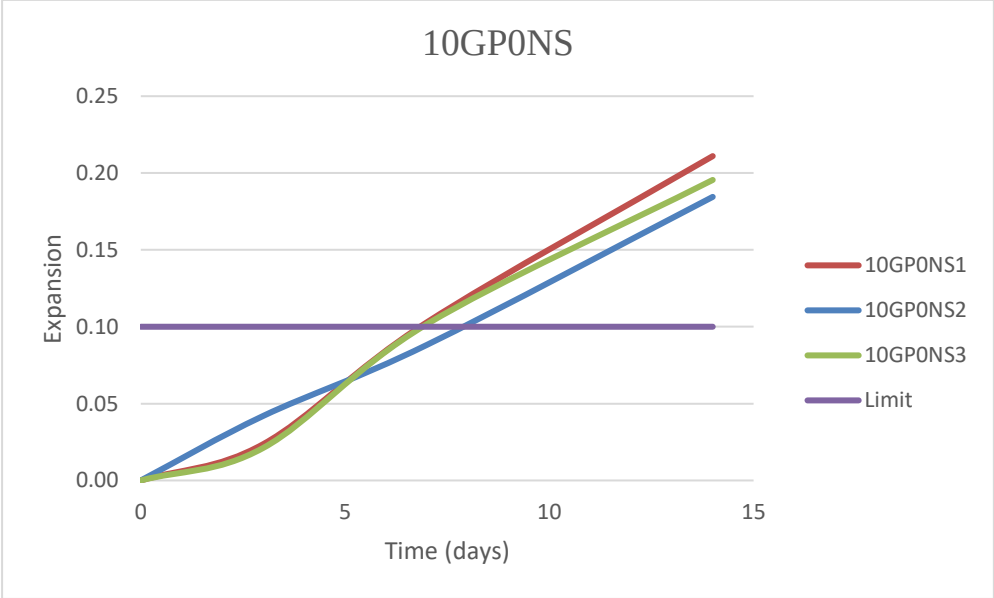

Figure C.6: ASR test results for 10%GP 0%NS.

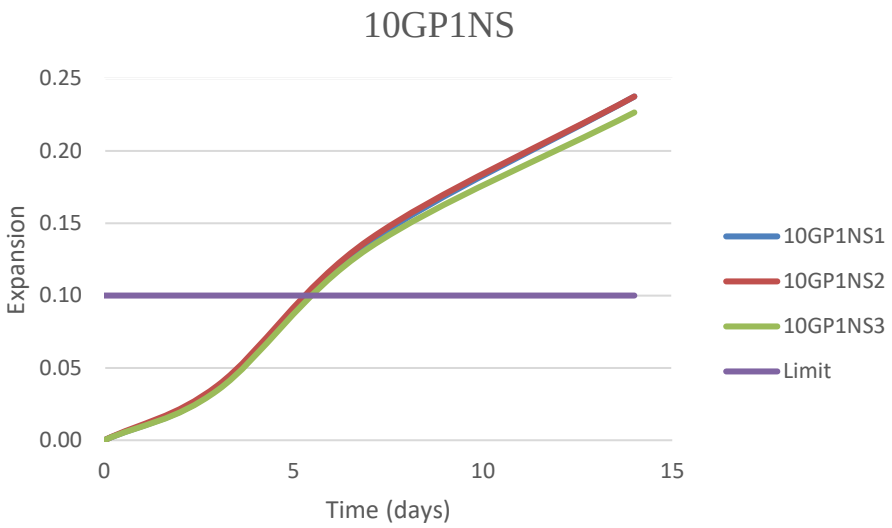

Figure C.7: ASR test results for 10%GP 1%NS.

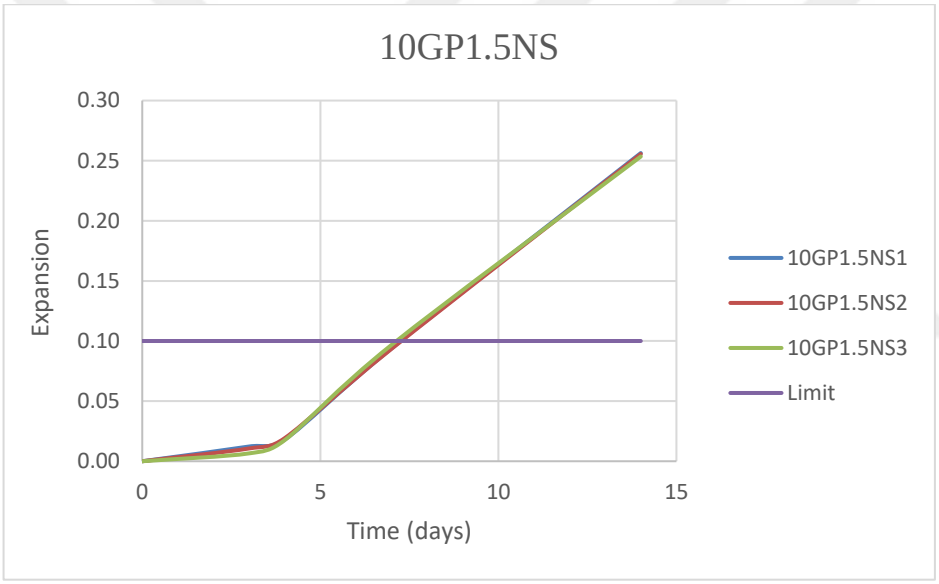

Figure C.8: ASR test results for 10%GP 1.5%NS.

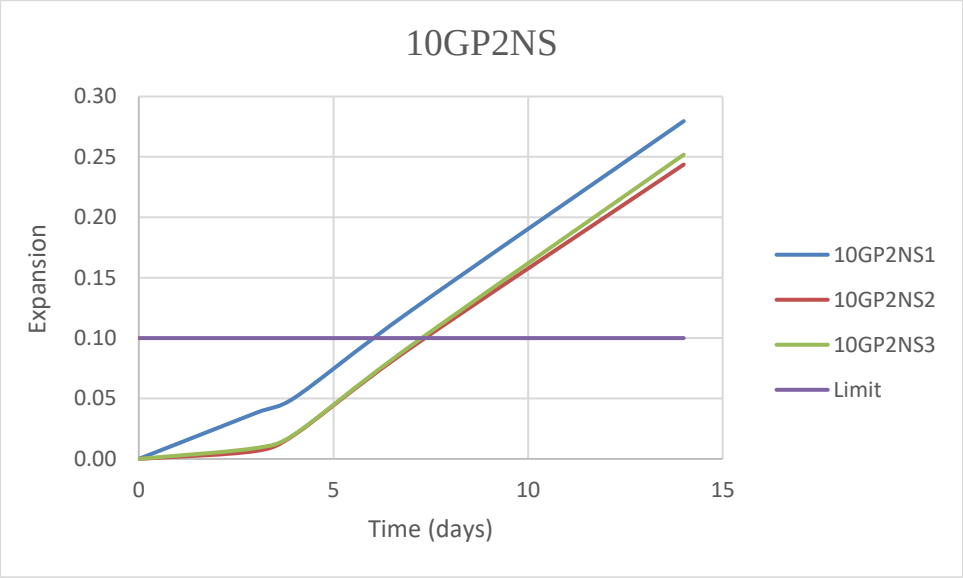

Figure C.9: ASR test results for 10%GP 2%NS.

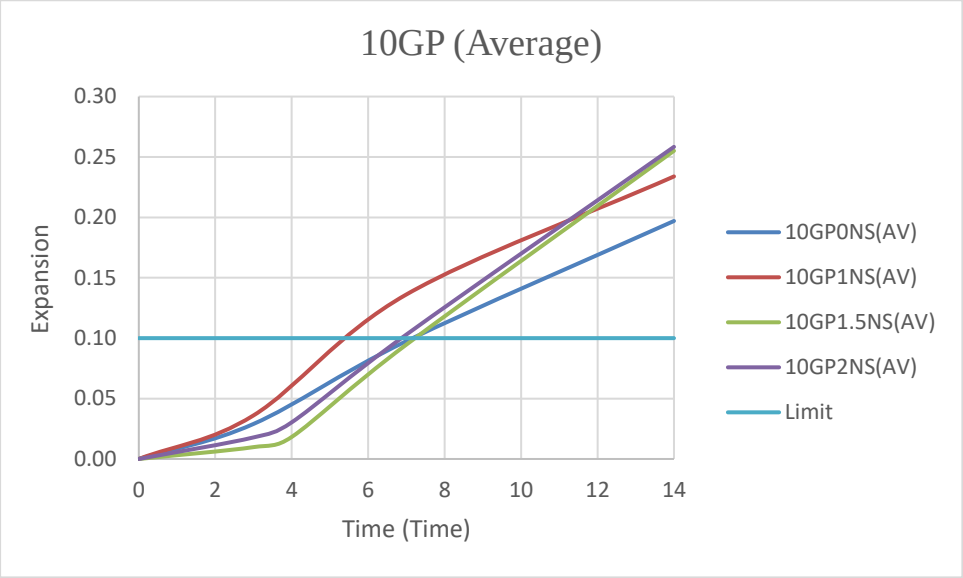

Figure C.10: Average ASR test results for 10%GP with different NS content.

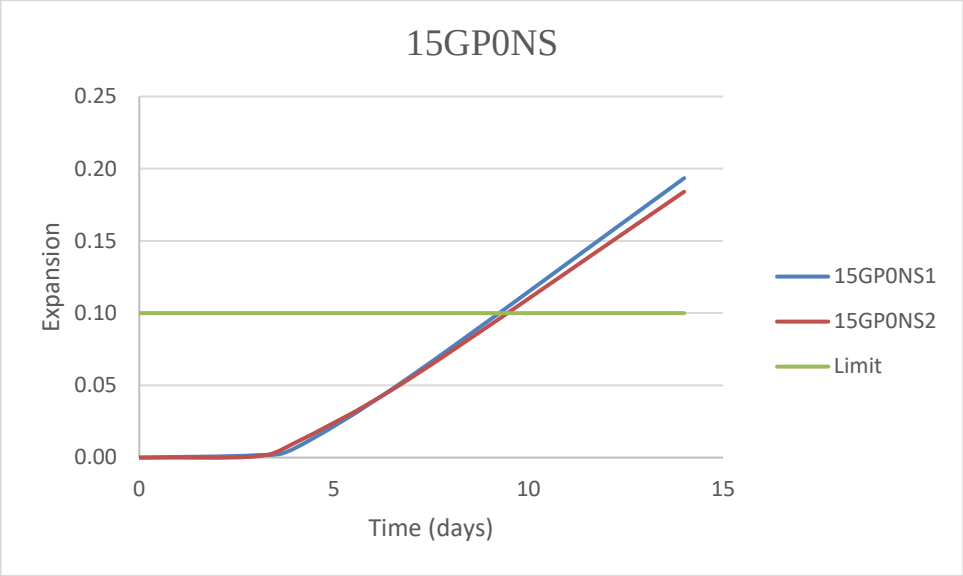

Figure C.11: ASR test results for 15% GP 0% NS.

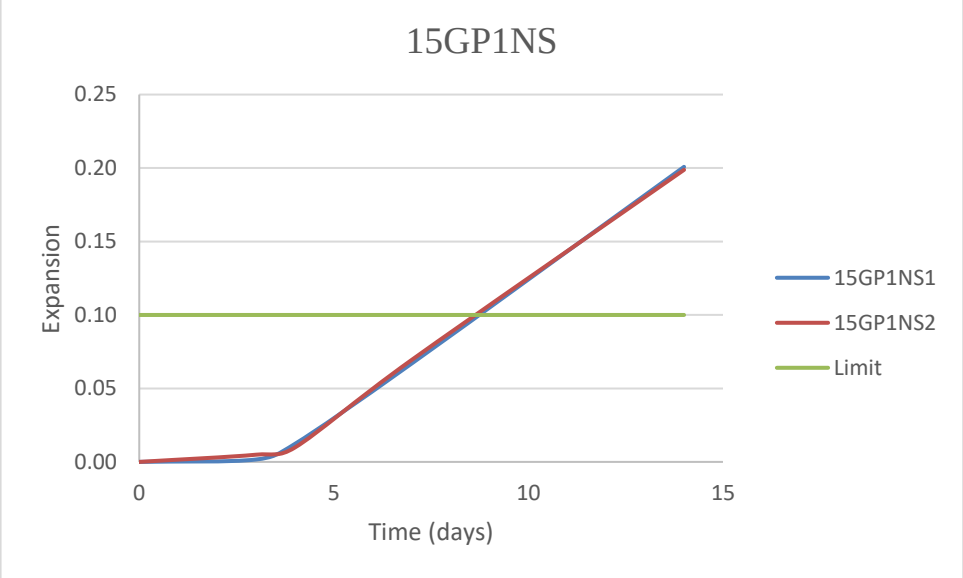

Figure C.12: ASR test results for 15%GP 1%NS.

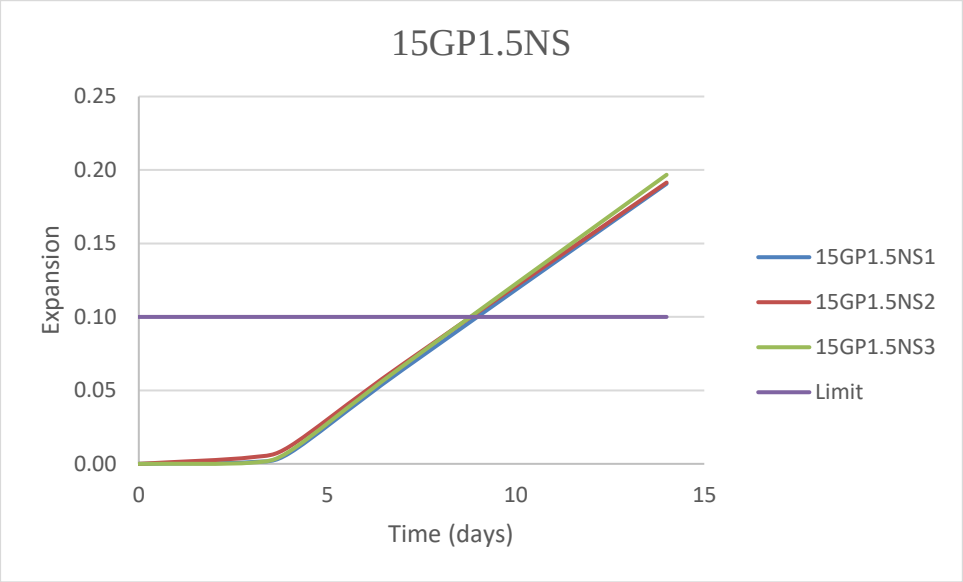

Figure C.13: ASR test results for 15%GP 1.5%NS.

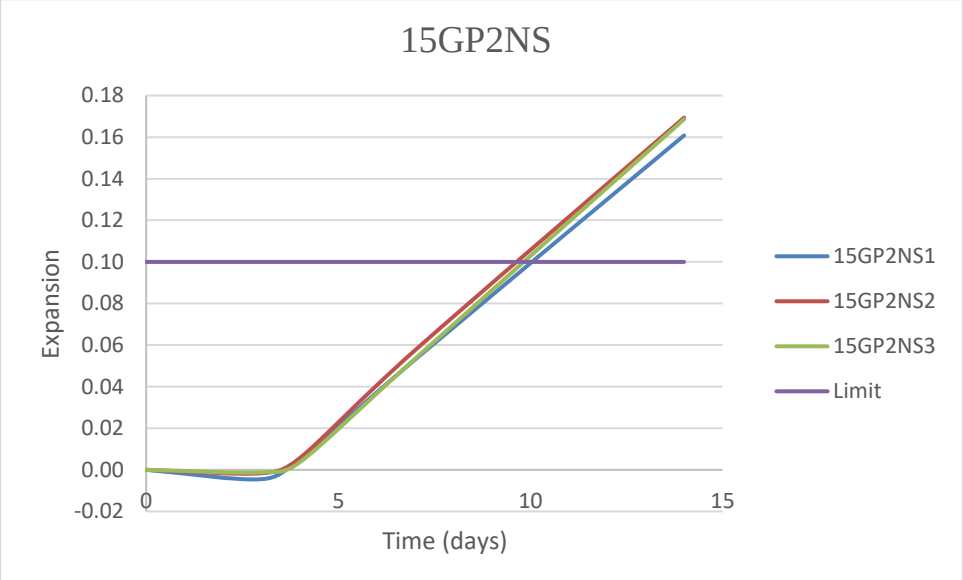

Figure C.14: ASR test results for 15%GP 2%NS.

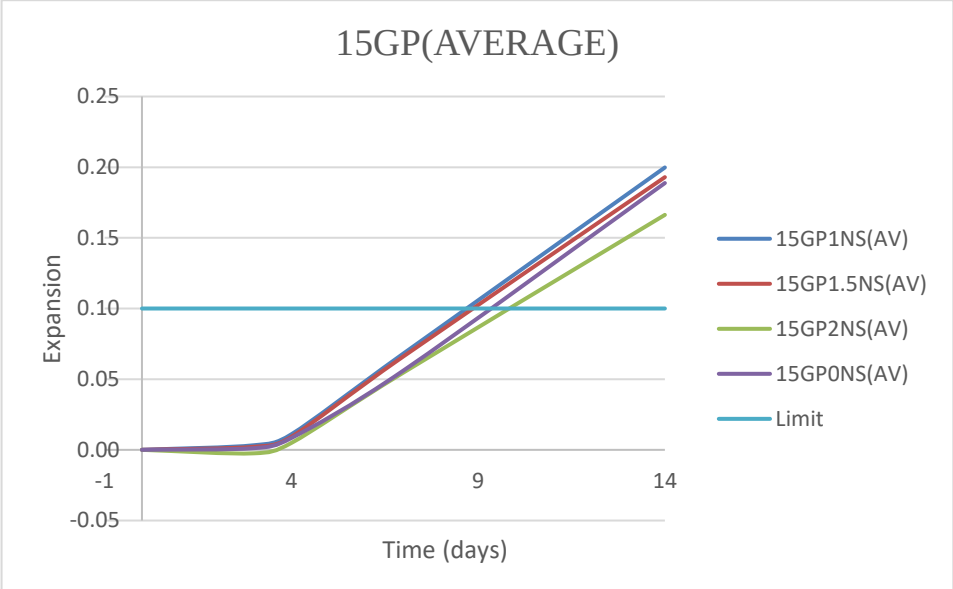

Figure C.15: Average ASR test results for 15%GP with different NS content.

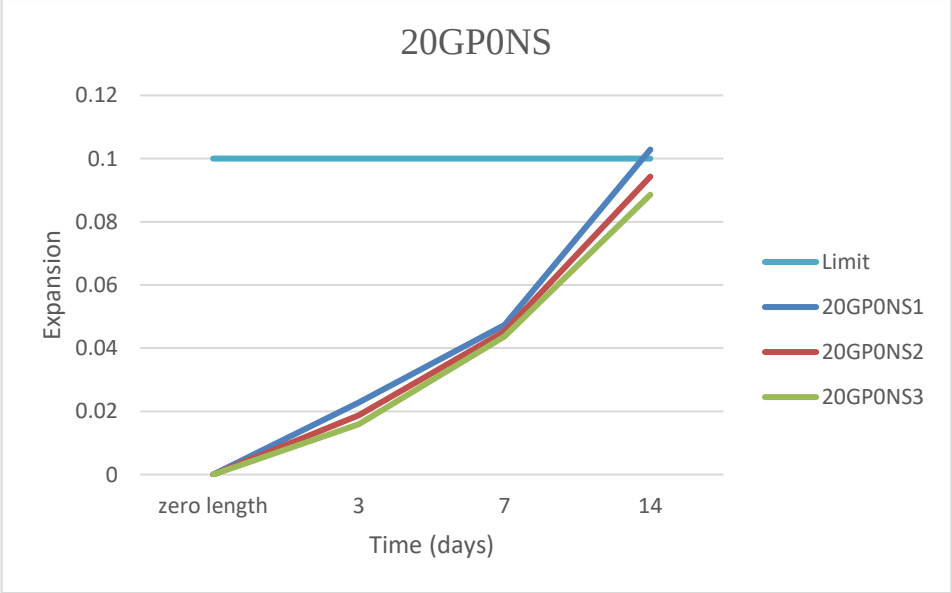

Figure C.16: ASR test results for 20%GP 0%NS.

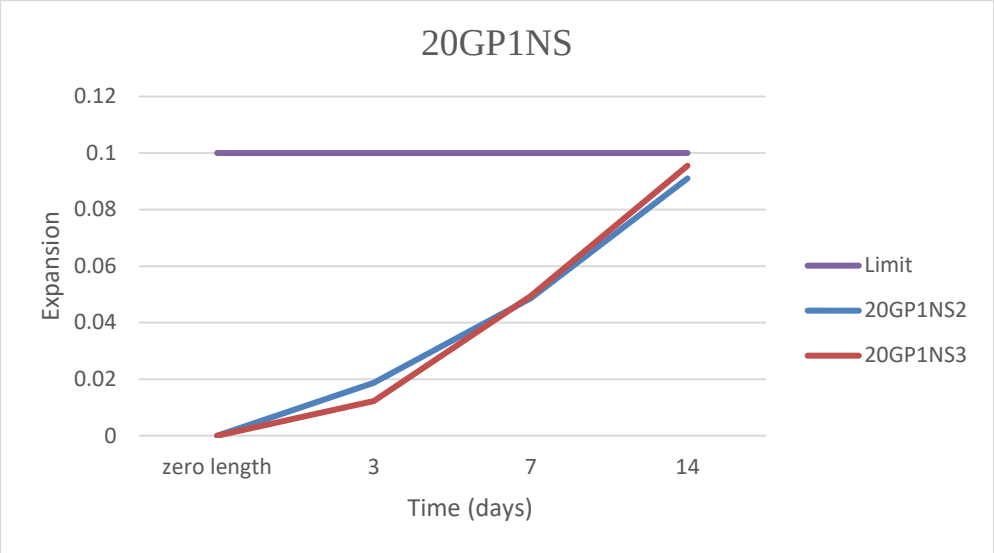

Figure C.17: ASR test results for 20%GP 1%NS.

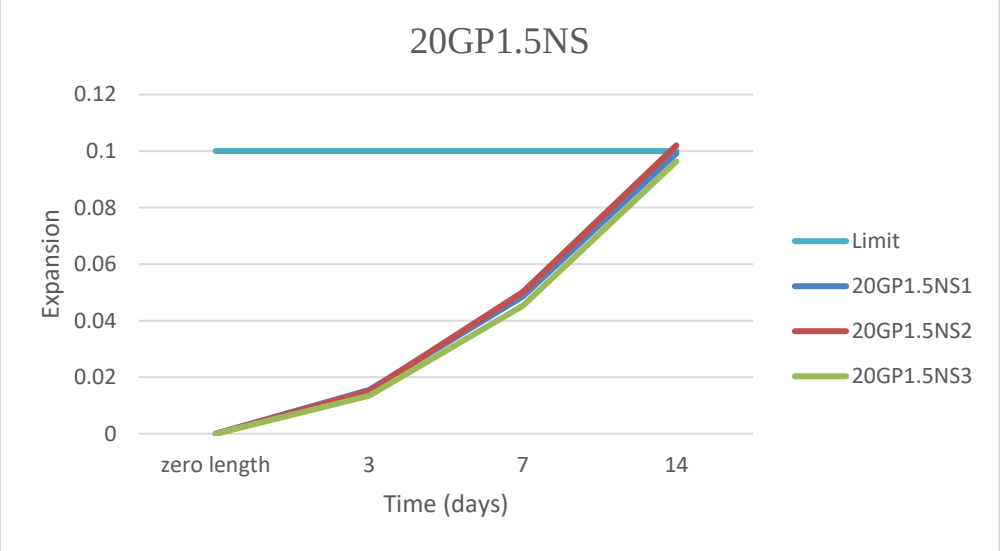

Figure C.18: ASR test results for 20%GP 1.5%NS.

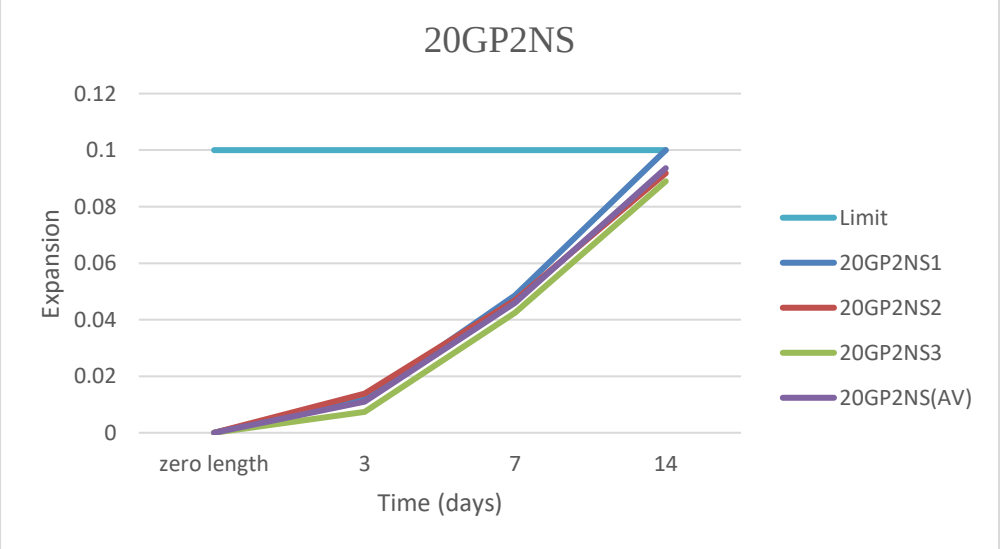

Figure C.19: ASR test results for 20%GP 2%NS.

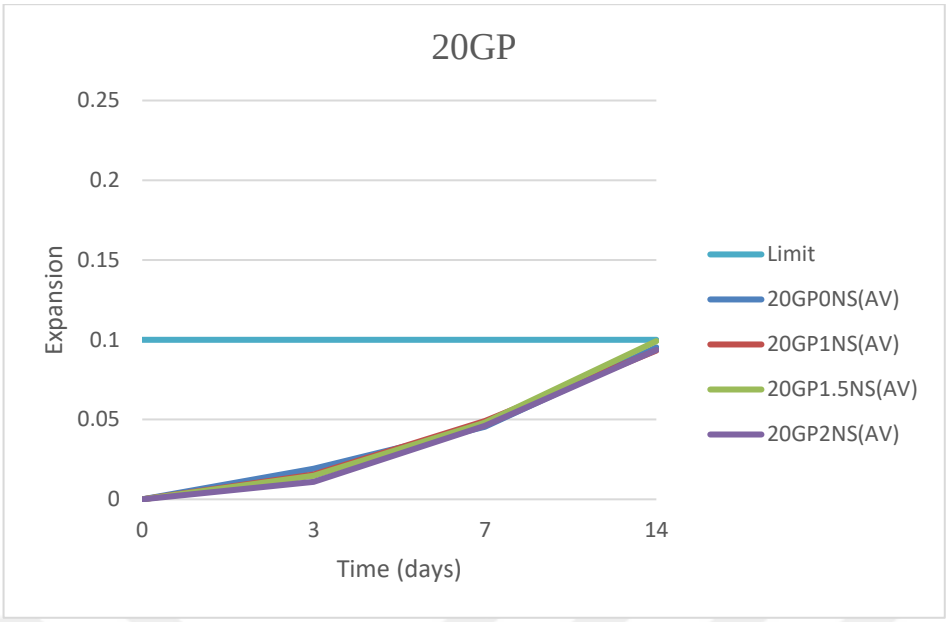

Figure C.20: Average ASR test results for 20%GP with different NS content.

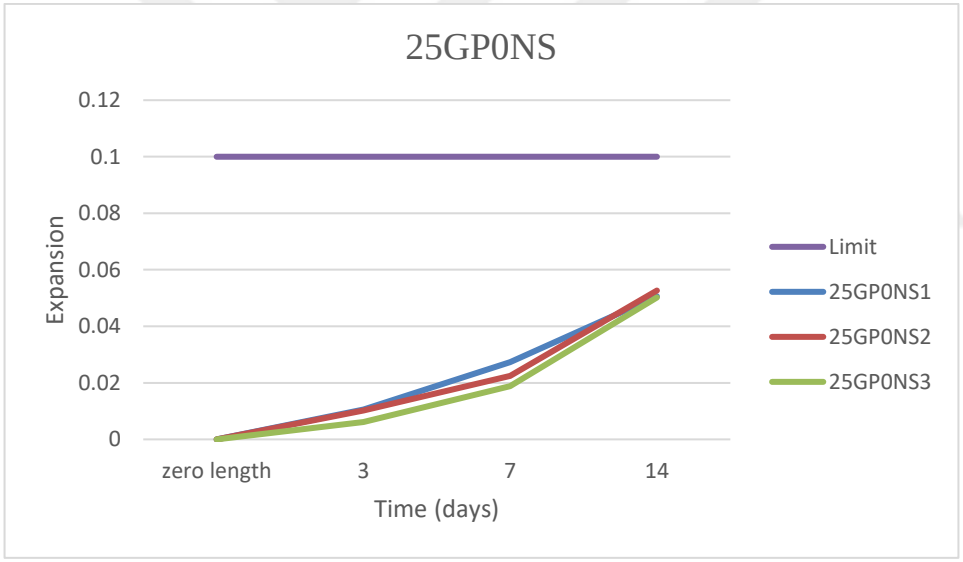

Figure C.21: ASR test results for 25%GP 0%NS.

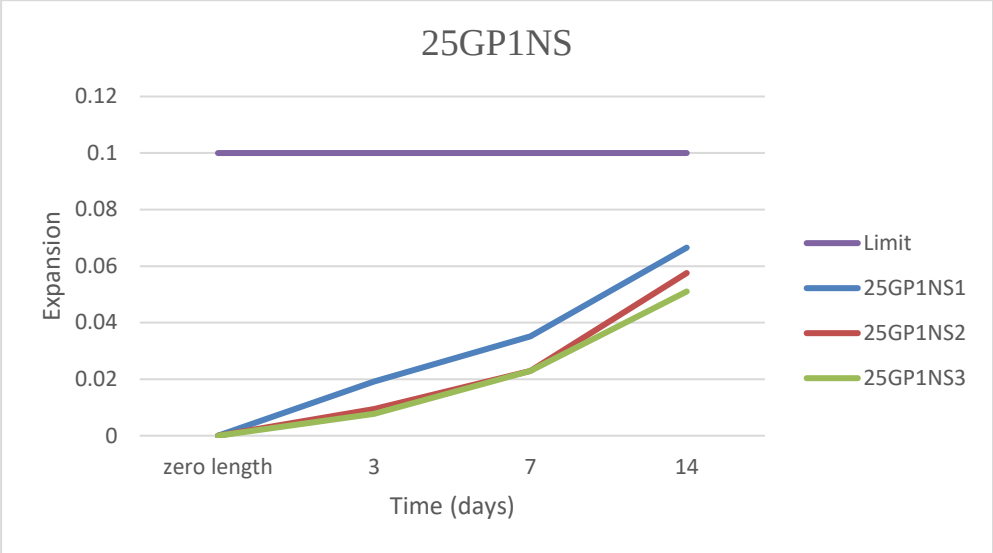

Figure C.22: ASR test results for 25%GP 1%NS.

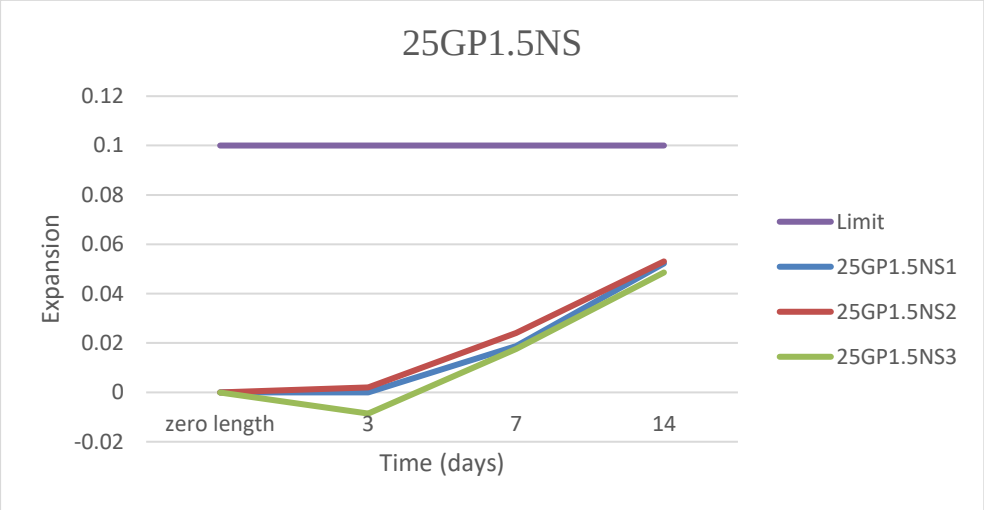

Figure C.23: ASR test results for 25%GP 1.5%NS.

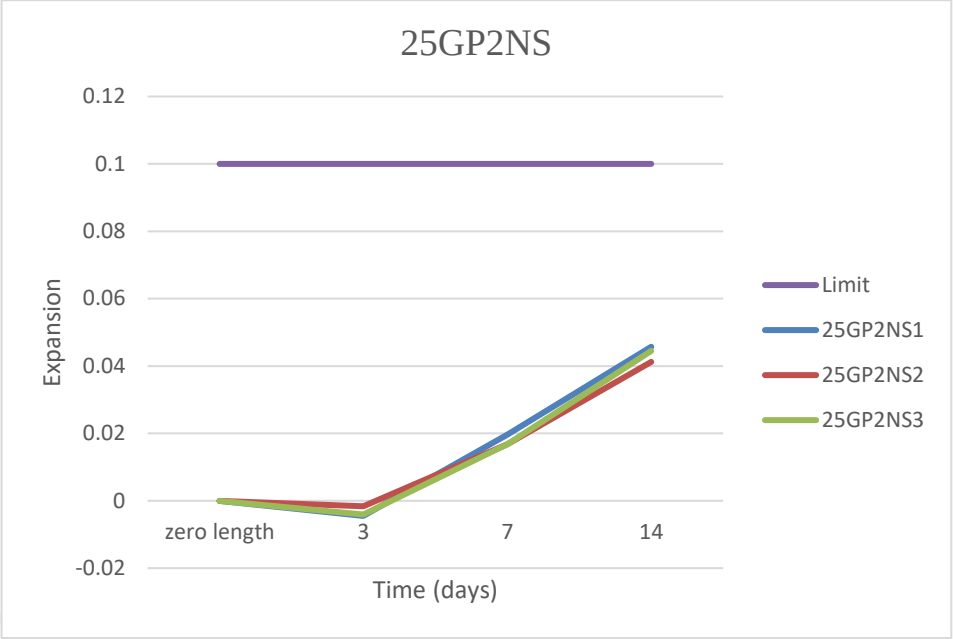

Figure C.24: ASR test results for 25%GP 2%NS.

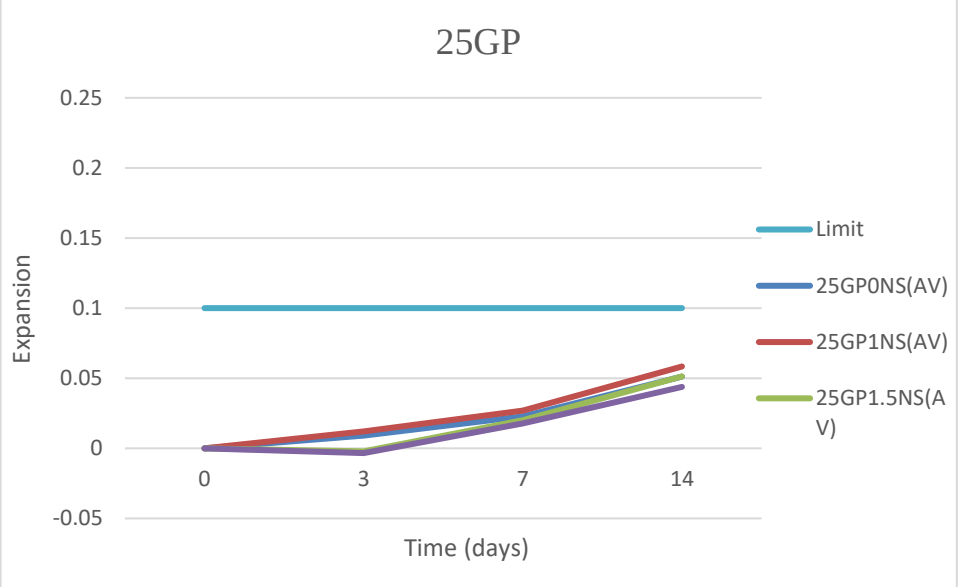

Figure C.25: Average ASR test results for 25%GP with different NS content.

Appendix D: XRD results for cement, glass powder, and mortars with different combinations of WGP and NS.

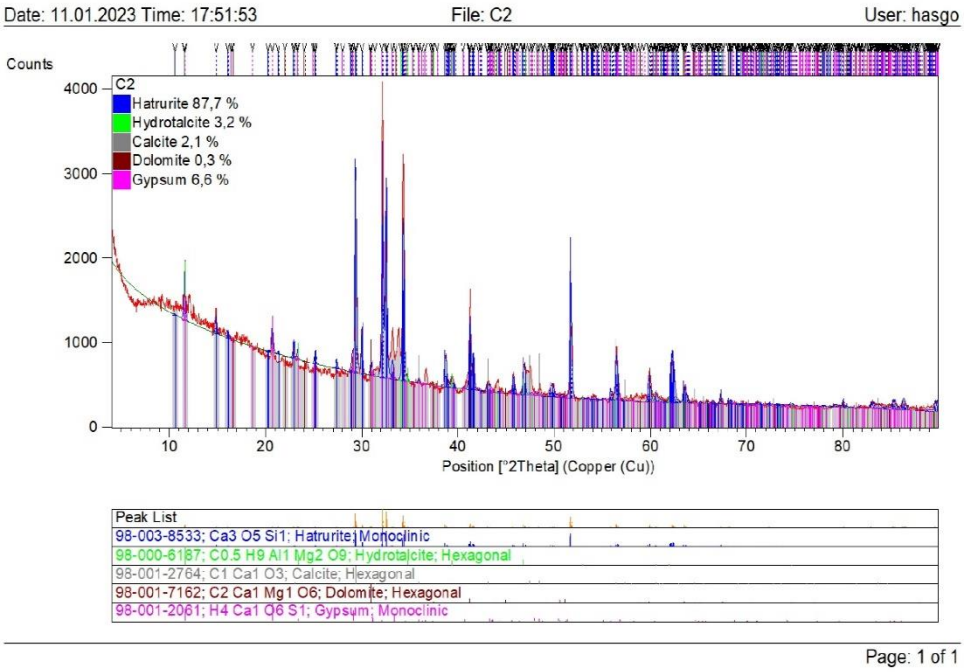

Figure D.1: XRD result for cement (RPC).

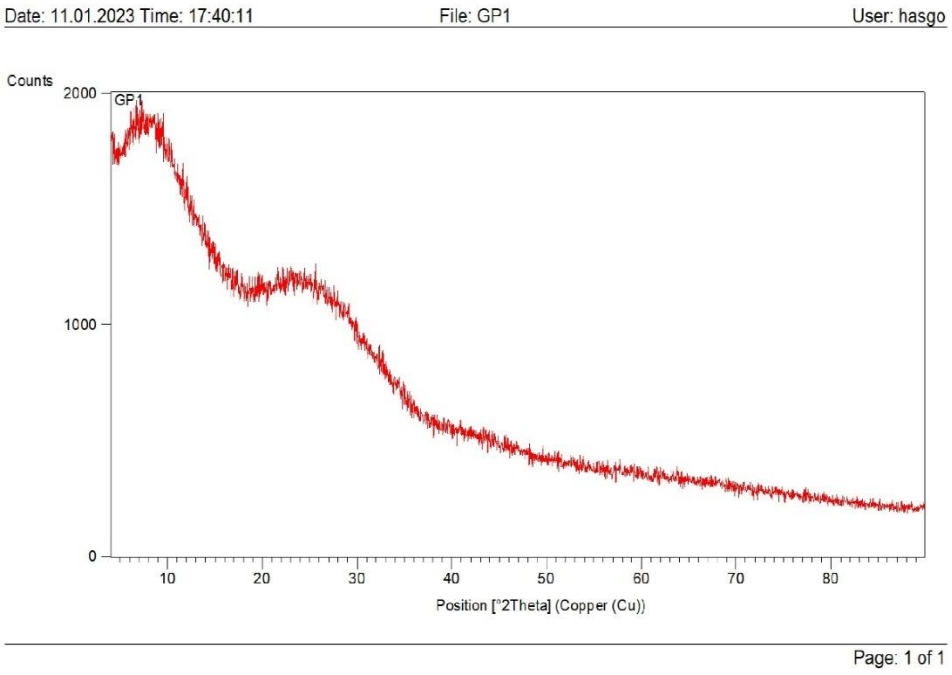

Figure D.2: XRD results for Glass powder (E- Fiber).

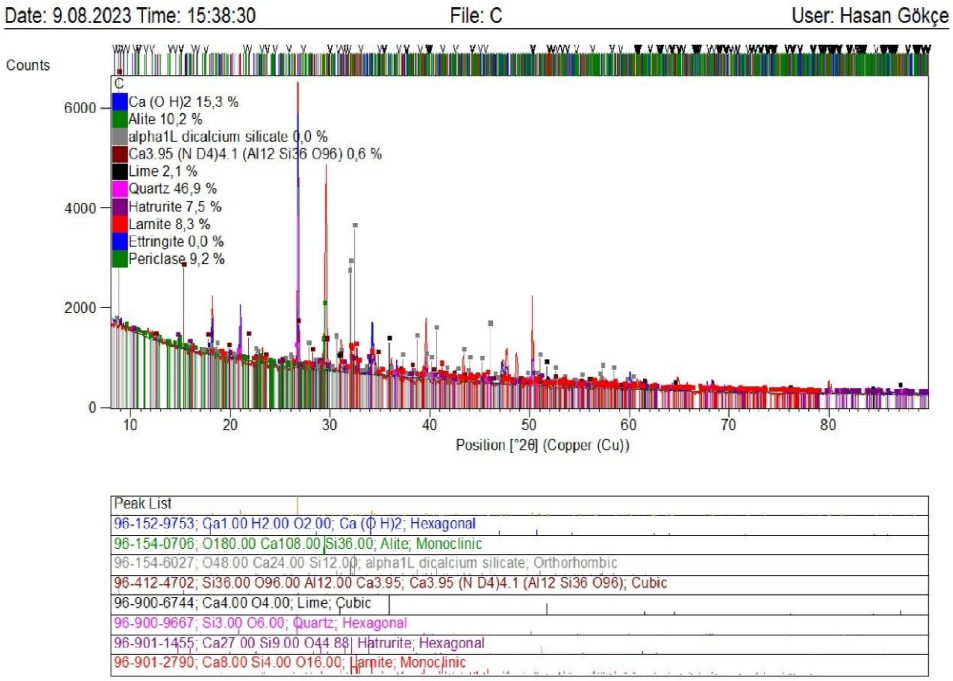

Figure D.3: XRD results for control paste.

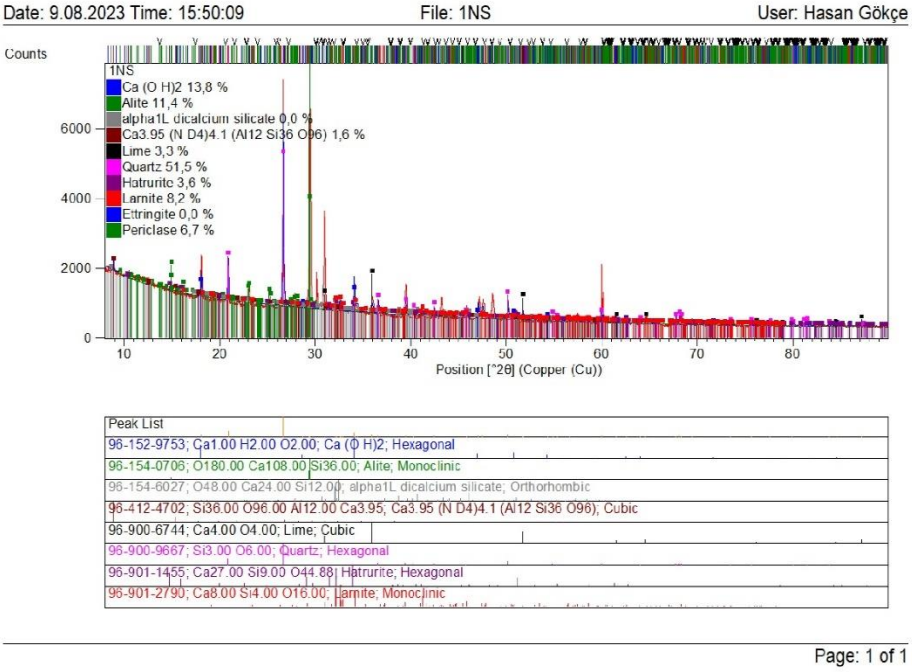

Figure D.4: XRD results for 1%NS paste.

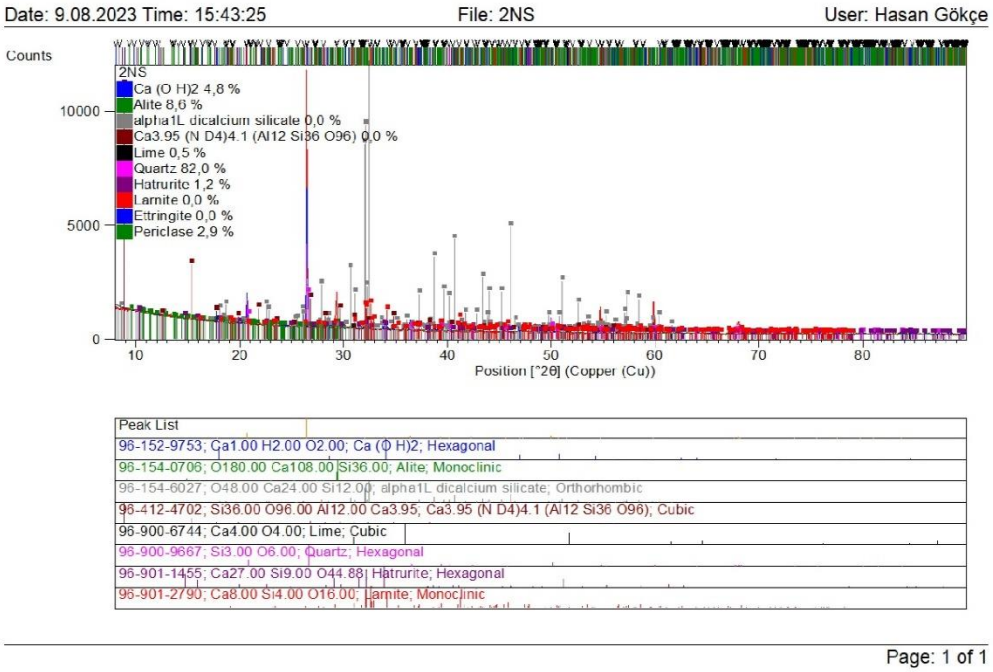

Figure D.5: XRD test results for 2%NS paste.

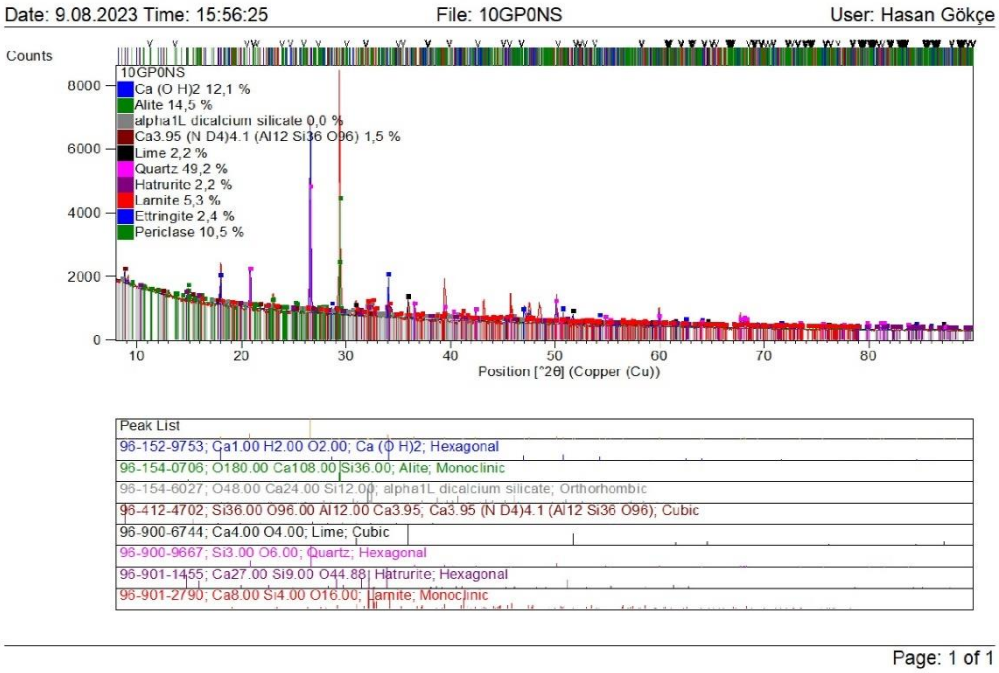

Figure D.6: XRD test results for 10%GP 0%NS paste.

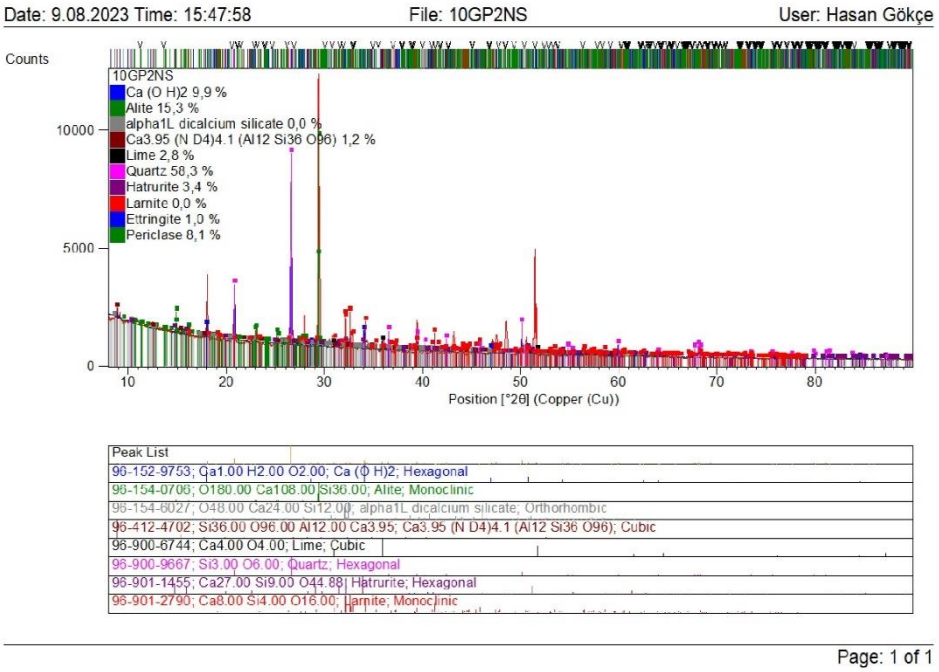

Figure D.7: XRD test results for 10%GP 2%NS paste.

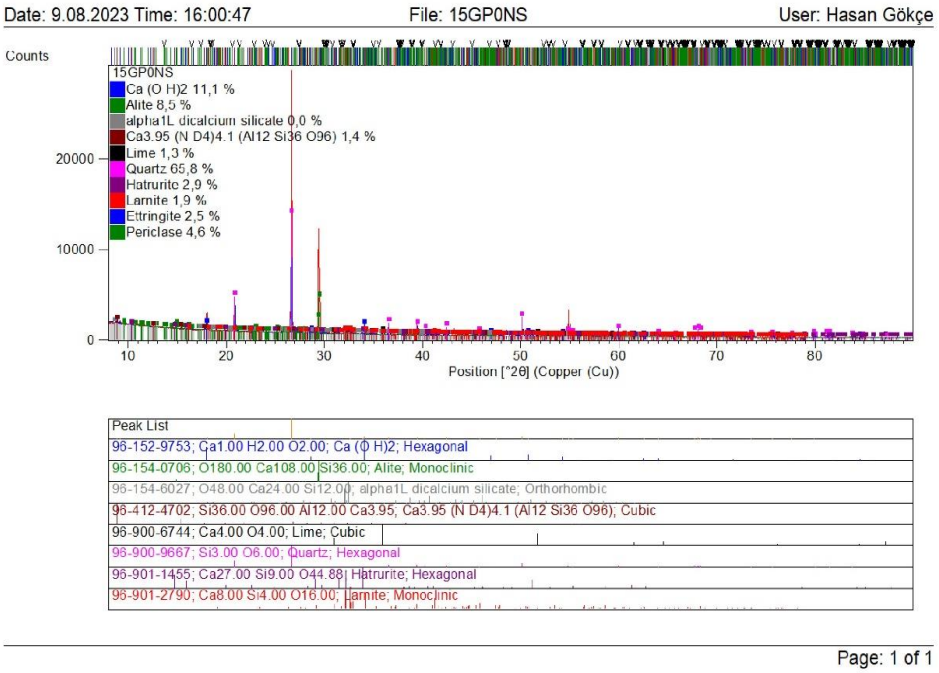

Figure D.8: XRD test results for 15%GP 0%NS paste.

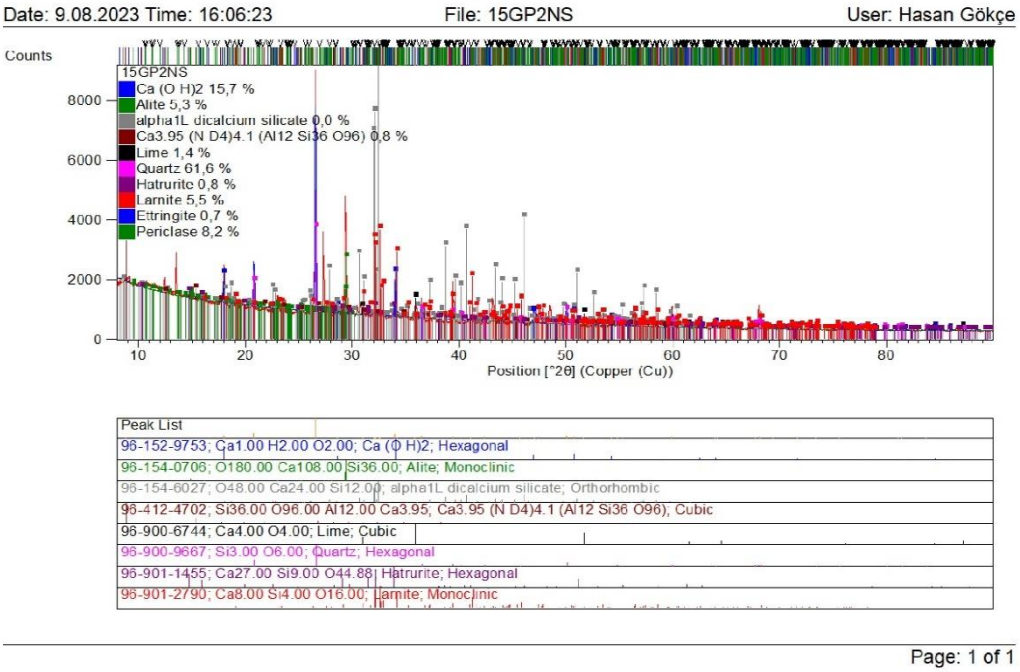

Figure D.9: XRD test results for 15%GP 2%NS paste.

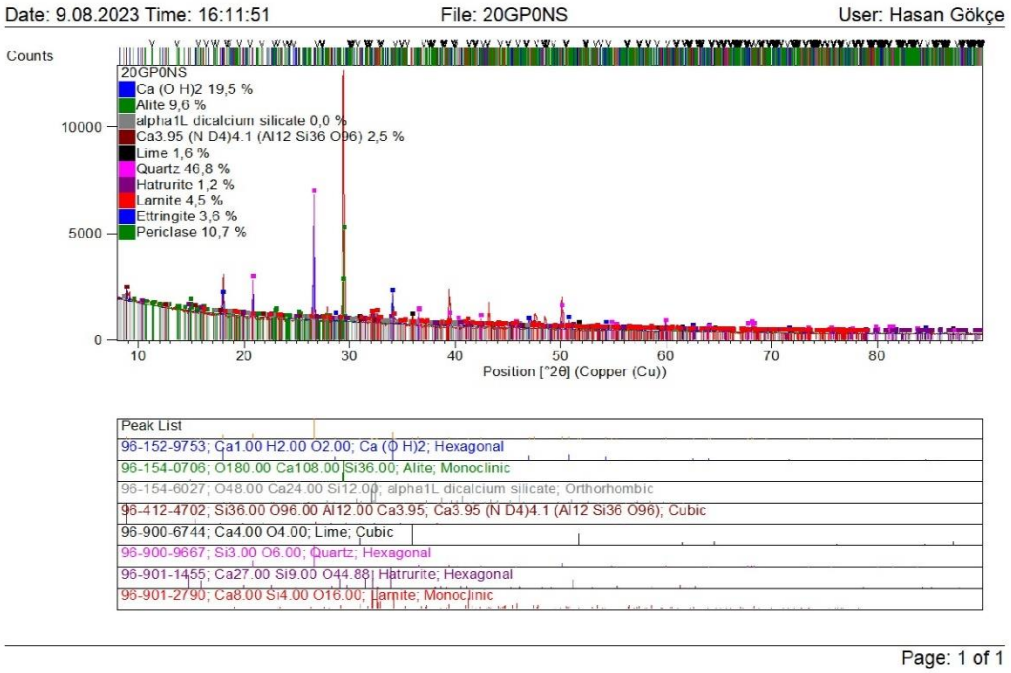

Figure D.10: XRD test results for 20%GP 0%NS paste.

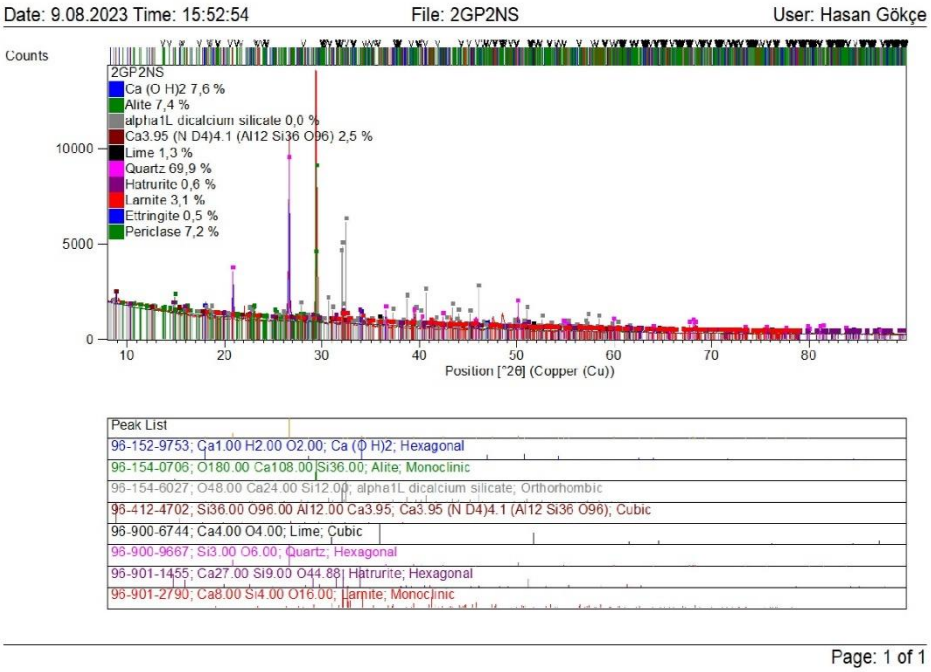

Figure D.11: XRD test results for 20%GP 2%NS paste.

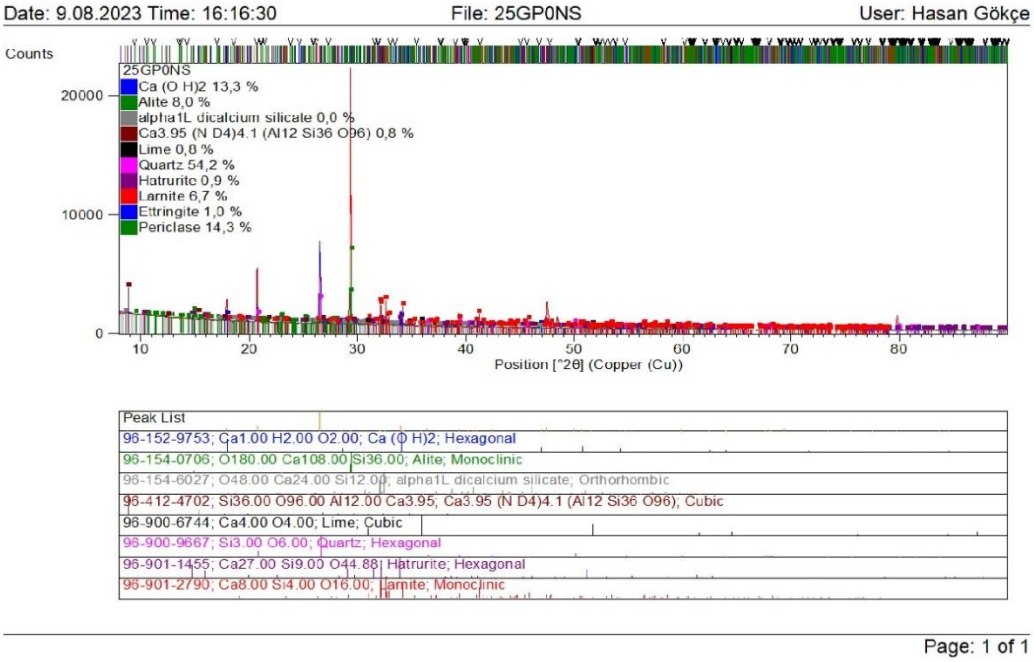

Figure D.12: XRD test results for 25%GP 0%NS paste.

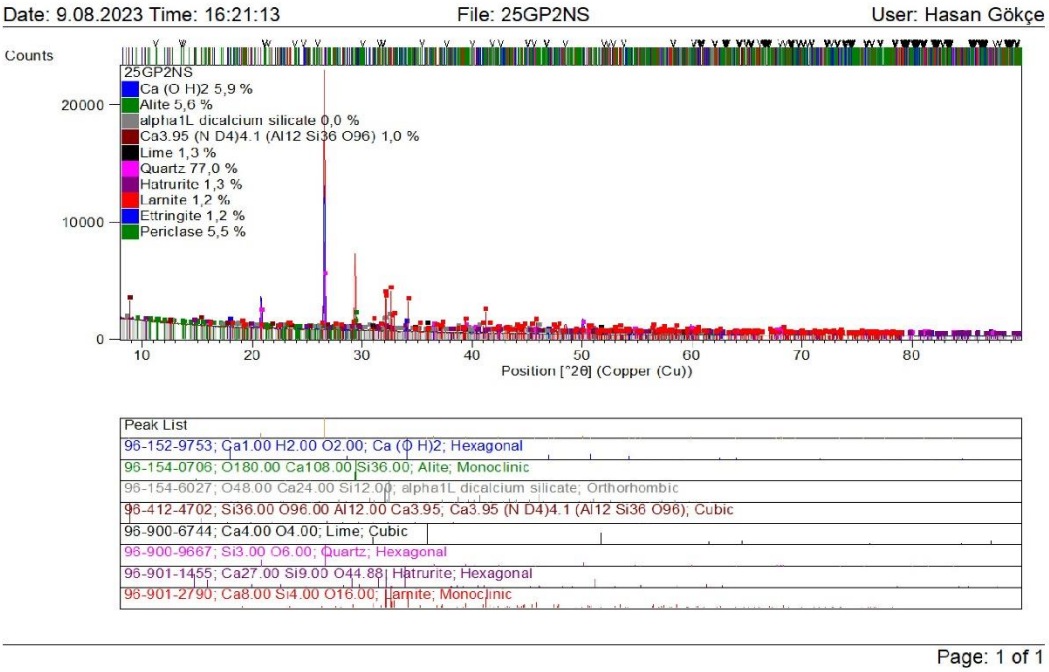

Figure D.13: XRD test results for 25%GP 2%NS paste.

CURRICULUM VITAE

Name Surname	**: Abed ALIOGLU**
EDUCATION	:
• B.Sc.	: 2019, Near East University, Faculty of Civil and Environmental Engineering, Civil Engineering Department.
• M.Sc.	: 2024, Istanbul Technical University, Faculty of Civil Engineering, Structural Engineering Department.

PUBLICATIONS, PRESENTATIONS AND PATENTS ON THE THESIS:

● ALIOGLU, A., & EKİNCİOĞLU, Ö. (2023) Mitigating Alkali-Silica Reaction Using Waste Glass Powder. 2nd International Graduate Research Symposium (IGRS'23) – May 16-18, 2023 İstanbul – TÜRKİYE. (n.d.). https://igrs.itu.edu.tr/